Experimental and Numerical Investigation of Nanotechnology on Foam Stability for Hydraulic Fracturing Application

A thesis submitted for the degree of Doctor of Philosophy (Ph.D.)

Australian School of Petroleum

Faculty of Engineering, Computer and Mathematical Sciences

University of Adelaide

By:

Yang Fei

Committee in charge:

Mary Gonzalez

Manouchehr Haghighi

August 2017

Abstract

Hydraulic fracturing is a well-known stimulation technique for creating fractures in a subsurface formation to achieve profitable production rates in a wellbore. The process involves the injection of a high-pressure fracturing fluid to induce fractures around the wellbore in a target interval enhancing oil and gas production in damaged wells or low permeability reservoirs. The pressure of injecting fracturing fluid should be high enough to overcome the subsurface in situ stresses and tensile strength of a fluid saturated porous rock, forming a tensile crack or fracture. Sand or other hard solid particles, referred to as proppant, is added in later stages of pumping. The fracturing fluid is required to have sufficient viscosity to suspend and carry the proppant deep into the created fracture system to keep the fractures open after hydraulic fracturing operation and during flowback and hydrocarbon production.

Slick water or cross-linked gel is currently used as fracturing fluid in almost all hydraulic fracturing operations. Foam as an alternative fracturing fluid is attracting attention because their liquid content (water) is small, reducing the water usage and reducing damage potential to water-sensitive formations. Foam as a fracturing fluid should remain stable to be able to carry a large amount of proppant. Gas-in-water foams is generally not stable in the presence of a surfactant, particularly in high temperatures reservoirs. Previously, guar gel and synthetic polymers were used as foam stabiliser. However, the damage to the formation increases because of the presence of gelling residue. Thus, stable foam with low formation damage is a key factor for the extensive use of foam as a fracturing fluid.

The principal goal of this study is to develop non-damaging and stable foam, which can transport proppant effectively. The secondary objective is to evaluate the performance and the stability of the developed foam using proppant placement efficiency (large uniform proppant distribution) and water usage efficiency (less water consumption to generate comparable or better productivity).

In this study, a non-damaging and stable foam is developed using silica nanoparticles and a living polymer made of worm-like surfactant micelles. The experimental results show that foam stability increases two to three times in the presence of 0.8 wt% silica nanoparticles under 90 ℃. The enhancement of foam lifetime by nanoparticle application allows better proppant suspension, which maintains post-fracture conductivity and minimise productivity loss. The simulation results show that foam stability is directly dependent on proppant placement and fracture conductivity distribution. When foam fracturing fluids experience long closure time, foam breakage leads to proppant settling and accumulation at the bottom of the formation; which causes reduction of the propped dimension. Both a high pumping rate and high foam quality provide a large initial propped area; however, foam stability is still the major factor that controls the final propped area, and the resulting productivity. Those results are critical findings for developing a guideline for an optimized application of nano-stabilised foams in unconventional reservoirs.

Declaration

I certify that this work contains no material which has been accepted for the award of any other degree or diploma in my name, in any university or other tertiary institution and, to the best of my knowledge and belief, contains no material previously published or written by another person, except where due reference has been made in the text. In addition, I certify that no part of this work will, in the future, be used in a submission in my name, for any other degree or diploma in any university or other tertiary institution without the prior approval of the University of Adelaide and where applicable, any partner institution responsible for the joint-award of this degree.

I give consent to this copy of my thesis, when deposited in the University Library, being made available for loan and photocopying, subject to the provisions of the Copyright Act 1968.

I also give permission for the digital version of my thesis to be made available on the web, via the University's digital research repository, the Library Search and also through web search engines, unless permission has been granted by the University to restrict access for a period of time.

Signature:

Date: 17-08-2017

Acknowledgements

First and foremost, I want to thank my two supervisors, **Mrs. Mary Gonzalez** and **AProf. Manouchehr Haghighi**. Among other things, Mary assisted me in setting the foundation to successfully conduct my studies, while Manouchehr provided valuable technical knowledge, which assisted me greatly. I would like to thank both for encouraging me in my research and for allowing me to grow as a research scientist. Their advices on both my research as well as on my career have been priceless.

I would also like to express my gratitude to **Dr. Raymond Johnson**. It has been an honour to have him as a co-author in my publications. I appreciate all his contributions.

A special thanks to my family. Words cannot express how grateful I am to my mother and father for all the sacrifices they made on my behalf. Their prayer for me was what sustained me thus far. Finally, I would like to thank all my friends, who provided much support during my study and writing.

List of publications

Published Journal Papers:

- Fei, Y., Gonzalez, M., Nguyen, V. Q., Lei, Z. Y., Pokalai, K., Sarkar, S., & Haghighi, M. (2016). Simulation of hydraulic fracturing with propane-based fluid using a fracture propagation model coupled with multiphase flow simulation in the Cooper Basin, South Australia. APPEA Journal, 56, 415-426.

- Fei, Y., Zhu, J., Xu, B., Li, X., Gonzalez, M., & Haghighi, M. (2017). Experimental investigation of nanotechnology on worm-like micelles for high-temperature foam stimulation. Journal of Industrial and Engineering Chemistry. doi:http://dx.doi.org/10.1016/j.jiec.2017.02.015.

Submitted Manuscript:

- Fei, Y., Pokalai, K., Johnson, R., Gonzalez, M., & Haghighi, M. (2017). Experimental and simulation study of foam stability and the effects on hydraulic fracture proppant placement submitted to Journal of Natural Gas Science and Engineering.
- Fei, Y., Johnson, R., Gonzalez, M., Haghighi, M., & Pokalai, K. (2017). Experimental and numerical investigation into nano-stabilised foam on hydraulic fracturing application, submitted to Fuel.
- Fei, Y., Zhu, J., Xu, B., Li, X., Gonzalez, M., & Haghighi, M. (2017). Free Drainage of foam mixed with coarse particles in the presence of nanoparticles submitted to SPE Hydraulic Fracturing Technology conference.

Table of Contents

List of Figures

List of Tables

Statement of Authorship

Statement of Authorship

Title of Paper	Free Drainage of foam mixed with coarse particles in the presence of nanoparticles
Publication Status	○ **Published** ○ **Accepted for publication** ◉ **Submitted for publication** ○ **Unsubmitted but in manuscript form**
Publication Details	Fei, Y., Zhu, J., Xu, B., Li, X., Gonzalez, M., & Haghighi, M. (2017). Free Drainage of foam mixed with coarse particles in the presence of nanoparticles submitted to SPE Hydraulic Fracturing Technology conference.

Principal Author

Name of Principal Author (Candidate)	Yang Fei		
Contribution to the Paper	Experimental study, Data collection, interpretation, analysis, and writing.		
Overall percentage (%)	70%		
Certification:	This paper reports on original research I conducted during the period of my Higher Degree by Research candidature and is not subject to any obligations or contractual agreements with a third party that would constrain its inclusion in this thesis. I am the primary author of this paper.		
Signature		Date	16-08-2017

Co-Author Contribution

By signing the Statement of Authorship, each author certifies that:

i. the candidate's stated contribution to the publication is accurate (as detailed above);
ii. permission is granted for the candidate to include the publication in the thesis; and
iii. the sum of all co-author contributions is equal to 100% less the candidate's stated contribution.

Name of Co-Author	Jingyi Zhu		
Contribution to the Paper	Supported with all the lab work (10 %)		
Signature		Date	16-08-2017

Name of Co-Author	Binyu Xu		
Contribution to the Paper	Supported with most of lab work. (5 %)		
Signature	Binyu Xu	Date	16-08-2017

Name of Co-Author	Xiaogang Li		
Contribution to the Paper	Supported with the structure, writing and review of paper. (5 %)		
Signature		Date	16-08-2017

Name of Co-Author	Mary Gonzalez Perdomo		
Contribution to the Paper	Supported with the structure, writing and review of paper. (5 %)		
Signature		Date	16-08-2017

Name of Co-Author	Manouchehr Haghighi		
Contribution to the Paper	Supported with the structure, writing and review of paper. (5 %)		
Signature		Date	16-08-2017

Statement of Authorship

Title of Paper	Experimental investigation of nanotechnology on worm-like micelles for high-temperature foam stimulation
Publication Status	◉ Published ○ Accepted for publication ○ Submitted for publication ○ Unsubmitted but in manuscript form
Publication Details	Fei, Y., Zhu, J., Xu, B., Li, X., Gonzalez, M., & Haghighi, M. (2017). Experimental investigation of nanotechnology on worm-like micelles for high-temperature foam stimulation. Journal of Industrial and Engineering Chemistry. doi:http://dx.doi.org/10.1016/j.jiec.2017.02.015.

Principal Author

Name of Principal Author (Candidate)	Yang Fei
Contribution to the Paper	Experimental study, Data collection, interpretation, analysis, and writing.
Overall percentage (%)	70%
Certification:	This paper reports on original research I conducted during the period of my Higher Degree by Research candidature and is not subject to any obligations or contractual agreements with a third party that would constrain its inclusion in this thesis. I am the primary author of this paper.
Signature	Date: 1/8/2017

Co-Author Contribution

By signing the Statement of Authorship, each author certifies that:

i. the candidate's stated contribution to the publication is accurate (as detailed above);

ii. permission is granted for the candidate to include the publication in the thesis; and

iii. the sum of all co-author contributions is equal to 100% less the candidate's stated contribution.

Name of Co-Author	Jingyi Zhu
Contribution to the Paper	Supported with all the lab work (10 %)
Signature	Date: 10/08/2017

Name of Co-Author	Binyu Xu
Contribution to the Paper	Supported with most of lab work. (5 %)
Signature	Date: illegible

Name of Co-Author	Xiaogang Li
Contribution to the Paper	Supported with the structure, writing and review of paper. (5 %)
Signature	Date: 10/08/2017

Name of Co-Author	Mary Gonzalez Perdomo
Contribution to the Paper	Supported with the structure, writing and review of paper. (5 %)
Signature	Date: 1/08/2017

Name of Co-Author	Manouchehr Haghighi
Contribution to the Paper	Supported with the structure, writing and review of paper. (5 %)
Signature	Date: 4-8-2017

Statement of Authorship

Title of Paper	Experimental and simulation study of foam stability and the effects on hydraulic fracture proppant placement
Publication Status	○ Published ○ Accepted for publication ◉ Submitted for publication ○ Unsubmitted but in manuscript form
Publication Details	Fei, Y., Pokalai, K., Johnson, Jr R., Gonzalez, M. , Haghighi, M.,2017 'Foam stability and the effects on hydraulic fracture proppant placement and overall effectiveness' (Major Review by Journal)

Principal Author

Name of Principal Author (Candidate)	Yang Fei
Contribution to the Paper	Data collection, interpretation, analysis, and writing.
Overall percentage (%)	60%
Certification:	This paper reports on original research I conducted during the period of my Higher Degree by Research candidature and is not subject to any obligations or contractual agreements with a third party that would constrain its inclusion in this thesis. I am the primary author of this paper.
Signature	Date 1/8/2017

Co-Author Contribution

By signing the Statement of Authorship, each author certifies that:

i. the candidate's stated contribution to the publication is accurate (as detailed above);

ii. permission is granted for the candidate to include the publication in the thesis; and

iii. the sum of all co-author contributions is equal to 100% less the candidate's stated contribution.

Name of Co-Author	Kunakorn Pokalai
Contribution to the Paper	Supported with the structure and review of paper (10 %)
Signature	Date 16/08/17

Name of Co-Author	Raymond (Ray) L. Johnson, Jr
Contribution to the Paper	Supported with the structure, writing and review of paper. (10 %)
Signature	Date 16/8/2017

Name of Co-Author	Mary Gonzalez Perdomo
Contribution to the Paper	Supported with the structure, writing and review of paper. (10 %)
Signature	Date 01/08/2017

Name of Co-Author	Manouchehr Haghighi
Contribution to the Paper	Supported with the structure, writing and review of paper. (10 %)
Signature	Date 4-8-2017

Statement of Authorship

Title of Paper	Experimental and Numerical Investigation into Nano-Stabilized Foams in Low Permeability Reservoir Hydraulic Fracturing Applications
Publication Status	○ Published ○ Accepted for publication ◉ Submitted for publication ○ Unsubmitted but in manuscript form
Publication Details	Fei, Y., Johnson, R., Gonzalez, M., Haghighi, M., & Pokalai, K. (2017). Experimental and Numerical Investigation into Nano-Stabilized Foams in Low Permeability Reservoir Hydraulic Fracturing Applications (Under review by Journal).

Principal Author

Name of Principal Author (Candidate)	Yang Fei
Contribution to the Paper	Data collection, interpretation, analysis, and writing.
Overall percentage (%)	65%
Certification:	This paper reports on original research I conducted during the period of my Higher Degree by Research candidature and is not subject to any obligations or contractual agreements with a third party that would constrain its inclusion in this thesis. I am the primary author of this paper.
Signature	Date 1/8/2017

Co-Author Contribution

By signing the Statement of Authorship, each author certifies that:

i. the candidate's stated contribution to the publication is accurate (as detailed above);

ii. permission is granted for the candidate to include the publication in the thesis; and

iii. the sum of all co-author contributions is equal to 100% less the candidate's stated contribution.

Name of Co-Author	Raymond (Ray) L. Johnson, Jr
Contribution to the Paper	Supported with the structure, writing and review of paper. (20 %)
Signature	Date 14/8/2017

Name of Co-Author	Mary Gonzalez Perdomo
Contribution to the Paper	Supported with the review of paper. (5 %)
Signature	Date 01/08/2017

Name of Co-Author	Manouchehr Haghighi
Contribution to the Paper	Supported with the review of paper. (5 %)
Signature	Date 4-8-2017

Name of Co-Author	Kunakorn Pokalai
Contribution to the Paper	Supported with the mathematical formulas (5 %)
Signature	Date 16/08/2017

Statement of Authorship

Title of Paper	Simulation of Hydraulic Fracturing with Propane-Based Fluid using a Fracture Propagation Model Coupled with Multiphase Flow Simulation in the Cooper Basin, South Australia.
Publication Status	(•) Published ( ) Accepted for publication ( ) Submitted for publication ( ) Unsubmitted but in manuscript form
Publication Details	Fei, Y., Gonzalez , Nguyen, V, Lei, ZY, Pokalai, K., Sarkar, S & Haghighi, M 2016 Simulation of Hydraulic Fracturing with Propane-Based Fluid using a Fracture Propagation Model Coupled with Multiphase Flow Simulation in the Cooper Basin, South Australia. The APPEA Journal, vol. 56.

Principal Author

Name of Principal Author (Candidate)	Yang Fei		
Contribution to the Paper	Data collection, interpretation, analysis, and writing.		
Overall percentage (%)	60%		
Certification:	This paper reports on original research I conducted during the period of my Higher Degree by Research candidature and is not subject to any obligations or contractual agreements with a third party that would constrain its inclusion in this thesis. I am the primary author of this paper.		
Signature		Date	28/03/17

Co-Author Contribution

By signing the Statement of Authorship, each author certifies that:

i. the candidate's stated contribution to the publication is accurate (as detailed above);
ii. permission is granted for the candidate to include the publication in the thesis; and
iii. the sum of all co-author contributions is equal to 100% less the candidate's stated contribution.

Name of Co-Author	Mary Gonzalez Perdomo		
Contribution to the Paper	Supported with the structure, writing and review of paper. (10 %)		
Signature		Date	01/08/2017

Name of Co-Author	Viet Quoc Nguyen		
Contribution to the Paper	Supported with the structure, writing and review (5 %)		
Signature		Date	14/08/2017

Name of Co-Author	Zhongyu Lei		
Contribution to the Paper	Interpreted image log and fracture (5 %)		
Signature		Date	16/08/2017

Name of Co-Author	Kunakorn Pokalai		
Contribution to the Paper	Supported with the structure and review of paper (5 %)		
Signature		Date	29/03/17

Name of Co-Author	Sume Sarkar		
Contribution to the Paper	Review of paper. (5 %)		
Signature		Date	07/08/2017

Name of Co-Author	Manouchehr (Manny) Haghighi		
Contribution to the Paper	Review of paper. (10 %)		
Signature		Date	27/3/2017

Nomenclature

Roman		
C_f	Fracture conductivity	$md.ft$
C_v	Volume fraction of particles	$dimensionless$
D_b	Bubble diameter	$inch$
E	Young's modulus	$Mpsi$
F_n	Network force	$kg.m/s^2$
F_p	Pressure force	$kg.m/s^2$
F_{ds}	Drainage drag force	$kg.m/s^2$
F_z	Total pulling force in vertical direction	$kg.m/s^2$
G	Gravity force	$kg.m/s^2$
g	Gravitational constant	$m^3.kg^{-1}.s^{-2}$
g_c	Gravitational unit conversion constant	$dimensionless$
H	Foam height	ft
k_{Foam}	Foam flow consistency index	$Pa.s^n$
k_{Liquid}	Base fluid flow consistency index	$Pa.s^n$
k	Boltzmann constant	$m^3.kg.s^{-2}K^{-1}$
K_s	Packed permeability	md
L	Length of Plateau border	ft
M	Interfacial mobility ratio	$dimensionless$
n	Ionic concentration	$dimensionless$
n_{Foam}	Foam flow behaviour index	$dimensionless$
n_{Liquid}	Base fluid flow behaviour index	$dimensionless$
P_{net}	Net pressure	psi
P_f	Fluid pressure	psi
P	Pressure	psi

Q_g	Foam quality	%
r_p	Particle radius	in
S	Distance along fracture surface	ft
$S(t)$	Travelling distance at time t	ft
T_F	Formation temperature	°F
t	Drainage time	s
$V_{(t)}$	Drained liquid volume at time t	ml
$V_{(l0)}$	Total liquid volume	ml
v_d	Drainage rate	ml/s
$v_d^{channel}$	Drainage front velocity at channel dominated flow	ml/s
v_d^{node}	Drainage front velocity at node dominated flow	ml/s
v_s	Vertical slurry velocity	ft/s
w_s	Packed width	in
w	Fracture width	in
z	Ion valency	dimensionless
Z	Vertical distance	ft
Greek		
η_l	Fluid viscosity	$lbm/ft \cdot s$
μ_s	Surface viscosity	$lbm/ft \cdot s$
ν	Poisson's ratio	$dimensionless$
κ^{-1}	Debye length	$dimensionless$
μ_a	Apparent slurry viscosity	$lbm/ft \cdot s$
ρ_s	Slurry bulk density	lbm/ft^3
ρ_l	Liquid phase density	lbm/ft^3
ρ_g	Gas phase density	lbm/ft^3
ρ_p	Particle density	lbm/ft^3

ε_o	Initial liquid fraction	$dimensionless$
ε_t	Time dependent liquid fraction	$dimensionless$
ϵ^*	Permittivity of free space	$dimensionless$
ϵ_r	Dielectric constant of liquid film	$dimensionless$
τ	Drainage half-time	s

Chapter 1: Introduction

1.1 Research Background and Rationale

The purpose of hydraulic fracturing is to generate a large conductive proppant pack area to improve the flow of reservoir fluids to the wellbore relative to natural flow (Economides and Nolte, 2000). Proppants, such as coated sand and ceramics, are mixed with fracturing fluids so that after injection has stopped, there will be physical support to maintain a conductive channel or network for reservoir fluids to flow. However, settling of proppant particles can occur particularly in low viscosity fluids during pumping and after pumping before fracture closure. This settling behaviour can lead to an accumulation of proppant particles in the lower part of the vertical fracture. The higher part of a vertical fracture could then have insufficient proppant to be conductive. **Figure 0.1** shows a typical proppant distribution in a vertical fracture at the end of treatment. With adequate fluid viscosity, proppant settling can be minimised, resulting in a more uniform distribution as shown in **Figure 0.1a**. With low viscosity fracturing fluids (**Figure 0.1b**), a less uniform propped fracture geometry results and can be characterised by a packed bed of proppants at the bottom of the fracture. The proppant at the top of the pack, or dune-like structure, will experience higher stresses (Warpinski, 2010) because it is supporting the open arch; this may lead to proppant crushing and additional formation damage (i.e. proppant embedment and fines migration). Therefore, it is generally recognised that failure to achieve sufficient vertical pay coverage with a propped fracture can seriously reduce the overall stimulation performance. Several experimental studies (Alotaibi and Miskimins, 2015; Beg et al., 1998; Fredd et al., 2001; Jansen et al., 2015; Li et al., 2016; Pyrak-Nolte and Morris, 2000; Wu et al., 2017) and numerical studies (Chang et al., 2017; Clark and Guler, 1983; Liu et al., 2017; Shiozawa and McClure, 2016; Yu et al., 2015; Zhang et al., 2016) have investigated the relationship between proppant transportation, distribution, and proppant pack conductivity.

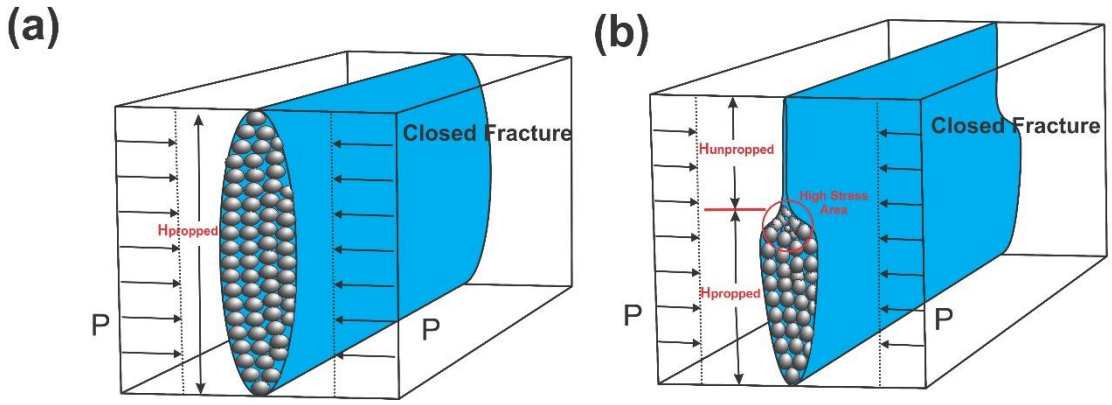

Figure 0.1. Schematic of proppant placement before fracture closure: (a) evenly distributed proppant; (b) unevenly distributed proppant.

Previously, foams were introduced as fracturing fluids in the early 1980s, and they have been extensively used in various liquid-sensitive and depleted reservoirs (Craft et al., 1992; Goelitz and Evertz, 1982; Wamock et al., 1985). It has been commonly reported that foams can achieve faster clean-up, low leak-off, and less formation damage than conventional water-based fracturing fluids (Burke et al., 2011; Garbis and Taylor, 1986; Goelitz and Evertz, 1982; Harris,

1985; Toney and Mack, 1991). Other reported benefits include a lower water consumption and reduced swabbing (Blauer and Kohlhaas, 1974; Gaydos and Harris, 1980). Increasing transportation costs in remote locations, storage costs, and high surface pumping requirements have been identified as limitations for field application (Wanniarachchi et al., 2015). Given the ability of foams to induce fractures and carry proppants, it is essential to maintain foam stability at high shear rates while pumping and at low shear rates during fracture closing. Failure to maintain foam stability results in proppant screen-out either in the fracture or at the wellbore or inadequate proppant distribution in the targeted interval at fracture closure, owing to inadequate foam stability and proppant redistribution during closure (Johnson, 1995). Therefore, the main issue of using foam in hydraulic fracture treatments is foam stability, particularly in high temperature conditions when foam becomes more unstable.

The gap in research has created a new research area for foam stability and it is focused on nanotechnology. The mechanism of nanoparticle-stabilised foam is explained in the literature review chapter. Therefore, one of the focuses of this study is to determine the nanoparticle effect on foam stability as well as on proppant placement during hydraulic fracturing.

1.2 Research objectives

The main goals in this study are to develop a non-damaging and stable foam, which can transport proppants effectively and to investigate the potential use of nanoparticles to stabilise foam and accordingly influence the proppant placement performance for hydraulic fracturing applications. The purpose behind this research is to provide general guidelines for the oil and gas industry in designing foam fracturing treatment. The specific objectives of this thesis are as follows:

1. To determine the relationship between foam drainage mechanism and proppant settling in the presence of nanoparticles.
2. To develop a polymer-free nano-stabilised foam and understand the effects of hydrophilic nanoparticles on foam stability at high temperatures.
3. To determine the relationship between foam stability and proppant settling with and without nanoparticles.
4. To establish a methodology for foam rheological characterisation with foam stability factors.
5. To investigate the effects of foam stability on proppant concentration distribution and post-fracture conductivity and productivity.
6. To develop screening criteria, indicating the treatment design and foam properties, which are more favourable to the application of foam-based fracturing to enhance hydrocarbon recovery.

1.3 Thesis Structure

The thesis comprises three main sections: literature review, experimental study, and numerical study. The overall thesis structure is illustrated in **Figure 0.2**.

The first section (chapter 2) involves the review on the theory of foam stability, current practice of foam stability enhancement, foam rheology, and proppant settling.

The second section (Chapter 3 and 4) can be split into two experimental parts. The first part details the free drainage experiment under 25℃. The effect of free drainage on the rheology of four different foams without proppant was investigated by generating the liquid fraction profiles. Afterwards, the proppant settling experiment was performed and the settling relationship with foam stability was studied. Based on the results of the first part, the next set of foam stability experiment is conducted under an 90 ℃ environment to simulate the actual reservoir condition. In this study, a regular anionic surfactant was employed as the foaming agent and a worm-like micelle (WLM) surfactant was employed as foam viscosifer with silica nanoparticles.

The final section (chapter 5, 6, and 7) consists of three simulation studies as follows:

The first study investigated the fundamental relationship between foam stability and proppant placement during hydraulic fracturing. The rheological characterisation of WLM foams was performed based on foam quality changes during the foam drainage experiments and also based on viscosity breakdown by disproportionation. A 3D hydraulic fracture simulation was conducted to evaluate the foam performance as a fracturing fluid using different vertical well scenarios. Based on simulation results, like fracture geometries and proppant distributions; the impact of WLM foams on hydraulic fracturing were evaluated.

The next study investigated a new concept to overcome the problem of proppant settling by introducing nanoparticles into the WLM foam system. In this study, following a previous experimental work, the rheological properties of the developed foam were characterised based on experimental results of drainage rate and foam volume decay rate. Then, the developed foam rheological model is integrated into the fracturing model. The impact of the WLM foams and nanoparticles on proppant distributions and fracture conductivities are evaluated under different pumping rates, foam quality, and shut-in time.

The last study investigated a propane-based fracturing fluid considered as an alternative to foam-based fracturing fluids. A multiphase flow model has been developed and linked with the 3D fracturing propagation model to simulate the flowback and gas production of the fractured wells.

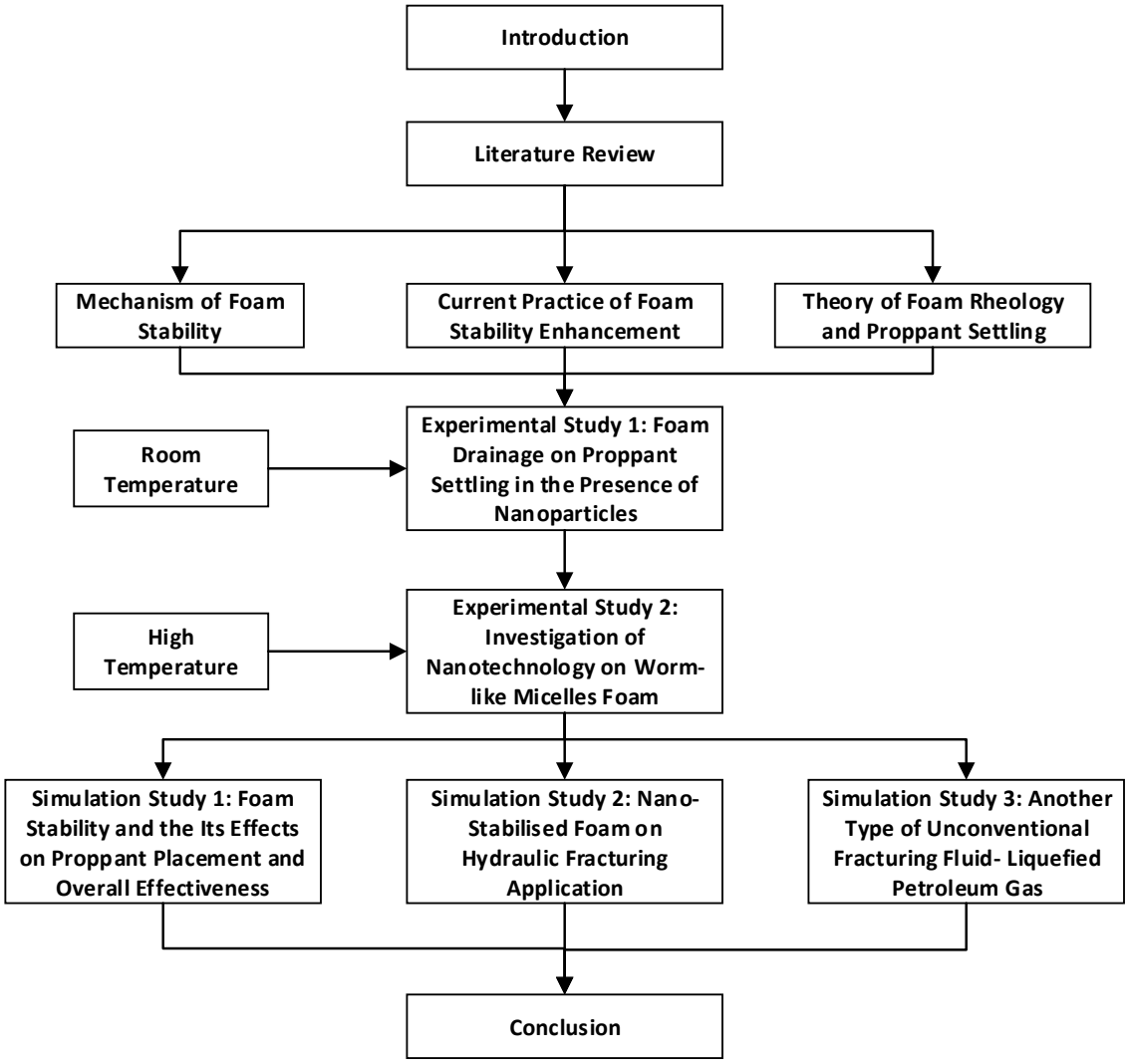

Figure 0.2. Structure of the thesis

1.4 Overview of chapters

This thesis is a hybrid dissertation (thesis with publication). Five papers are included in the thesis, of which two papers have been published in peer-reviewed journals, two papers have been submitted to academic journals and one paper is currently under review (Table 1). The thesis contains eight chapters and the details of each are as follows:

Chapter 1: Introduces the background and motivation, objective and methodology, and structure of the dissertation.

Chapter 2: Presents a literature review of current concepts on foam-based fracturing fluids.

Chapter 3: Presents an experimental study of free drainage of different foam designs and its impact on proppant settling.

Chapter 4: Presents the development of nano-stabilised WLM foams through foam stability test and foam rheology test and their impact on proppant settling.

Chapter 5: Incorporates the results of previous experiments, and presents the development of hydraulic fracturing modelling to predict proppant distribution and productivity.

Chapter 6: Incorporating the results of previous experiments, this chapter presents numerical investigation into nano-stabilised foams which provide a solution of proppant settling in a low permeability reservoir.

Chapter 7: Presents another type of unconventional fracturing fluid consideration-liquefied petroleum gas, which compares hydraulic fracturing effectiveness with foam-base fluid.

Chapter 8: Summarises the research work in this thesis and presents recommendations for future work.

Table 1.1 Chapter Outlines

Chapter	Title	Status
Chapter 3	Foam drainage on proppant sedimentation in the presence of nanoparticles	Submitted
Chapter 4	Investigation of nanotechnology on worm-like micelles for high temperature foam stimulation	Published
Chapter 5	Foam stability and its effects on proppant placement and overall effectiveness	Submitted
Chapter 6	Hydraulic fracturing by nano-assisted foam-based fluids using a fracture propagation model	Manuscript
Chapter 7	Another type of unconventional fracturing fluid—liquefied petroleum gas	Published

Chapter 2: Literature reviews

2.1 Theory of foam stability

Foam stability can be explained by three mechanisms: drainage, disproportionation, and coalescence. Foam drainage is caused by liquid gravity segregation (Angarska et al., 2007; Koehler et al., 2000). During foam drainage, the foam quality increases with time, influencing the foam rheology (Höhler and Cohen-Addad, 2005; Weaire, 2008). Disproportionation is caused by the gas transfer between bubbles induced by capillary pressure differences (Maestro et al., 2014a). During disproportionation, the bubble size increases, causing the bubble to become more 'fragile', affecting the rheology and increasing proppant settling in the fracture. Finally, bubble coalescence is caused by the rupture of liquid films between neighbouring bubbles (Saye and Sethian, 2013). The inter-relationship between foam drainage, disproportionation and coalescence determines the foam quality, proppant carrying capacity, and foam volume (i.e. bulk deformation of bubbles), thereby controlling the fracturing fluid effectiveness.

2.1.1 Foam drainage

Figure 0.1 shows a schematic of free drainage which considers a foam sample of initial foam height H_o and initial uniform liquid fraction ε_o at $t = 0$ in a cylinder with a closed base. Over time, the downward flow of the liquid dries the foam and the liquid accumulates at the base of the cylinder. The interface between the foam and the accumulated liquid over time is labelled L_t. Foam drainage is the flow of liquid through the channels (Plateau borders) and nodes between bubbles of the foam whilst experiencing resistance due to viscous friction from the walls (Bhakta and Ruckenstein, 1995; Leonard and Lemlich, 1965; Magrabi et al., 2001). Drainage can be described as a complex hydrodynamic process governed by gravity and capillary pressure (Hutzler et al., 2005; Koehler et al., 2004; Neethling et al., 2002).

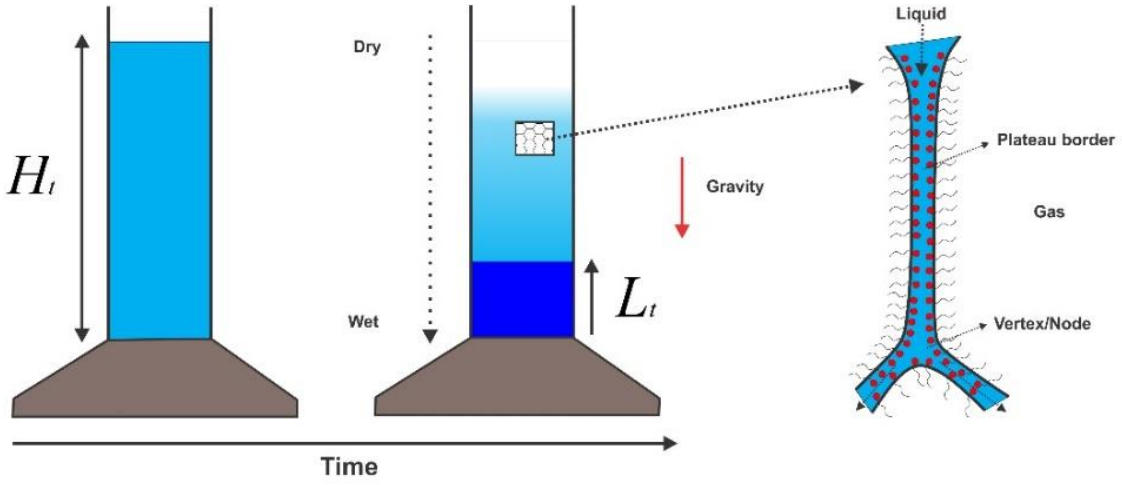

Figure 0.1. Schematic of a free drainage experiment

Drainage rate is crucially important for foam stability and rheology (see details in **Section 2.4**) as it increases the foam quality (Q_g) as a function of time as follows:

$$Q_g^t = Q_g^o + v_d t \quad (1)$$

Where Q_g^o is the initial foam quality, Q_g^t is the foam quality after draining for a certain time t, and v_D is the foam drainage rate.

2.1.2 Disproportionation

Disproportionation is also known as Ostwald ripening and is a process involving the diffusion of gas from smaller to larger bubbles. The driving force for this process is the Laplace pressure, or the pressure difference between bubbles of different sizes (**Figure 0.2**):

$$P_A = P + {}^{2\sigma}/_{r_A} \quad (2)$$

$$P_B = P + {}^{2\sigma}/_{r_B} \quad (3)$$

$$P_{capillary} = P_A - P_B = 2\sigma(\frac{1}{r_A} + \frac{1}{r_B}) \quad (4)$$

Where σ is the surface tension and r_A, r_B are the radii of bubble A and bubble B respectively. Capillary pressure coupled with gas solubility in the aqueous phase initiates gas diffusion, leading to growth of larger bubbles whilst smaller ones are shrinking. The mechanism of diffusive disproportionation in foams has been reviewed both theoretically and experimentally in terms of foam film permeability (Farajzadeh et al., 2008).

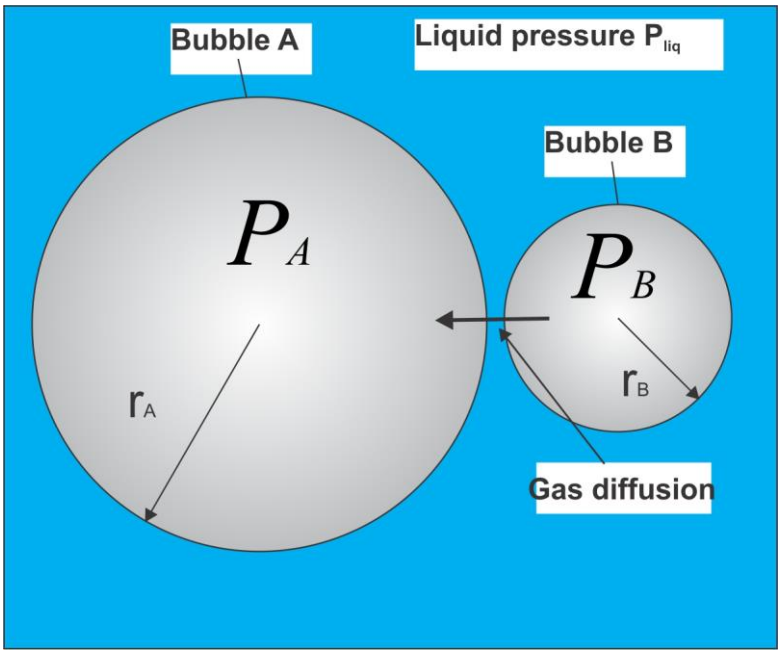

Figure 0.2. Schematic of Ostwald ripening: bubble A growth from gas diffusion of bubble B by capillary pressure driving force (reproduced from Stevenson (2010).

2.1.3 Foam stability analysis by DLVO theory (Derjaguin and Landau, Verwey and Overbeek)

When a foam film is first created, its wall thickness h_w can be up to a few hundred nanometres. The liquid in the film flows away driven by the capillary pressure across the bubbles. The DLVO disjoining pressure appears and acts as an opposite force. A positive disjoining pressure in the film is necessary to attain film stability and existence of foam.

The disjoining pressure is based on the attractive and repulsive interactions (Churaev, 2003; Cosima and Regine von, 2003; Vance, 1999; Wang et al., 2016). It is a function of the thickness

of the foam film, h_w, and can be calculated from three independent terms: Π_{vw} is the van der Waals force, Π_{el} is the electrostatic force, and Π_{st} is the steric force.

$$\Pi = \Pi_{vw} + \Pi_{el} + \Pi_{st} \quad (5)$$

The van der Waals force (Π_{vw}) depends on the Hamaker constant A_H, which is the generalised attractive force between any two surfaces:

$$\Pi_{vw} = -\frac{A_H}{6\pi h_w^3} \quad (6)$$

The van der Waals attractions always destabilise foam films. Therefore, repulsive forces (electrostatic force, Π_{el}) produced by surfactant and electrolyte molecules are required to balance the attractive force to stabilise the foam films. The electrostatic repulsion (Π_{el}) to the disjoining pressure is approximately calculated as follows:

$$\Pi_{el} = 64cRTs^2e^{-\frac{h_w}{D}} \quad (7)$$

Where D is the Debye length, s is an intermediate value, c is the molar concentration of salt, and T is the absolute temperature. In addition to van der Waals and electrostatic pressures, the steric repulsion (Π_{st}) has also been considered:

$$\Pi_{st} = \frac{0.035qb}{h_w(h_w - b)} \quad (8)$$

Where b is the steric length, below which the disjoining pressure is 'infinite' and above which **Eq. 8** is an adequate approximation, whereas q is the surface charge with values between 0 (no steric interaction) and 1 (maximum steric interaction). **Figure 0.3** shows an example of the disjoining pressure versus film thickness.

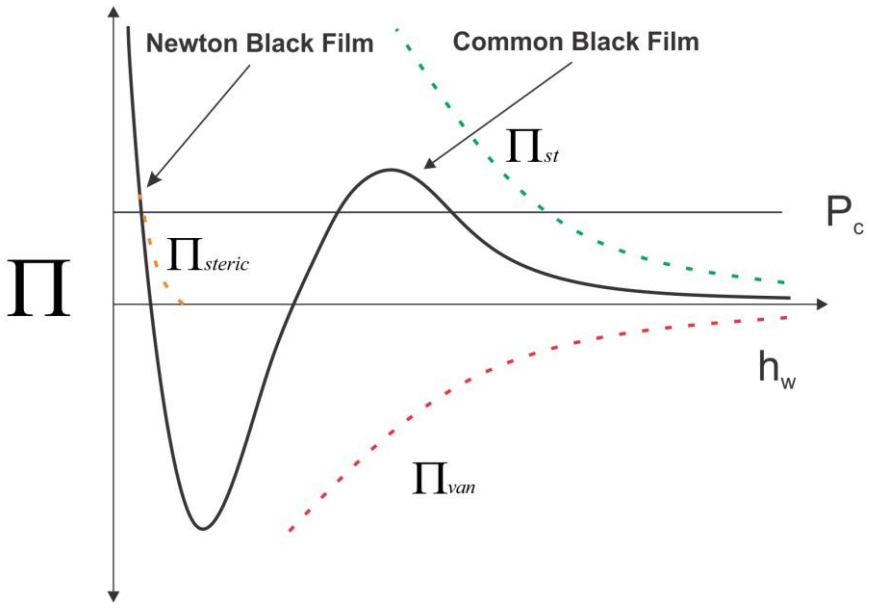

Figure 0.3. Disjoining pressure isotherm for foam films including contributions from $\boldsymbol{\Pi_{el}}$, $\boldsymbol{\Pi_{van}}$, and $\boldsymbol{\Pi_{steric}}$ (reproduced from Vance (1999).

There are two equilibrium states of foam films that are defined by thermodynamic conditions. Common black films (CBF, 8–100 nm thick) are usually formed when the salt concentration in the film-forming solution is low and the electrostatic double layer repulsion between the

films is strong. The film thickness decreases as the salt concentration in the film-forming solution increases, resulting in a reduction of the double layer repulsion. Very thin Newton black films (NBF, 5 nm thick) are formed at that point, which are stabilised by steric repulsion. The strong steric repulsion can oppose high ionic strength but are strongly influenced by the different polarisabilities of the ions (Karakashev and Manev, 2001).

2.2 Foam stability enhancement

There are two ways to reduce ripening: 1) decrease the solubility of the gas so it diffuses more slowly, and 2) increase the resistance to diffusion across the film wall. The first method is used depending on the type of gas. In the petroleum industry, N_2 and CO_2 are most commonly used for foam stimulation (Harris, 1992; Harris and Heath, 1996; Watkins et al., 1983). Given that nitrogen has a relatively lower solubility in water than CO_2, the rate of inter-bubble gas diffusion is lower, and this results in a more stable foam. The second method can be achieved by adding polyelectrolytes or worm-like micelles (shown in **Figure 0.4**). The enhancement of bulk viscosity is due to the high polymer molecular weight or entanglement of WLMs. Those rheology improvements can reduce the film permeability, which retard gas diffusion, and therefore, improve foam stability.

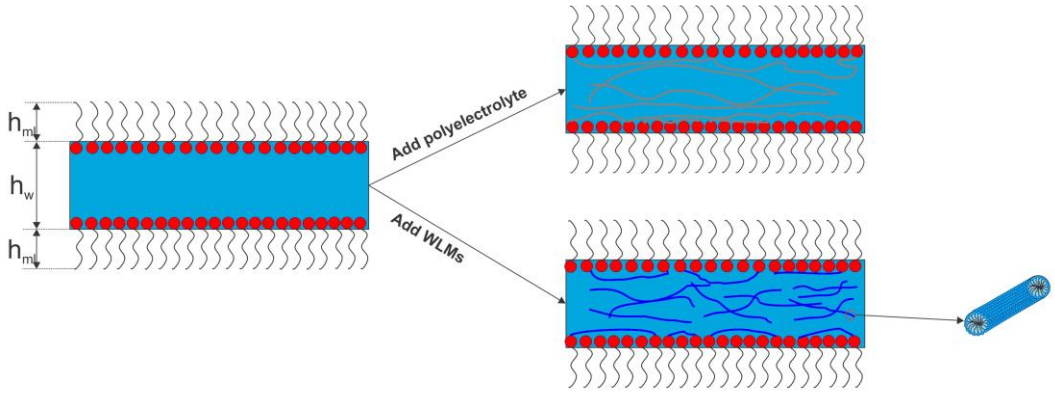

Figure 0.4. A single foam film containing liquid with thickness, $\boldsymbol{h_w}$, between two adsorbed monolayers of surfactant with thickness, $\boldsymbol{h_{ml}}$. Addition of polyelectrolytes or WLMs enhances the bulk and surface rheology, causing more difficulty in gas diffusion.

In recent years, the development of nanotechnology has provided an alternative to use nanoparticles as foam stabilisers (Carl et al., 2015; Carn et al., 2009; Lv et al., 2017; Zhu et al., 2015). Many studies (Alargova et al., 2004; Binks and Horozov, 2005; Dickinson et al., 2004; Fujii et al., 2006; Urs T. Gonzenbach et al., 2006) demonstrated that nanoparticle-stabilised foams can survive for weeks or more, even under extremely harsh conditions. The role of nanoparticles in foam stability is that the nanoparticles are adsorbed at the interface, and can inhibit bubble coalescence by creating a steric barrier that prevents the advancement of the interfaces (Bournival et al., 2015; Stocco et al., 2011). **Figure 0.5** shows a schematic of the foam interface between bubbles with and without nanoparticles. The attachment energy of a nanoparticle to the gas-water interface is usually irreversible and its adsorption energy determines the foam stability (Binks et al., 2008b). In addition, experimental results (Binks et

al., 2008b; Hunter et al., 2008; Maestro et al., 2014b; Sun et al., 2015b; Zargartalebi et al., 2014) reported that SiO_2 nanoparticles have a synergistic effect on foam stability with proper surfactant concentration, which influences the contact angle of nanoparticles on the interface. In the absence of a surfactant, several researchers (Carl et al., 2015; Carn et al., 2009; Lv et al., 2017; Zhu et al., 2015) introduced hydrophilic or partially hydrophobic nanoparticle-surfactant mixtures for developing stable foam.

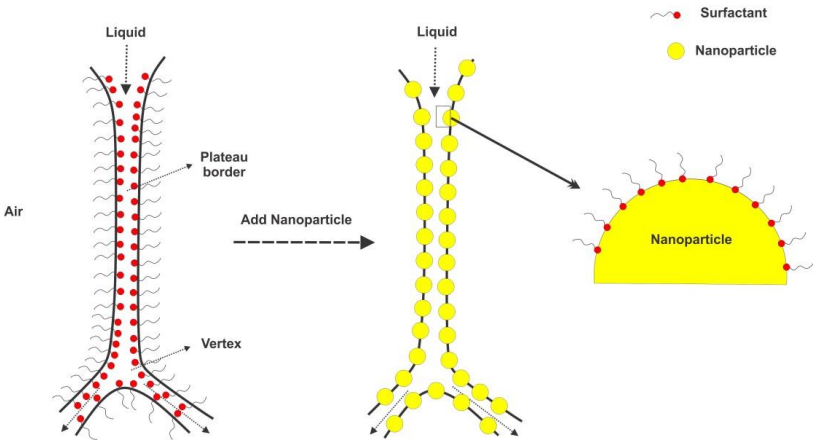

Figure 0.5. Schematic of a foam structure filled by surfactant molecules (left) and nanoparticles (right)

2.3 Foam rheology versus foam stability

Foam rheology is an important property for fracture-treatment design. It influences the fracture geometry, proppant transport, fluid loss to the matrix, etc. It is affected by foam quality, texture, viscosity of the base aqueous phase, pressure, and temperature. **Figure 0.6** shows an example on how foam viscosity typically varies as a function of foam quality. When foam is relatively wet (i.e. low foam quality), the dispersed bubbles do not interact significantly, because the majority of the liquid content still exists in the plateau border and both film and gas diffusion rates are still low. However, as free drainage occurs, the friction between individual bubbles increases the foam viscosity non-linearly with respect to time (Gu and Mohanty, 2015; Safouane et al., 2006). When foams become relatively dry (i.e. high foam quality), the bubbles interact significantly, which is a condition where bubbles cannot maintain stability, leading to a sharp reduction in foam viscosity. Moreover, as the foam quality increases, the proppant carrying capacity increases as well and the maximum will be reached at a critical time. This proppant capacity is shown in **Figure 0.6** by the number of grey circles.

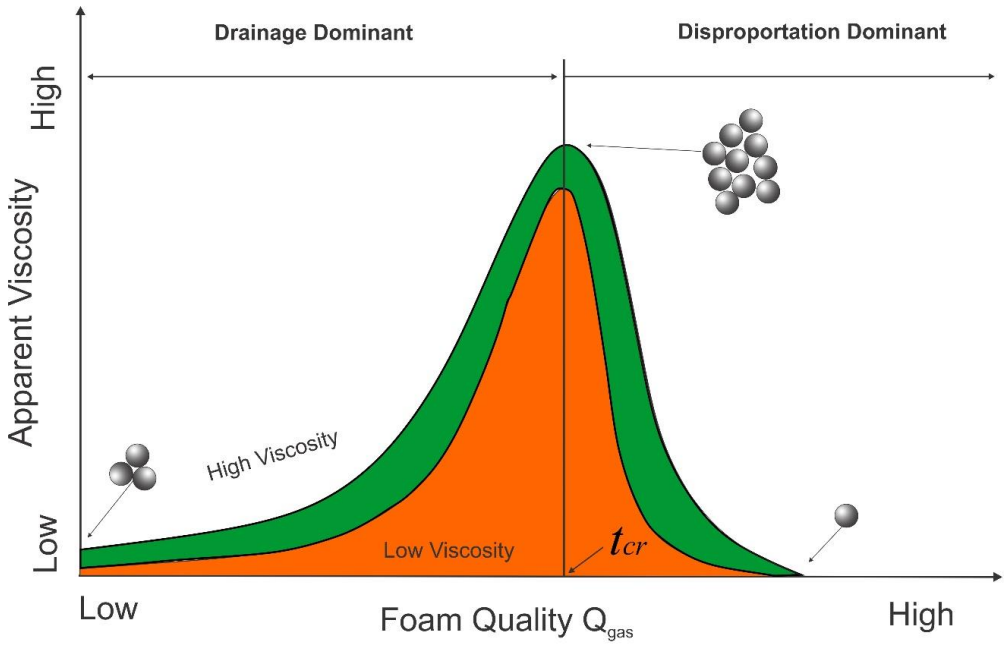

Figure 0.6. Schematic of apparent foam viscosity as a function of foam quality

In addition, shear rate, gelling concentration, and temperature also affect the rheology of the foam system. These relationships have been investigated by several research studies (Gu and Mohanty, 2015; Harris and Health, 1996; Harris and Reidenbach, 1987; Khade and Shah, 2004; Sun et al., 2014) which illustrated in **Figure 0.7**. In **Figure 0.7(a),** apparent viscosity decreases with increasing shear rate for any type of gelling agent. In **Figure 0.7(b)**, the apparent viscosity increases with increasing gelling concentration and the viscosity decreases with increasing temperature for a given shear rate. This is because of the enhancement of bulk viscosity owing to the high polymer molecular weight. On the other hand, increasing the temperature destabilises the foam by thinning the liquid phase and the foam film thickness.

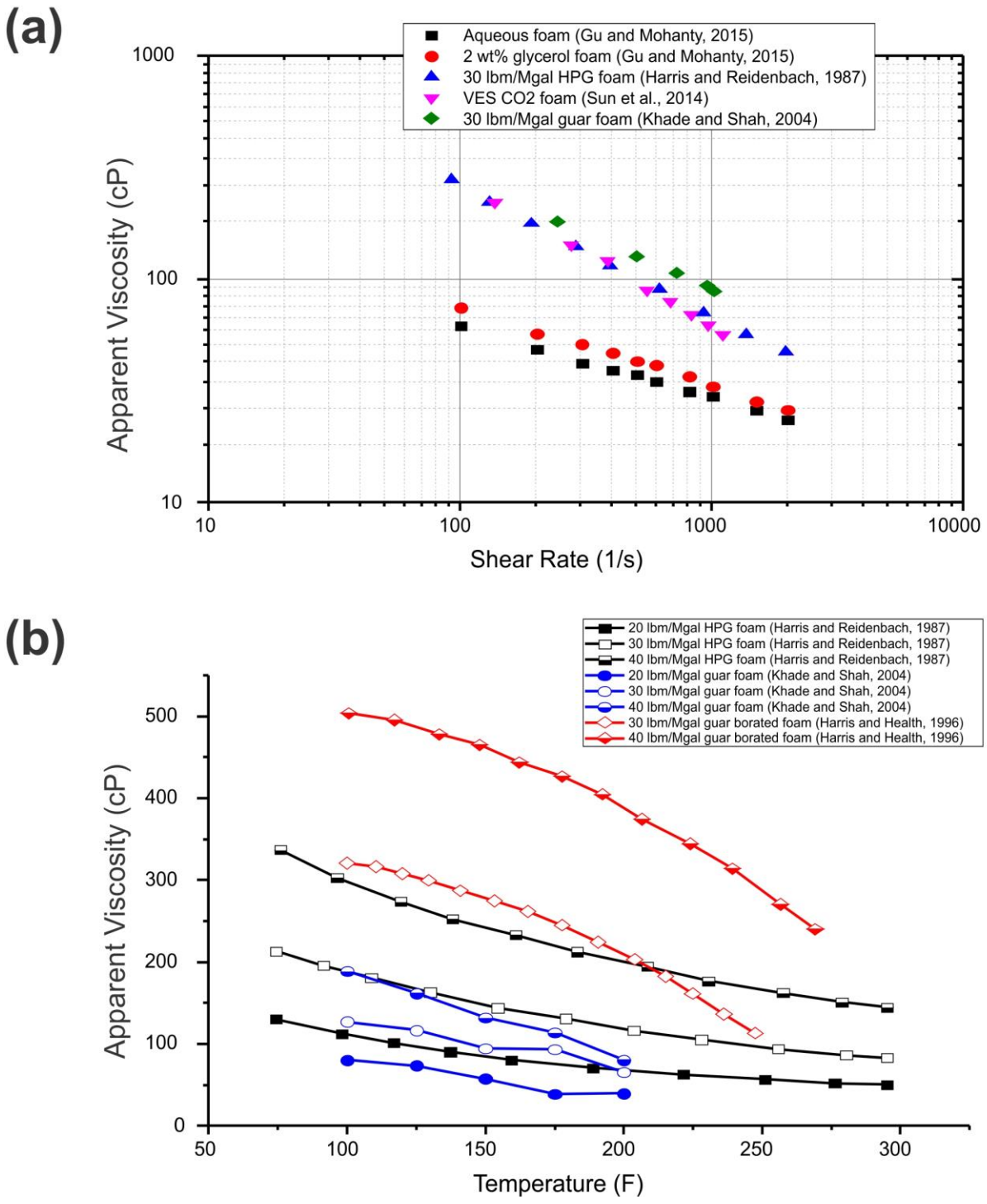

Figure 0.7. Foam viscosity depends on a number of variables: (a) shear rate and gelling type, (b) temperature and gelling concentration.

Currently, there is no universal correlation available for the presentation of rheology data for foamed fracturing fluids. Those developed correlations (Gu and Mohanty, 2015; Harris and Reidenbach, 1987; Khade and Shah, 2004; Sani et al., 2001; Sun et al., 2014) estimate foam rheology under typical field conditions (shear rate, temperature, and pressure) during fracturing are summarised in **Table 0.1**. It is also shown that one of most important parameters in foam

quality is the percentage of volume occupied by the internal gas phase, which is controlled by the foam drainage.

Table 0.1. Correlations of rheological parameters

Equations	Conditions	Paper
<u>For Γ less than 60%:</u> ➢ $n_F = 1.54 - 1.64\,\Gamma^2$ ➢ $k_F = 10^{(5.89\,\Gamma^2+0.43\,\Gamma-4)}$ <u>For Γ higher than 60%:</u> ➢ $n_{F1} = n_F + (0.21 - 0.89\Gamma)[\log\left(\frac{P}{1000}\right)]$ ➢ $k_{F1} = k_F + (8.6 \times 10^{-11} e^{21*\Gamma})[P - 1000]$	<u>Aqueous N_2 foam</u> ● $T < 150$°F ● $p < 2000\ psi$ ● Power law model	Gu and Mohanty (2015)
For 0–80 lbm/Mgal HPG ➢ $n_t = n_{75} e^{(0.0028-0.0019\Gamma)(T-75)}$ ➢ $C_2 = e^{-(3.1+3n_{75})}$ ➢ $k_t = k_{75} e^{(C_2\Gamma-0.018)(T-75)}$	<u>Uncrosslinked (gelled) N_2 foam</u> ● 75°F $< T <$ 300°F ● Power law model	Harris and Reidenbach (1987)
For 20 lbm/Mgal guar: ➢ $\frac{n_F}{n_L} = 1 - 2.1006\Gamma^{7.3003}$ ➢ $\frac{k_F}{k_L} = e^{(-1.9913\Gamma+8.9722\Gamma^2)}$ For 30 lbm/Mgal guar: ➢ $\frac{n_F}{n_L} = 1 - 0.1535\Gamma^{6.5152}$ ➢ $\frac{k_F}{k_L} = e^{(-2.3761\Gamma+8.883\Gamma^2)}$ For 40 lbm/Mgal guar: ➢ $\frac{n_F}{n_L} = 1 - 0.6633\Gamma^{5.168}$ ➢ $\frac{k_F}{k_L} = e^{(-0.4891\Gamma+5.6203\Gamma^2)}$	<u>Uncrosslinked (gelled) N_2 foam</u> ● $60\% < \Gamma < 80\%$ ● 100°F $< T <$ 200°F ● Power law model	Khade and Shah (2004)
For 20 lbm/Mgal xanthan: ➢ $\frac{k_F}{k_L} = e^{(1.556\Gamma+2.813\Gamma^2)}$ ➢ $\tau_o = 0.013e^{3.5\Gamma}$ For 30 lbm/Mgal xanthan: ➢ $\frac{k_F}{k_L} = e^{(0.754\Gamma+3.237\Gamma^2)}$ ➢ $\tau_o = 0.038e^{2.5\Gamma}$ For 40 lbm/Mgal xanthan: ➢ $\frac{k_F}{k_L} = e^{(-0.055\Gamma+4.563\Gamma^2)}$ ➢ $\tau_o = 0.073e^{2\Gamma}$	<u>Xanthan-gelled N_2 foam</u> ● $60\% < \Gamma < 80\%$ ● 100°F $< T <$ 200°F ● Herschel-Buckley model	Sani et al. (2001)
➢ $n_F = \frac{0.341\exp[(0.349-0.5001\Gamma)\times 0.108\times(\mathrm{T}-10)]}{\exp[\left(\left(\frac{\mathrm{P}}{25}\right)-1\right)^{9.36}]}$ ➢ $k_F = 7.94\exp[(0.455\Gamma - 0.248) \times (10 - \mathrm{T})] \times \exp[25.44\Gamma + 0.89\Gamma^2] \times \exp[\left(\left(\frac{\mathrm{P}}{25}\right) - 1\right)^{9.36}]$	<u>VES-CO_2 foam</u> ● $50\% < \Gamma < 75\%$ ● 104°F $< T <$ 176°F ● $1450 < p < 4350\ psi$ ● Power law model	Sun et al. (2014)

2.4 Proppant sedimentation

Proppant or particle sedimentation in hydraulic fracturing is of great interest from both fundamental and practical points of view. In a homogeneous Newtonian fluid, the sedimentation of particles has long been studied using Stokes' law (Stokes, 1851), where the terminal velocity of a particle depends on the viscosity of the liquid, density difference between particle and liquid, and square of particle radius. On the other hand, the sedimentation process has not been well known in non-Newtonian fluids such as foam, which is an excellent carrying medium to suspend particles due to its local structure (Jing et al., 2016; Wyn et al., 2008). Particle sedimentation can be explained by the amount of net force on a particle during drainage process. Generally, there are three different forces, namely gravity (g), pressure force (F_p), and pulling force of film network (F_n), which act on each particle during sedimentation as illustrated in **Figure 0.8**.

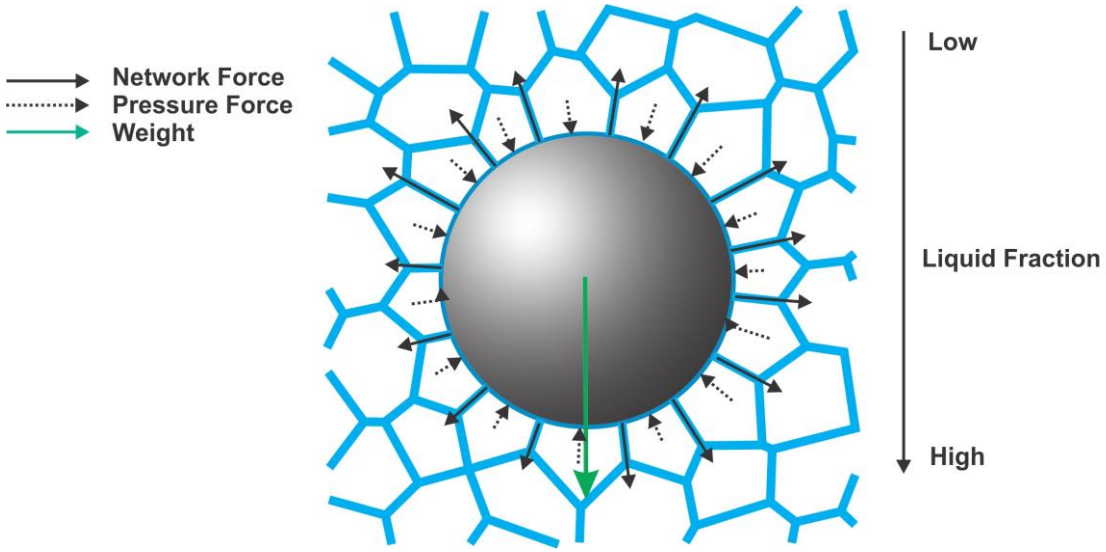

Figure 0.8. Different forces acting on films and bubbles in a particle: gravity (green arrow), network force (black solid arrow), and pressure force (black dashed arrow).

Several studies on sedimentation were performed by Cox and co-workers (Cox et al., 2006; Davies and Cox, 2009; Wyn et al., 2008) using simulations of drag force on disks moving relative to a 2D foam. The sedimentation depends mostly on drag force components due to local elasticity and plasticity in the structure. As foam is a naturally unstable medium, the structure is always changing; the liquid fraction effect (Jing et al., 2016; Raufaste et al., 2007) has been used to characterise the forces acting on particles.

2.5 Summary

In this chapter, the theory of gravity drainage and disproportionation as two main mechanisms in foam stability are first discussed. Then, foam stability analysis by disjoining pressure and DLVO theory is explained. Furthermore, the literatures on current research of foam stability enhancement are reviewed. The relationship between foam rheology and foam stability are discussed in a separate subsection. Finally, the theory and literature on sedimentation of proppant in foam are reviewed.

Chapter 3: Foam drainage on proppant sedimentation in the presence of nanoparticles

3.1 Introduction

This chapter presents an experimental analysis on the relationship between foam drainage and proppant suspension for different foam designs in the presence of nanoparticles. The chapter begins by describing the foam drainage experiment under 25℃. The effect of free drainage on the rheology of four different foams without proppant was investigated by generating the liquid fraction profiles. Then, a proppant sedimentation experiment was performed and the settling relationship with foam stability was investigated. This chapter is a modified and adjusted version of the manuscript, 'Fei, Y., Zhu, J., Xu, B., Li, X., Gonzalez, M., & Haghighi, M., (2017). Free drainage of foam mixed with coarse particles in the presence of nanoparticles (manuscript submitted to SPE Hydraulic Fracturing Technology conference)'.

3.2 Materials

Sodium dodecyl sulfate (SDS) and sodium dodecyl benzene sulfonate (SDBS) were provided as solid powder by Chengdu Kelong Co., Ltd, China (95 wt% active content). Carboxymethyl hydroxypropyl guar (CMHPG) was provided by Halliburton China Pty Ltd. Nano-fumed silica (with an average size of 40 nm) powder was purchased from China Aladdin Chemical Co., Ltd. Sodium chloride (NaCl) and 20/40 mesh size carbon proppant were provided by the State Key Laboratory of Oil and Gas Geology and Exploitation, South West Petroleum University, China. All of these chemicals were used without further purification. Deionised water was used in all experiments. All working solutions were prepared immediately before each experiment at 25 ± 1 ℃ temperature.

3.3 Sample preparation

Foam A. Foam sample A was prepared using a mixture of anionic surfactant of 0.05 wt% SDS and 0.05 wt% SDBS. The surfactants were added into 100 mL of deionised water and a glass rod was gently rotated to dissolve the surfactant powder to avoid bubble formation. The viscosity was measured using a FANN35 viscometer.

Foam B. Foam sample B was prepared by mixing 0.8 wt% hydrophilic nano-fumed silica with sample A. Nanoparticle size measurements were conducted on Mastersizer 2000 from Malvern Instrument (UK) using laser diffraction. The intensity of light scattered as a laser beam passes through a dispersed particulate sample was measured. Then, the light intensity was analysed to calculate the size of particles that created the scattering pattern. The aggregate particle size distribution of the silica particles is shown in **Figure 0.1** with an average size of 11 μm. Nanoparticles were added after the surfactants were dissolved into the solution. Once all the nanoparticles were completely mixed, high-speed homogenisation of the chemical mixture at 8,000 rpm for 1 min with entrained air was performed to produce fine foam. The high speed was used to generate very small bubbles to minimise film rupture and coarsening impact on the free drainage stage. After complete mixing, the foam was immediately transferred to the same 500 ml measurable cylinder as foam A and free drainage data were recorded for the foam without coarse particles. Then, the sedimentation experiment was repeated with foam B mixed with 1 wt% of coarse particle concentration similar to foam A.

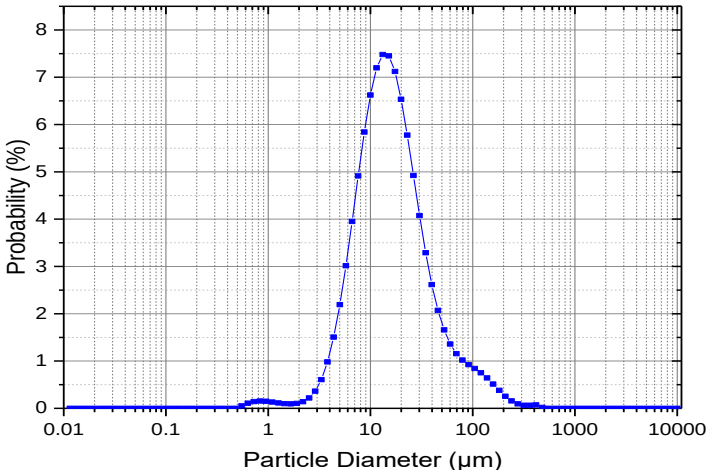

Figure 0.1. Particle diameter distribution of nanoparticles

Foam C. In order to investigate the effects of viscosity on gravity drainage in foam mixed with coarse particles, foam sample C was prepared by adding 0.36 wt% CMHPG to foam sample A.

Foam D. To study the effect of ion strength on foam drainage and settling of coarse particles, foam sample D was prepared by adding 7% NaCl to foam sample A.

3.4 Experimental procedure

After preparing each sample, the foam was immediately transferred to a 500 ml measurable cylinder and the starting height with a foam column having a uniform vertical liquid fraction was recorded. During the experiments, the total height of foam H_t, height of drained liquid L_t, and time t were recorded. **Figure 0.2** shows a schematic of the recorded parameters versus time during free drainage. After the experiment of the base case was completed, the same foam was mixed with 1 wt% carbon particle concentration with a 20/40 mesh size (equivalent diameter $D_p = 700$ μm) and density $\rho_p = 2000$ kg/m^3. We used a 500 ml cylinder to ensure that the cylinder diameter was at least 25 times larger than the diameter of the particles to minimise the wall effect on the settling velocity. The process time was recorded to calculate the sedimentation velocity. First, free drainage data were recorded for the foam without particles followed by the sedimentation experiment when the foam was mixed with coarse particles.

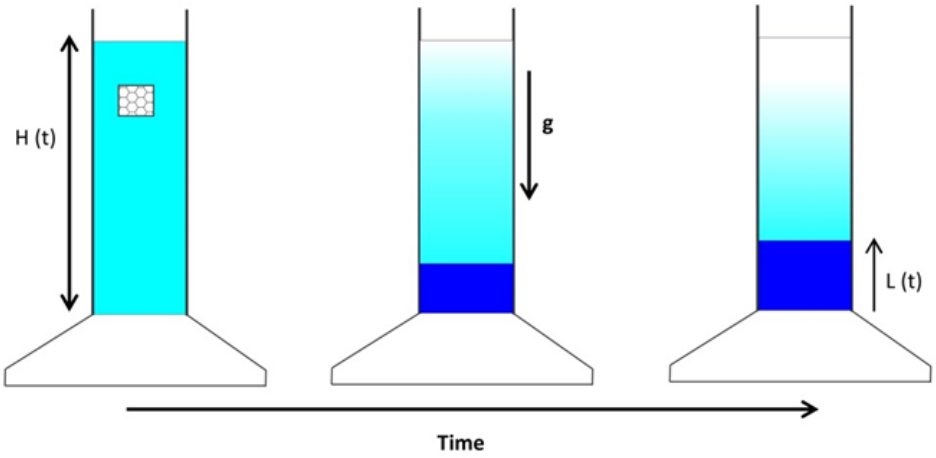

Figure 0.2. Schematic of free drainage experiment

3.5 Results and discussion

3.5.1 Free drainage

The results of foam height H_t versus time are shown in **Figure 0.3**Figure 0.3. As can be observed**,** foam A and foam B show a foam volume of approximately 450 mL corresponding to a foamability of 80% gas quality. While the foam volume of foam A starts to decrease after 2000 s (40 min), foam B remains stable for the entire duration of the 2 h test (7200 s). Therefore, the effect of nanoparticles in our tests on foam stability improvement was confirmed. Foam C and foam D demonstrate less foamability than A; however, they were stable for the entire 2 hours period.

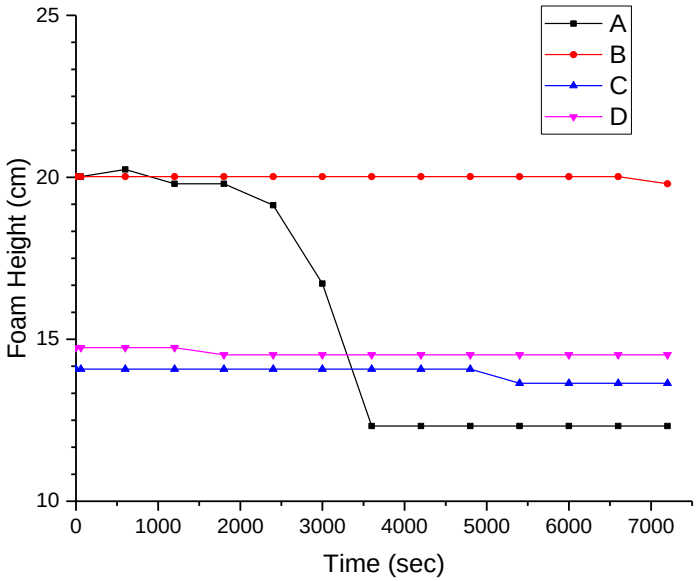

Figure 0.3. Foam height vs. time for four different samples

As a further stability analysis, we examined the trend of drainage profiles in our samples. A drainage profile is produced from the recorded drained liquid height (L) versus time. **Figure 0.4** displays the normalised drained liquid volume ($V_{(t)}$ / $V_{(l0)}$) versus time. $V_{(t)}$ is the foam volume that has been drained out of the foam, and $V_{(l0)}$ is the total volume of liquid in the foam at t = 0. In each sample, the drainage half-time τ was recorded when the drainage front reaches the bottom of the foam. The drainage half-time τ for each sample is also shown in the figure. We have calculated the drainage half-time from a theoretical formula and obtained a good agreement between the experimental and theoretical values for foam samples A to C. However, for high salinity foam, the results of the theoretical formula (see **Eqs**. **24** to 2**6** in **Appendix A**) are not consistent with those of the experiments. From the drainage profile, a critical time τ_1 is identified when the curve reaches an asymptotic value. Thus, two different drainage regimes of $t < \tau_1$ and $t > \tau_1$are identified for foams A, C, and D. We name the region for $t < \tau_1$ as free-drainage-dominated regime, and for $t > \tau_1$, the relaxation regime. By comparing the curves for different foam samples, it is observed that in the free-drainage-dominated regime, the drainage rate is strongly dependent on the liquid viscosity. For example, in **Figure 0.4(c)**, foam with high viscosity will result in a low drainage rate. Therefore, the liquid content will decrease more slowly and the remaining liquid in the foam acts as an 'obstacle', which delays the coarsening and coalescence process. However, in the relaxation regime, we reach a critical rate in which the drainage rate is not changing anymore. Because the foam is much drier than that in the free-drainage-dominated regime, we concluded that the radius of curvature of Plateau borders is smaller. Therefore, according to Young–Laplace equation, the capillary pressure is higher, which is balanced by gravity and the disjoining pressure. In this regime, bubble coarsening and rupture become more dominant.

Although, the liquid viscosity is a criterion for defining the two different regimes, a third regime can also be identified for the case of a nanoparticle foam in which two critical times of τ_1 and τ_2 are identified as shown in **Figure 0.4(b)**. This period when ($\tau_1 < t < \tau_2$) is called the transition period. As can be observed in foam B, the presence of nanoparticles can reduce the fast drainage rate during the gravity drainage-dominated regime. After that period, a transition regime can be observed in which the starting time of the relaxation regime is delayed. Therefore, more stable foam is produced. This mechanism can be explained by the blocking of Plateau borders by nanoparticles. When the Plateau border is reduced, the local geometry of the liquid drainage channel will be reduced as well. We observed that the transition period is more pronounced when the SiO_2 nanoparticle concentration is more than 2%. This mechanism was also discussed by Carn et al. (2009) and is called traffic jamming.

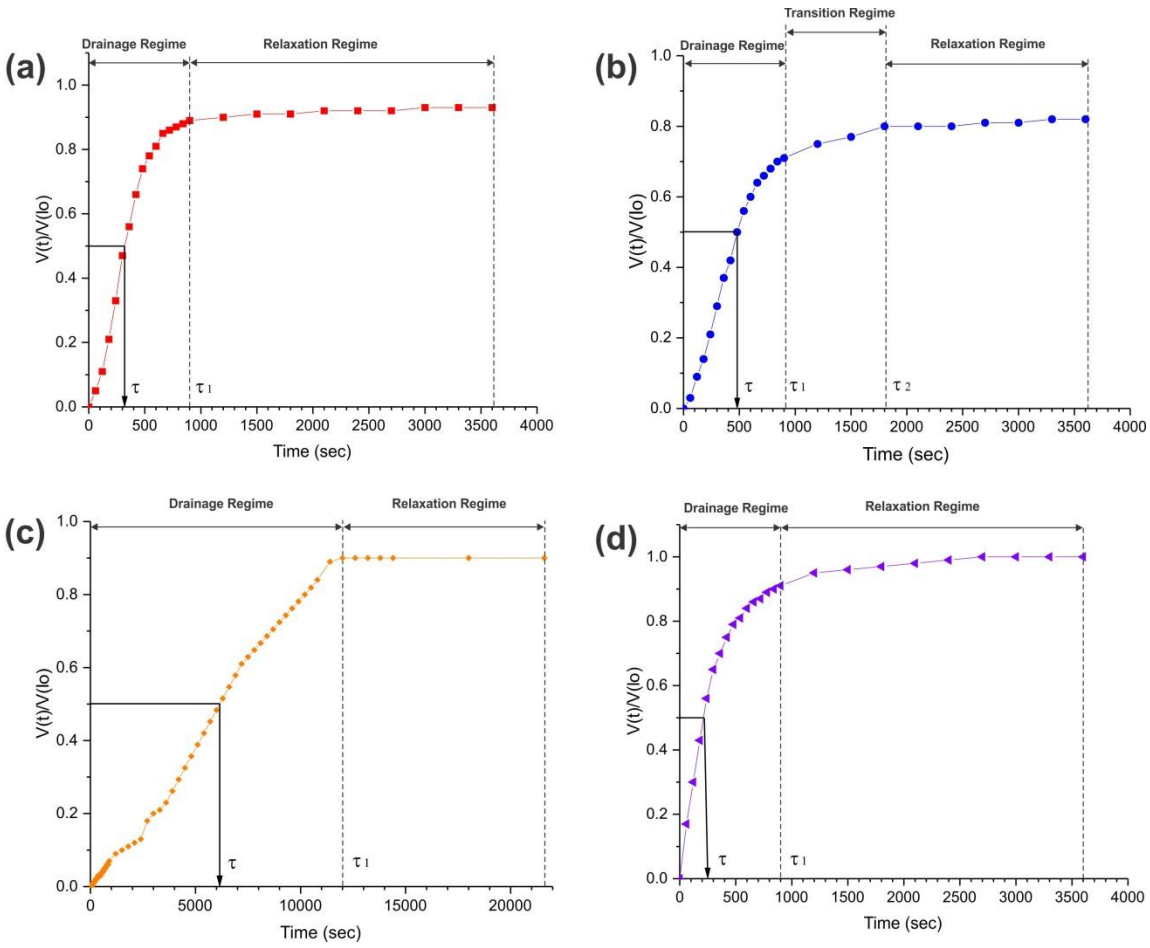

Figure 0.4. Free drainage curves for liquid foams: (a) foam A, (b) foam B, (c) foam C, and (d) foam D.

3.5.2 Liquid fraction profile

The liquid fraction profile was developed and displayed in **Figure 0.5** for all four samples. The main input parameters are the initial foam height, solution viscosity, liquid density, and initial liquid fraction (**Table 0.1**). The initial liquid fraction was calculated based on the ratio of the liquid volume to the initial foam volume. These profiles show the distribution of the liquid content in the foam from the top of the column, which is changing towards the bottom and also changing with time during the gravity drainage experiments. At $\boldsymbol{t = 0}$, the liquid fraction is uniform and constant ($\boldsymbol{\varepsilon_l^A}$ *and* $\boldsymbol{\varepsilon_l^B = 0.2}$, $\boldsymbol{\varepsilon_l^C = 0.31}$, *and* $\boldsymbol{\varepsilon_l^D = 0.3}$). The profile is produced from $t = 0$ to $t = \tau_1$ because after the time τ_1, the drainage rate is almost negligible. As can be observed in **Figure 0.5,** different foams show different patterns in their profiles. The profile in all samples shows that the upper section is always lower in liquid content, or relatively drier than the lower part of the container. This indicates that the overall uplift pulling forces exerted on the foam decreases from top to bottom. In addition to this general trend, we observed that the high viscosity foam C (CMHPG) exhibits a more homogeneous profile in comparison to the other 3 samples. In this study, we calculated the liquid fraction profile to quantify the effect of drainage. The following four steps comprise the calculation procedure: 1) defining the flow-drainage regime, 2) calculating the drainage velocity, 3) determining the theoretical drainage

half-time, and 4) calibrating the drainage half-time between theoretical and experimental values. The details of the calculations are given in **Appendix A**.

Table 0.1. Main input parameters to calculate drainage velocity

Parameter	Foam A	Foam B	Foam C	Foam D
Initial foam height, **H** (**cm**)	20.0	19.8	14.1	14.7
Average diameter of bubble, **D** (**μm**)	325	294	202	270
Solution viscosity, $\boldsymbol{\eta}$ ($\mathbf{g/(cm \cdot s)}$)	0.03	0.04	0.26	0.035
Density, $\boldsymbol{\rho}$ (**g/cc**)	1	1.02	1.003	1.15
Initial liquid fraction, $\boldsymbol{\varepsilon_o}$ (**dimensionless**)	0.2	0.2	0.31	0.3
Length of Plateau border, **L** (**μm**)	112	110	81	115
Calculated drainage velocity, $\boldsymbol{V_d}$ ($\mathbf{cm/s}$)	0.058	0.043	0.003	0.069
Mobility, **M** (**dimensionless**)	0.37	0.48	2.87	0.47
Theoretical drainage half-time, $\boldsymbol{\tau}$ (**s**)	301	477	5983	217
Experimental drainage half-time, $\boldsymbol{\tau}$ (**s**)	300	495	6010	250

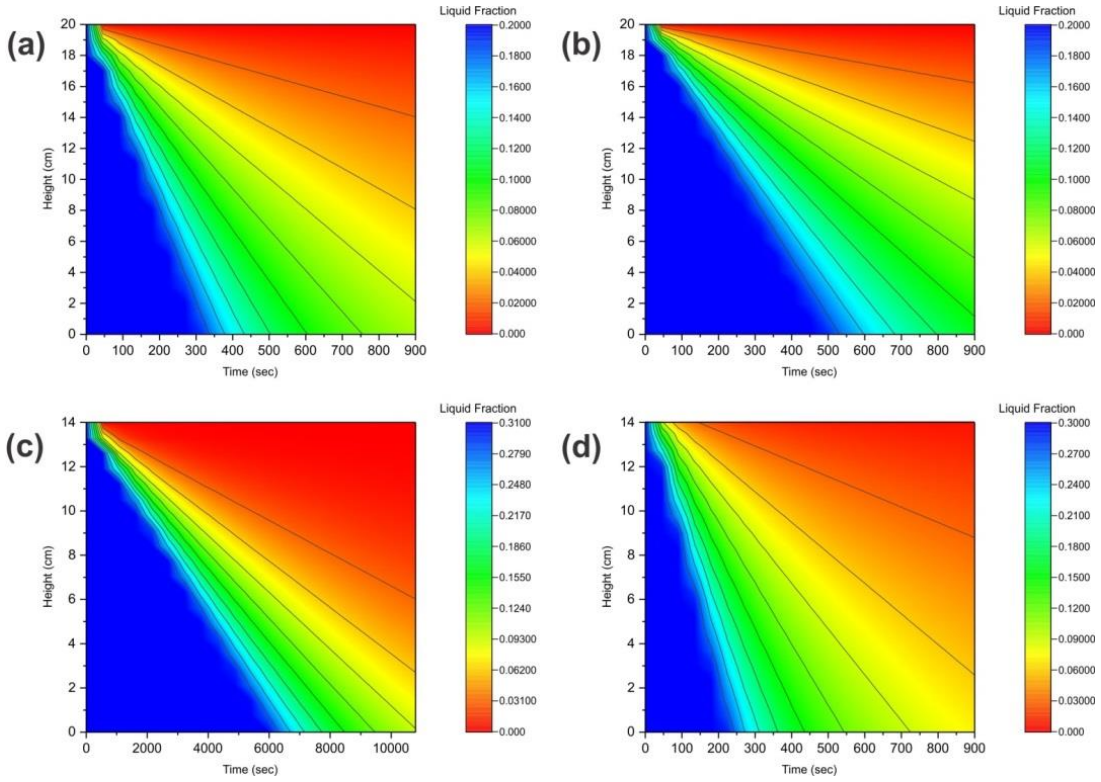

Figure 0.5. Vertical profiles of liquid fraction as a function of time and height for foam. The scale of the time ($\boldsymbol{t = \tau_1}$) is based on the drainage regime. The labels (a)–(d) refer to foams A–D.

3.5.3 Proppant sedimentation

Figure 0.6 shows the results of free drainage experiments for foams A–D mixed with 1 wt% carbon particles. The sedimentation versus time is measured in a 500 ml graduated glass cylinder during the free drainage regime. As the foam volume decreases, the particle starts to move downwards and accumulates at the bottom of the foam column. The increment of total particle concentration on the existing foam causes the acceleration of particle settling. Because foams A, B, and D have the same drainage time ($\boldsymbol{\tau_1}$ = 15 min), four snapshots of the sedimentation at 1, 5, 10, and 15 min are shown for those samples. However, the drainage time for the highly viscous foam C is 90 min and the sedimentation is shown in 1, 30, 60, and 90 min. By comparing the sedimentation in foams A and B, the settlement was found to be low for both cases and no significant difference was observed. However, foam D with high ionic strength exhibited a high sedimentation in the early times but was reduced at the end of the drainage-dominated regime.

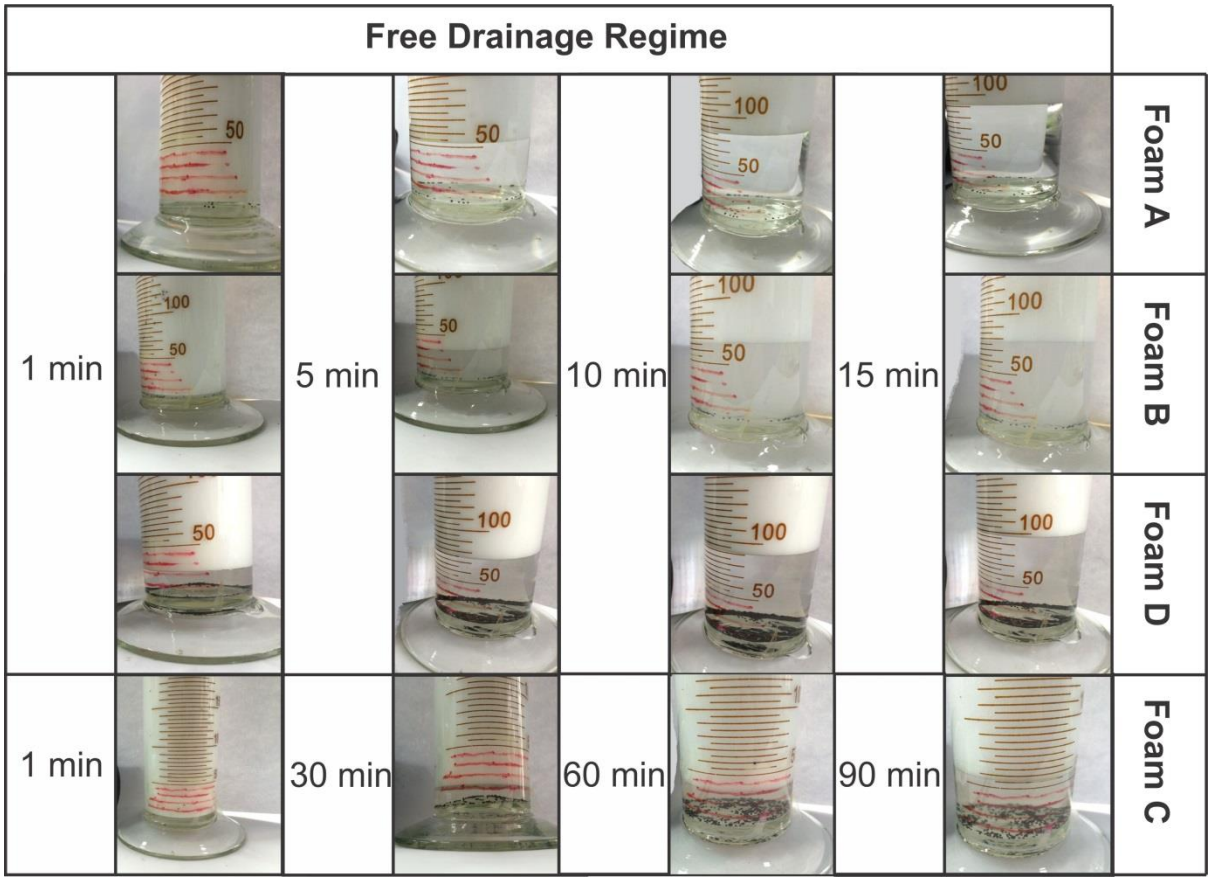

Figure 0.6. Different snapshots of particle sedimentation experiments for foams A–D during foam drainage regime

For foams A and B, we believe that the total pulling force at the initial liquid fraction $\varepsilon_o^{A\ or\ B} = 0.2$ is smaller than the gravitational force. Therefore, the particle is moving downwards. The pulling force F_z could be increased by fast liquid drainage, which decelerates the proppant sedimentation or makes the suspension more stable. However, after time τ_1, the proppant sedimentation tends to be more dependent on coarsening and coalescence, and thus, the total pulling force is reduced. Proppants in foam D exhibit an unstable scenario, where high amount of particles settle in the early stages of the drainage regime. This could be explained by the high ionic strength (7 wt% of NaCl) that contributes to a relatively lower electrostatic repulsion. This phenomenon accelerates the coarsening rate and therefore decreases the total pulling force. For foam C, which has high viscosity and high initial liquid content $\varepsilon_o^C = 0.31$, it requires a long draining time to reach the relaxation regime. This means that particles with weights greater than the initial total pulling force are moving downwards, reducing the liquid drainage rate. This is an indication of gradual increase of pulling force. This requires a long drainage time to reach the force balance, resulting in more particles settling during the drainage regime. However, in foam C, it is unclear whether the coarsening effect interferes during the free drainage stage. At this point, the particle settling mechanism contributes to the liquid fraction and thus to the drainage.

Based on our sedimentation results, we have developed an area chart (**Figure 0.7**) to visualise the effect of foam quality on apparent viscosity and total pulling force at two different regimes

during sedimentation. The number of particles in different areas in the figure indicates the suspension capacity of the proppant. As can be observed, in the free drainage regime, the suspension capacity generally increases with high foam quality and the maximum is reached when t =τ_1. Therefore, in order to reach the optimum foam quality, it is required to reach the drainage time τ_1. As high viscosity foam has a low drainage rate, or low slope, it requires a long time to reach that maximum gas quality. For example, the increase of polymer concentration will suppress the foam volume formation in highly viscous foam, requiring a long time to reach the optimum foam quality owing to the drainage rate and the high initial liquid fraction. Therefore, regardless of foam stability, we should have not only a large proppant carrying capacity with high viscosity, but also fast drainage to reach the maximum foam quality. Because it is believed that after the free drainage period the bubble diffusion becomes more dominant and results in bubble size growth and foam volume reduction, after the maximum point in the graph, the viscosities and total pulling force of dry foams start to decrease in both low and high viscosity foam cases.

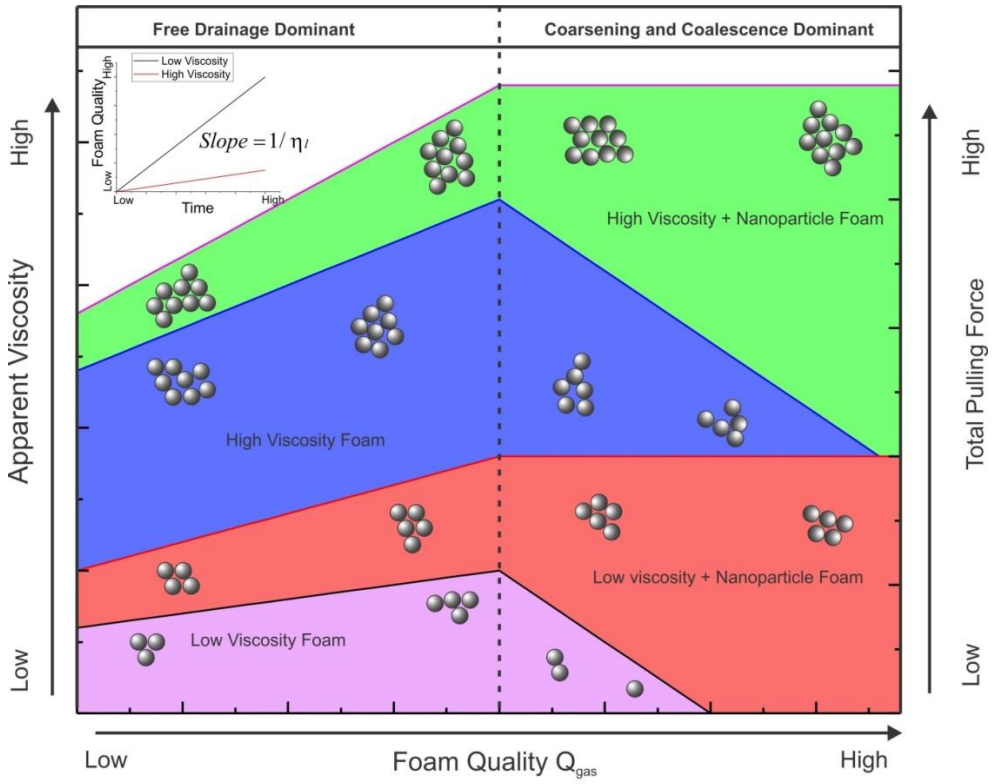

Figure 0.7. Area chart for foam quality vs. apparent viscosity and total pulling force at two different regimes during sedimentation

Furthermore, it was found that the addition of nanoparticles will result in slightly more proppants carried in the drainage regime as it is enhancing the viscosity. In addition, it was previously found that a rough bubble surface (Lv et al., 2015) and the presence of nanocomposite aggregates with micrometre size will contribute to creating a transition regime (**Figure 0.4b),** which will reduce the coarsening mechanism to some extent. We have concluded that nanoparticles, will maintain the dry foam stability when reaching the coarsening and coalescence region. The role of nanoparticles has previously been discussed in many

research studies (Binks et al., 2008a; Maestro et al., 2014a; Sun et al., 2015a; Sun et al., 2015b), which confirmed that nanoparticles can be adsorbed on the foam film in the presence of a suitable surfactant concentration (to increase the film rigidity and therefore to prevent bubble diffusion). This shows the possibility of solid silica adsorption on the foam film to prevent foam rupture. Therefore, for the enhancement of particle suspension, it is required to develop a foam with a suitable viscosity and sufficient total pulling force to carry the designed amount of proppants with a given initial foam quality. The author found that nanoparticles make the foam more stable and a high foam quality yields the largest particle carrying capacity.

3.6 Summary

In summary, the main finding as explained in this chapter is that foam drainage can help in suspending more proppant. However, the major question is how long can the proppant be kept in suspension, which is related to maintaining stability. When foam reaches a high gas quality, the structure becomes more 'fragile' and easily breaks. In the presence of high ionic strength, the foam structure can be damaged even more quickly and the particle suspension becomes worse. In addition, it is generally easy to suspend particles in highly viscous foam owing to the high total pulling force and long free drainage regime. Nanoparticle-stabilised foam has been found to create a transition regime that delays the foam coarsening and coalescence. Therefore, in order to maintain a high proppant suspension capacity, nanoparticles with polymers or other viscosifers in the mixture and with surfactants are proposed as potentially good additives to foam fracturing fluid under high temperature conditions.

Chapter 4: Investigation of nanotechnology on worm-like micelles for high temperature foam stimulation

Fei, Y., Zhu, J., Xu, B., Li, X., Gonzalez, M., & Haghighi, M. (2017). Experimental investigation of nanotechnology on worm-like micelles for high-temperature foam stimulation. Journal of Industrial and Engineering Chemistry. doi:http://dx.doi.org/10.1016/j.jiec.2017.02.015

Journal of Industrial and Engineering Chemistry 50 (2017) 190–198

Contents lists available at ScienceDirect

Journal of Industrial and Engineering Chemistry

journal homepage: www.elsevier.com/locate/jiec

Experimental investigation of nanotechnology on worm-like micelles for high-temperature foam stimulation

Yang Fei[a,*], Jingyi Zhu[b], Binyu Xu[b], Xiaogang Li[b], Mary Gonzalez[a], Manouchehr Haghighi[a]

[a] Australian School of Petroleum, University of Adelaide, South Australia, Australia
[b] State Key Laboratory of Oil and Gas Geology and Exploitation, South West Petroleum University, Chengdu, Sichuan, China

ARTICLE INFO

Article history:
Received 11 January 2017
Received in revised form 13 February 2017
Accepted 18 February 2017
Available online 27 February 2017

Keywords:
WLMs
Nanoparticle
Foam stability
Hydraulic fracturing

ABSTRACT

Regarding the novel application of nanoparticles in enhanced oil recovery, the objective of this study was to investigate the potential of silica nanoparticles to stabilize foam under high-temperature conditions and exhibit an improved capacity to suspend proppants for hydraulic fracturing applications. In this study, a regular anionic surfactant was employed as the foaming agent and a worm-like micelle (WLM) surfactant was employed as the foam viscosifer and silica nanoparticles. The results indicate that the SiO_2 nanoparticles and WLMs exhibit a synergistic effect in terms of foam rheology and stability, which significantly improves the proppant suspension capabilities for petroleum applications.

Introduction

Aqueous foam can be considered a dispersion of gas bubbles in a liquid that is stabilized by a surface-active agent adsorbed at the gas-liquid interface. Foams are widely applied in daily lives and various industries, such as food [1], froth flotation [2] and petroleum industries [3–6]. Their practical and industrial importance has motivated fundamental studies of foams. Because foam is typically unstable both thermodynamically and kinetically especially under high-temperature conditions, the collapse of the foam can be detrimental to many industrial applications. Foam stability can be divided into three mechanisms (i.e., drainage, coarsening and rupture). These mechanisms include foam drainage caused by gravity [7], coarsening caused by gas transfer between bubbles induced by capillary pressure differences [8], and bubble coalescence caused by rupture of liquid films between neighbouring bubbles [9]. Because foam drainage influences the liquid fraction of foam, which determines both coarsening and bubble coalescence, a possible strategy for enhancing foam stability involves reducing the liquid drainage by increasing the fluid viscosity [10,11].

In recent decades, worm-like micelle surfactants have receive considerable attention in many experimental and theoretical studies [12]. Unlike polymers, which consist of strong covalent bonds that are not easily broken, worm-like micelles are formed by weak, physical bonds that continuously break and re-form, resulting in dynamic or "living" structures [13]. For rheology, the transition from spherical micelle to worm-like micelle corresponds to a dramatic increase in the fluid elasticity and viscosity. WLMs are primarily formed by mixing a surfactant and an organic counter ion that screens the electrostatic repulsions between the charged headgroups of the surfactant. The main process is shown in Fig. 1 where spherical micelles transforms into worm-like micelles [14] upon addition of an electrolyte. This transformation occurs because the salt (electrolyte) with the counter ions that penetrate the hydrophobic interior of the micelles promote the self-assembly of the surfactant into long, flexible worm-like micelles. The concentration depends on the type of salt. For example, sodium salicylate (NaSal) is much more efficient at promoting self-assembly than sodium chloride (NaCl). Small concentrations of NaSal counter ions are sufficient to produce high viscosity solutions [15]. In addition, most previously studied worm-like micellar systems have been based on cationic surfactants [15–18]. However, more recent studies have demonstrated that zwitterionic surfactants can form worm-like micelles in deionized water in the absence of inorganic salt even at low amphiphile concentrations [19]. Despite being very gentle on the human skin and more environmentally friendly due to their neutral charge, WLM zwitterionic surfactants exhibit better biodegradability and less ecotoxicity compared to non-ionic,

* Corresponding author.
E-mail address: yang.fei@adelaide.edu.au (Y. Fei).

http://dx.doi.org/10.1016/j.jiec.2017.02.015
1226-086X/

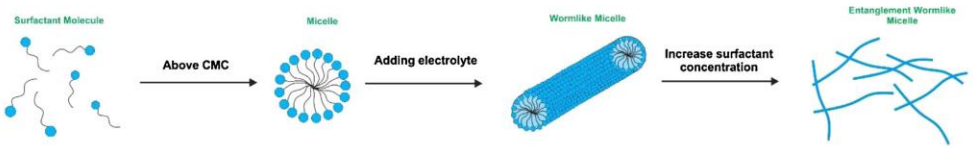

Fig. 1. Schematic illustration of the transformation of spherical micelles to worm-like micelles [19].

cationic, and anionic surfactants [20,21]. Therefore, this type of surfactant has the potential for used in the formation of worm-like micelles.

Furthermore, a current area of research in "foam stability" is focused on nanotechnology. The nanoparticles at an interface can inhibit bubble coalescence by creating a steric barrier that prevents advancement of the interfaces [22,23]. Experimental results [24,25] have indicated that the nanoparticle-surfactant mixtures have a synergistic effect on foam stability due to the adsorption of surfactant molecules onto particle surfaces. The attachment energy of a nanoparticle is related to the surfactant concentration, which influences the contact angle of the nanoparticle on the interface [23]. Another important aspect of inorganic nanoparticles is that they can act as a "pseudocrosslinking agent" to ionic WLMs in solution, or a "double network" comprised of micellar entanglements and particle junctions that result in significant improvement in the viscoelasticity properties [26,27].

A foam-based gel was developed using a mixed foaming agent in the presence of a zwitterionic surfactant (i.e., erucyl amidopropyl betaine (EAPB)) in a system consisting of water and nanoparticles. To the best of our knowledge, only a few studies on foam stabilisation by nanoparticles with zwitterionic worm-like micelles, which tend to be commercially popular, have been reported. The current study attempts to answer the following questions: how does the presence of hydrophilic nanoparticles affect foam stability in high temperature environments in terms of drainage and coalescence? What are the effects of the particles on the rheological properties of WLM foams?

Experimental section

Materials

Sodium dodecyl sulphate (SDS) and sodium dodecyl benzene sulfonate (SDBS) were provided as solid power by Chengdu Kelong Co., Ltd., China (95 wt% active content). Nano fumed silica (with an average size of 40 nm) powder was purchased from China Aladdin Chemical Co., Ltd. 20/40 mesh size carbon particles were kindly provided by State Key Laboratory of Oil and Gas Geology and Exploitation, South West Petroleum University, China. The EAPB surfactant is a commercial product manufactured by "Winsono New Material Technology LLC" (China, Shanghai). EAPB is a betaine-type zwitterionic surfactant based on its chemical structure (Fig. 2). The molecule possesses both a positively charged dimethyl ammonium moiety and a negatively charged carboxylate group. All these chemicals were used without further purification. Deionized water was used in all the experiments. All working solutions were prepared immediately prior to each experiment at 25 ± 1 °C.

Sample preparation

The foam sample was prepared using an anionic surfactant mixture consisting of 0.05 wt% sodium dodecyl sulphate [SDS] and 0.05 wt% sodium dodecyl benzene sulfonate [SDBS]. These foaming agents were added to 100 mL of deionized water using a glass rod to dissolve the powder with gentle stirring to avoid bubble formation in all cases. Then, 3–5 wt% EAPB surfactant was added as a viscosifer with continuous rod rotation. The 3–5 wt% guaranteed a concentration greater than the critical micelle concentration (CMC) to form worm-like micelles. To investigate the effects of the nanoparticles, as second set of experiment was performed with 0.8 wt% silica nanoparticles, which were introduced into the solution after the addition of EAPB. Once all additives were completely mixed, high-speed homogenization of the chemical mixture at 8,000 rpm for 1 min using entrained air was performed to produce a fine foam.

Experimental procedure

After the mixing was complete, the foam was immediately transferred to a 500 mL graduated cylinder in a pre-heated 90 °C oven. During the experiments, the free drainage volume and total foam volume were recorded (H_t is the total foam height, L_t is the drained liquid height and t is time). Then, the morphologies of the selected foam sample were imaged using a Quanta 450 scanning electron microscope (FEI, Netherlands). These samples were prepared by freezing a small drop of foam on a clean wafer with liquid nitrogen to maintain the microstructures of the mixtures. Next, the influence of the nanoparticle addition on the rheological properties of the worm-like micellar foam samples was investigated using a HAAKE MARS III Rheometer (Thermo Scientific, Germany). A double concentric cylinder (DG41) was used to carry out the steady rheological measurements. The apparent sample viscosity was measured by continuous shearing for 60 min at 90 °C. The entire process was performed at a constant shear rate of

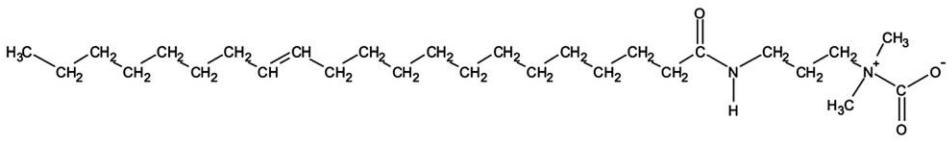

Fig. 2. Chemical structure of the erucyl amidopropyl betaine (EAPB) zwitterionic surfactant, reprinted from Gaynanova et al. [28].

$170\,s^{-1}$. Dynamic rheology was performed with a parallel-plate geometry P35 Ti L (the gap is 1 mm), and the stress amplitude was first confirmed to ensure that all measurements were performed within the linear viscoelastic region. The dynamic results were analysed based on the storage (G′) moduli and loss (G″) moduli at a frequency range of 0.1–10.0 Hz. After completion of the rheology experiment, the same foam was mixed with 1 wt% carbon particles with a 20/40 mesh size (Equivalent diameter $D_p = 700\,\mu m$) and density of $\rho_p = 2000\,kg/m^3$. A 500 mL cylinder was employed to ensure that the cylinder diameter was at least 25 times larger than the diameter of the particles to minimize the wall effect on the settling velocity.

Results and discussion

Foamability and foam stability

First, the effects of the EAPB surfactant and silica nanoparticles on the foamability and foam stability were studied. Based on our observations, a foam sample was selected for Cryo-SEM and rheological measurement.

In Fig. 3, the initial foam volume is shown as a function of the WLM (or EAPB) concentration. The best foamability was observed for the sample with a volume of 225 mL, which was generated using 3 wt% EAPB. In the presence of 0.8 wt% silica nanoparticles, the negative impact on the foaming ability was small because the foam volume was slightly lower compared to that of pure EAPB. The effect of EAPB on the damage of foam formation increased, which reduces the foam volume to 170 mL (5 wt% EAPB). This behaviour was due to the increase in the viscosity of the foaming solution with the addition of EAPB. Therefore, gas is more difficult to dissolve in the solution at the same mixing rate of the warning blender, reducing the foam volume. However, the special structure of EAPB is absorbed on the interface (occupied the adsorption space by SDS & SDBS), increasing the surface tension of the foam solution and decreasing the foam volume.

To compare the foam stabilities from dispersions with different foamabilities, the foam decay ratio (R_t^{foam}) is introduced:

$$R_t^{foam} = \frac{V_t^{Total} - V_t^{Drainage}}{V_t^{total}} \quad (1)$$

Table 1
Drainage half-life in foam prepared with 3–5 wt% EAPB with and without nanoparticle addition.

Free drainage half-life, $\tau_{1/2}$ 90 °C	EAPB concentration		
	3 wt%	4 wt%	5 wt%
Without silica nanoparticles	65 min	65 min	75 min
With 0.8 wt% silica nanoparticles	85 min	75 min	90 min
Incremental ratio	31%	15%	17%

where the V_t^{Total} is the total foam volume at time t and $V_t^{Drainage}$ is the free drainage volume at time t between 0 and 180 min. If the decay ratio is unity, the foam is completely stable to drainage and coalescence. However, a value of zero corresponds to complete foam breakdown. Fig. 4 shows the stability of the mix at 90 °C for surfactant-containing foams in the absence (black) and presence (red) of silica particles. For EAPB-only foams, the foam volume gradually decreases during the first 60 min and then more sharply decreases until no foam remains within 180 min. In contrast, the SiO_2-EAPB foams exhibited a significant improvement in stability because 40%–60% of the foam volume remains after 180 min at 90 °C. Fig. 4d shows the volume change for different foam samples at 90 °C. The enhanced stability resulted from both a reduction in the extent of free drainage due to increases in the aqueous phase viscosity as well as the adsorption of particles around bubbles to prevent coalescence and disproportionation. Therefore, to confirm this hypothesis, free drainage, Cryo-SEM and rheology experiments were conducted.

Free drainage

For all the cases, the drainage half-life ($\tau_{1/2}$) of the foam is summarized in Table 1. In general, the drainage rate tends to be slower with increasing EAPB concentration. For the EAPB-only (3–5 wt%) foams, the drainage half-life is between 65 min and 75 min, which is consistent with the previous observation (Fig. 4a–c). In the absence of nanoparticles, 3–5 wt% EAPB exhibited good foam stability during the initial 60 min because it is still in the drainage-dominated regime. After the addition of 0.8 wt% silica particles, the drainage half-life increased, especially for 3 wt% EAPB, which exhibited an increase of 31%. Therefore, the slowing free drainage

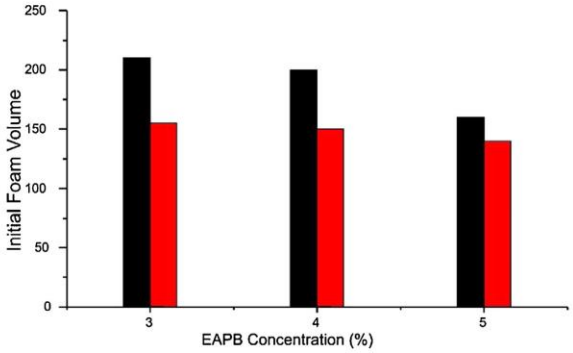

Fig. 3. Foam volume as a function of the EAPB concentration at room temperature. Without silica-particle: black bar and with 0.8 wt% silica-particle: red bar. (For interpretation of the references to colour in this figure legend, the reader is referred to the web version of this article.).

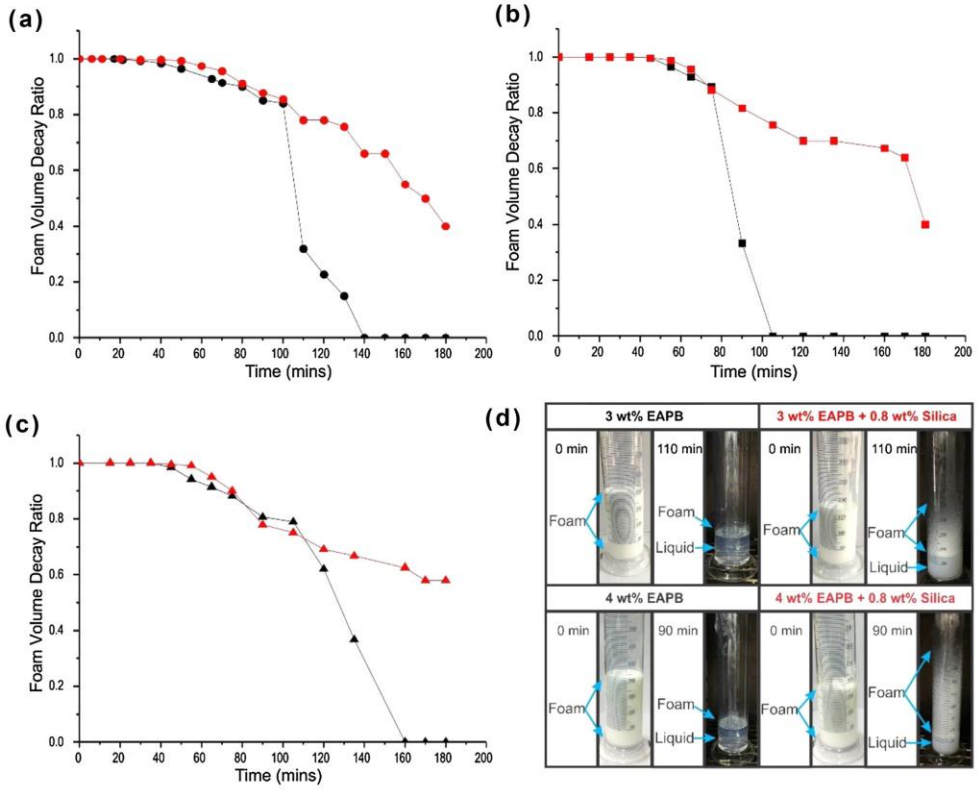

Fig. 4. Stability of the foams in particle-WLM mixtures as a function of the surfactant concentration at 90 °C: (a) 3 wt% EAPB, (b) 4 wt% EAPB and (c) 5 wt% EAPB (without silica particles (Black) and 0.8 wt% silica particles (Red)). (For interpretation of the references to colour in this figure legend, the reader is referred to the web version of this article.).

induced by the nanoparticles reduced the film thinning rate, which contributed to foam stabilisation as explained below.

To understand how the nanoparticle effect on free drainage, 3 wt% EAPB was selected as an example, and the drainage profile is produced from the recorded drained liquid volume as a function of time. Fig. 5a shows the normalized drained liquid ($V_{(t)}/V_{(l0)}$) as a function of time, where the $V_{(t)}$ is the volume of liquid drained out of the foam and $V_{(l0)}$ is the total volume of liquid in the foam at t = 0. The effect of the nanoparticles on foam drainage can be classified into three different regions. The first drainage-dominated regime is primarily controlled by viscosity. The addition of nanoparticles increases the viscosity of the foam solution, slowing gravitational drainage. This result is confirmed in the rheology section. In the second relaxation regime, the foams reach a critical rate where the drainage rate no longer changes. In this regime, the bubble coarsening and rupture become more dominant. Therefore, the foam becomes unstable. For the SiO_2-EAPB mixture, the relaxation regime starts at 150 min. However, for EAPB only, the relaxation regime starts at 83 min, which yields a total delay of 67 min prior to reaching this unstable regime. This results is due to the lower drainage rate via viscosity enhancement, which is also observed in the third transition regime created by the nanoparticles. This mechanism can be explained by [29] particle jamming or "cork formation" (Fig. 5b), resulting from collision between large aggregates that may be progressively formed after crossing several node intersections. These blockages reduce the number of liquid drainage channels.

Cryo-SEM

The foam morphologies were analysed using the Cryo-SEM technique to provide evidence to confirm our hypotheses. The 3 wt % SiO_2-EAPB mixtures exhibited good foam stability and drainage half-life, and the Cryo-SEM images are shown in Fig. 6. The first observation (Fig. 6a) is after the addition of SiO_2 nanoparticles, which results in particle aggregation and "cork formation". This phenomenon was previously confirmed (Fig. 5b) and results in a decrease in the drainage rate as well as the creation of a transition regime that delays the relaxation time. In addition, the interface of the bubbles adsorbed by the nanoparticles is shown in Fig. 6b. When the two bubble surfaces become sufficiently close, attractive forces, such as van der Waals forces, become significant, and the amplitude of the disturbance increases, which leads to film rupture. The purpose of the particle adsorption is to maintain a film

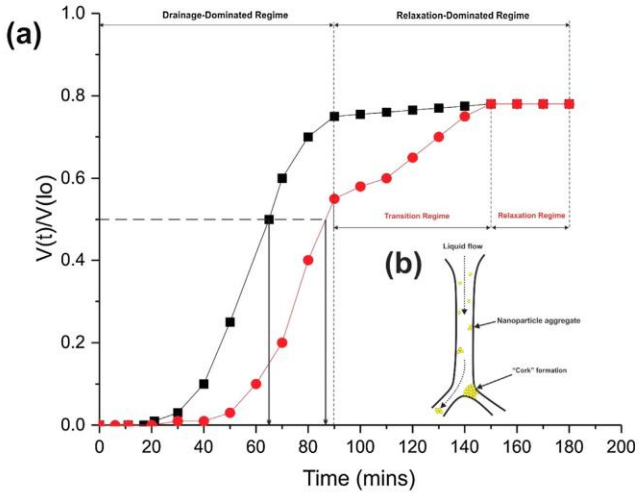

Fig. 5. Effect of nanoparticles on foam drainage. In (a), the 3 wt% EAPB results are represented by the black line and the 3 wt% silica nanoparticle results are represented by the red line. (b) Schematic representation of "Cork formation" by nanoparticle aggregates. (For interpretation of the references to colour in this figure legend, the reader is referred to the web version of this article.).

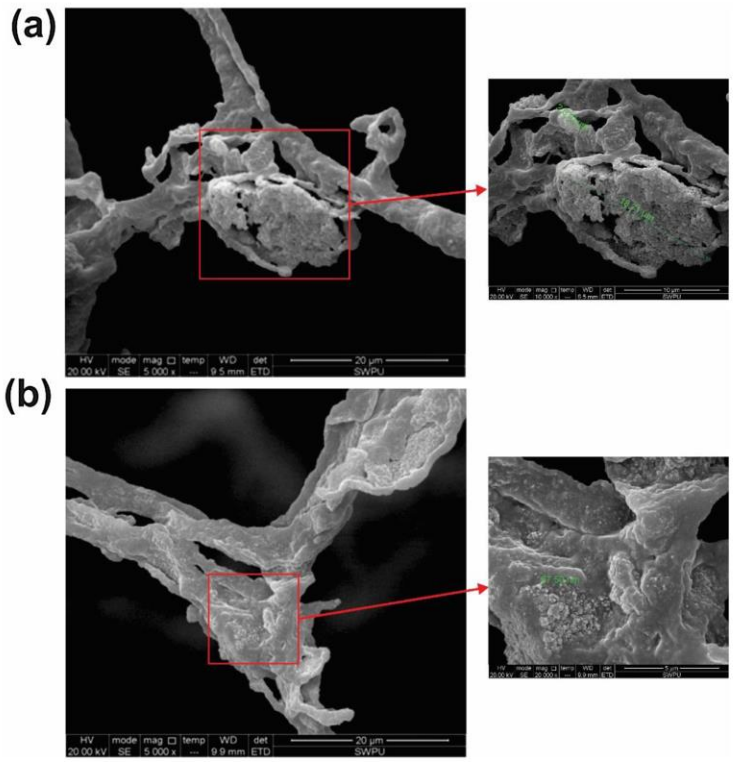

Fig. 6. Cryo-SEM images of frozen aqueous foams of 3 wt% EAPB with 0.8 wt% silica nanoparticles. (a) Foam node blockage by nanoaggregates and (b) nanoparticle attachment at the gas–water interface.

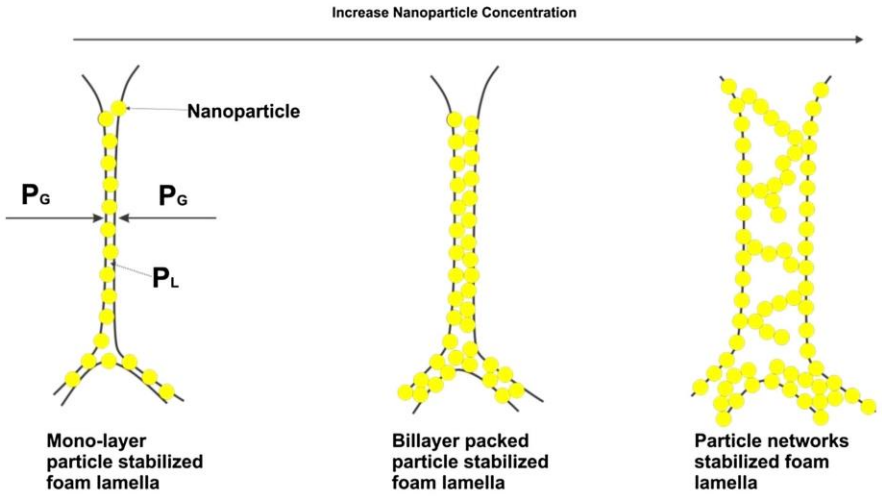

Fig. 7. Schematic representation of nanoparticles (yellow circles) at the air–liquid interface. The picture shows the effect of nanoparticle aggregation on the film thickness due to capillary suction, reprinted from Horozov [31]. (For interpretation of the references to colour in this figure legend, the reader is referred to the web version of this article.).

thickness that is larger than the film critical rupture thickness (H_{cr}) [30]. Even if most of the liquid drains out, the particles can maintain the thickness of the film. To improve the stability against coalescence and Ostwald ripening, a film that is thicker than the critical rupture thickness must be created, which can be achieved by a higher nanoparticle concentration. This higher concentration could result in the formation of a closed-packed bilayer or particle network that leads to a lower probability of film rupture. A schematic representation of the geometrical configurations for particles at the bubble interface is shown in Fig. 7. Therefore, the foam stabilisation occurs via nanoparticle attachment for film prevention and foam node blockage by nanoaggregates for drainage retardation.

Rheology

As previously mentioned, the drainage rate decreased due to the introduction of nanoparticles. Therefore, the silica nanoparticle interaction with the EAPB foam must be investigated in terms of the rheological properties. As shown in Fig. 8, the apparent viscosity of the foam mixtures proportional to the shear rate, and typical shear thinning behaviour [32] (i.e., pseudoplastic) was observed. The apparent viscosity of the foam mixtures exhibited a shear rate-dependent behaviour due to the orientation of the entanglement WLMs resulting from a high shear rate disturbance.

Next, the linear viscoelasticity of 3% EAPB with SiO_2 nanoparticles was determined using the oscillation shear sweep test. The elastic modulus (G') and viscous modulus (G'') are plotted as functions of the frequency (ω) under different temperatures, as

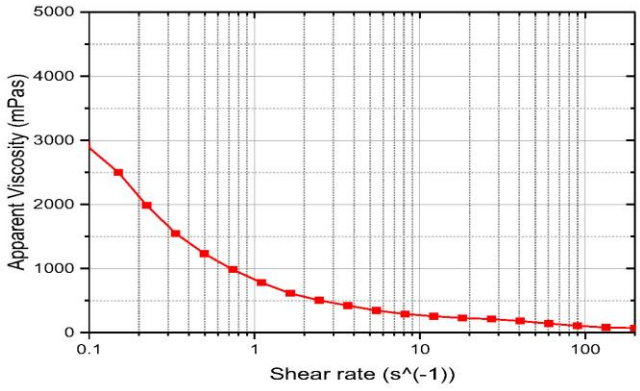

Fig. 8. Apparent viscosity as a function of the shear rate for 3 wt% EAPB with 0.8 wt% silica nanoparticles at 90 °C.

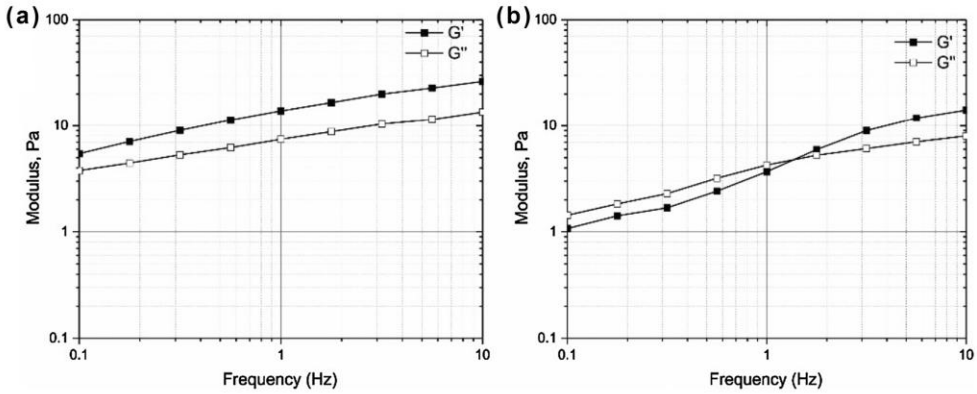

Fig. 9. Dynamic rheology measurement of 3 wt% EAPB with 0.8 wt% silica nanoparticles: (a) 25 °C and (b) 90 °C.

shown in Fig. 9. Both G′ and G″ increased as the frequency increased. At room temperature (25 °C), the elastic modulus was dominant over the viscous modulus in the tested frequency range (Fig. 10a). At higher temperatures (90 °C), the elastic modulus crosses over and decreases below the viscous modulus to a critical frequency value (ω_c) (Fig. 9b). The response of the sample was elastic at low temperatures and switched to viscoelastic at higher temperatures, which indicates the thermo responsiveness [33] of EAPB on the rheological property. This behaviour can also be explained by the high temperature influence on both the micellar elongation and entanglement of WLMs, which results in viscoelasticity. In addition, some of our results are consistent with those reported by Kumar et al. [34] in the field of dynamic rheology.

Then, a steady state apparent viscosity experiment was performed at a constant shear rate of 170 s^{-1} for 60 min at 90 °C. The apparent viscosity as a function of time is shown in Fig. 10. For EAPB only, the viscosity gradually increased from 70 mPa s to 95 mPa s (t = 60 min) due to the free drainage effect on

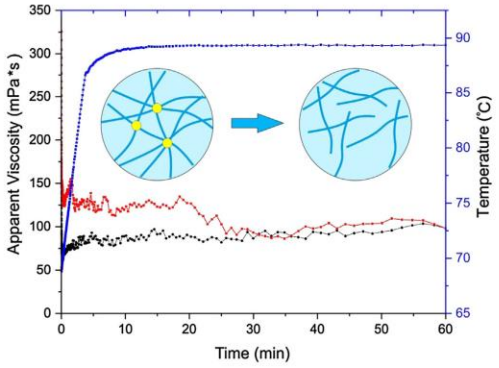

Fig. 10. Apparent viscosity as a function of time at a shear rate of 170 s^{-1} t 90 °C. The 3 wt% EAPB results are represented by the black line, and the 0.8 wt% silica nanoparticle results are represented by the red line of apparent viscosity. The dark blue line shows the temperature. (For interpretation of the references to colour in this figure legend, the reader is referred to the web version of this article.).

the liquid fraction inside the structure. The drier foam tends to become more solid like, which creates more friction for the shear force. The overall EAPB foam can maintain a fairly stable viscosity at approximately 85 mPa*s at 90 °C. However, the addition of 0.8 wt % SiO_2 nanoparticles results in a significant viscosity enhancement for the first 30 min, which may be due to the nanoparticles physically participating in the WLM network (as shown in Fig. 10). The formation of micelle-particle junctions leads to the formation of physically crosslinked micellar aggregates, which effectively join two or more micellar chains and results in additional viscoelasticity. For example, a particle with two junctions will join two micelles, resulting in an effectively longer micelle that will result in a greater number of entanglements per effective micelle. Particles with three or more junctions will serve as physical crosslinks of a micellar network that is similar to that in a crosslinked polymer gel [35]. However, these crosslink effects only last 30 min, and then, the particles detach from the micellar-like Gel Breaker [36]. In the junctions, this behaviour is governed by a balance between the end-cap energy [26] and the micellar adsorption energy [12], which can be analysed by structural and thermodynamic measurements [37].

Fig. 11 shows the rheological modification due to the formation of micelle-nanoparticle junctions. The presence of these junctions significantly increases the viscosity in the foam during the initial 30 min due to the decrease in the drainage rate (Fig. 5), which resulted in stability enhancement. After 30 min, all nanoparticles break from these junctions, and the viscosity returns to the initial conditions. The breaking point of the micelle junctions depends on many factors that may be useful for industrial applications, as previously mentioned. For example, the WLM foam can be used as a hydraulic fracturing fluid for carrying proppants. The sample is required to have sufficient viscosity to transport large concentrations of dense proppant until it reaches the desired subsurface location to keep the fractures open. An additional benefit is that when the treatment has finished, the foam would easily breakdown and facilitate flow back to the surface to prevent formation damage. Therefore, the micelle junction break mechanism is important to investigate and tailor for different purposes. In addition, a positive increase in the viscosity was observed after 30 min most likely due to the foam coarsening effect on the growth of the bubbles size, which affects the foam rheology.

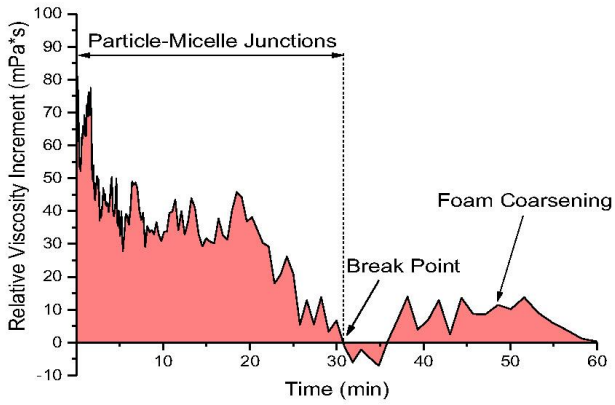

Fig. 11. Apparent viscosity comparison chart with and without nanoparticles.

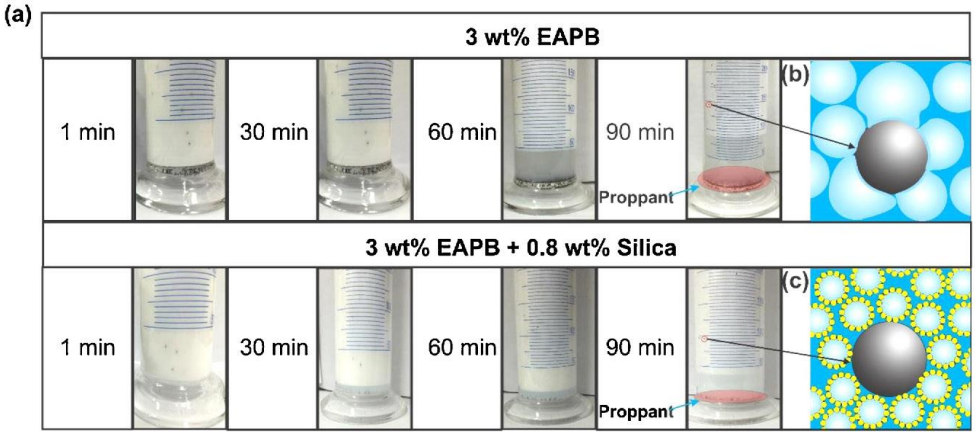

Fig. 12. Four snapshots of the particle sedimentation experiments from 0 min to 90 min (a). Soft bubble film easily deformed by proppant settling and provided weak uplifting force for the proppant (b). Particle-stabilized film maintains homogenous size and provides strong uplifting force for the proppant (c).

Proppant sedimentation

Fig. 12a shows the results for the 3% EAPB and 3% SiO_2-EAPB mixtures mixed with 1 wt% proppant at 90 °C. The sedimentation as a function of time was measured in a 500 mL graduated cylinder. Four snapshots of the sedimentation at 1, 30, 60 and 90 min are shown for these samples. In comparison, the proppant in the EAPB foam settled much faster than that in the SiO_2-EAPB foam, which is primarily due to the surface of the SiO_2-EAPB bubbles being rougher than the EAPB bubbles due to nanoparticle adsorption. When the proppant settled through the deformed bubbles, the SiO2-EAPB bubbles produced more resistance than the EAPB foam. The proppant did not easily slip through the surface of the SiO_2-EAPB bubbles (as shown in Fig. 12b and c). Similar observations were also reported by Lv et al. [4]. Other factors, such as rheology enhancement by particle-micelle junctions and bubble diffusion retardation by particle adsorption, could prevent the proppant from settling due to an increase in the total uplifting force of the proppant.

Conclusions

This experimental study highlights the improvement of foam stability by silica nanoparticles under high temperature environments. The enhancement of the foam stability with hydrophilic silica nanoparticles may be due to two aspects. 1. The particles adsorbed at the air/water interface prevent thinning of the films to the critical rupture thickness. 2. In addition, the particles decreased the drainage rate by creating an "obstacle" in the liquid channel or intersection. The EAPB surfactant behaves either as an elastic gel or as a viscoelastic material, and this behaviour depends on the temperature conditions. Based on the rheological experiment, a synergistic enhancement of the viscosity by the SiO_2-EAPB foam system results in a good combination of properties from the single

components due to the formation of micellar-particle junctions. This unique rheology characteristic is due to the SiO_2-EAPB mixture, which exhibits a longer foam drainage, and the overall improvement in the efficiency of the foam as a fracturing fluid under high temperature environments in terms of the proppant carrying capacity. Our results provide motivation for further experimental studies to control the viscoelasticity (micellar-particle junction) under high temperature environments in petroleum engineering applications.

Acknowledgements

The authors acknowledge the financial support provided by the National Science and Technology Major Project (2016zx04404002). The authors also acknowledge support from the Fracturing & Acidizing research team lead by Prof. Yang Zhaozhong, who provided the research facilities used in this work.

References

[1] E. Dickinson, Curr. Opin. Colloid Interface Sci. 15 (2010) 40.
[2] T.N. Hunter, R.J. Pugh, G.V. Franks, G.J. Jameson, Adv. Colloid Interface Sci. 137 (2008) 57.
[3] D. Oussoltsev, I. Fomin, K.K. Butula, K. Mullen, A. Gaifullin, A. Ivshin, D. Senchenko, I. Faizullin, Foam Fracturing: New Stimulation Edge in Western Siberia (Russian), Society of Petroleum Engineers, Moscow, Russia, 2008.
[4] Q. Lv, Z. Li, B. Li, S. Li, Q. Sun, Ind. Eng. Chem. Res. 54 (2015) 9468.
[5] F. Guo, S. Aryana, Fuel 186 (2016) 430.
[6] S.H. Talebian, R. Masoudi, I.M. Tan, P.L.J. Zitha, J. Petrol. Sci. Eng. 120 (2014) 202.
[7] J. Angarska, C. Stubenrauch, E. Manev, Colloids Surf. A: Physicochem. Eng. Asp. 309 (2007) 189.
[8] A. Maestro, E. Rio, W. Drenckhan, D. Langevin, A. Salonen, Soft Matter 10 (2014) 6975.
[9] R.I. Saye, J.A. Sethian, Science 340 (2013) 720.
[10] J. Wang, A.V. Nguyen, Soft Matter 12 (2016) 3004.
[11] S. Guignot, S. Faure, M. Vignes-Adler, O. Pitois, Chem. Eng. Sci. 65 (2010) 2579.
[12] V.A. Pletneva, V.S. Molchanov, O.E. Philippova, Langmuir 31 (2015) 110.
[13] C.A. Dreiss, Soft Matter 3 (2007) 956.
[14] A. Sambasivam, A.V. Sangwai, R. Sureshkumar, Langmuir 32 (2016) 1214.
[15] S.R. Raghavan, E.W. Kaler, Langmuir 17 (2001) 300.
[16] S. Ezrahi, E. Tuval, A. Aserin, Adv. Colloid Interface Sci. 128–130 (2006) 77.
[17] S.-i. Imai, T. Shikata, J. Colloid Interface Sci. 244 (2001) 399.
[18] W.-J. Kim, S.-M. Yang, Langmuir 16 (2000) 6084.
[19] Z. Chu, Y. Feng, X. Su, Y. Han, Langmuir 26 (2010) 7783.
[20] J.G. Weers, J.F. Rathman, F.U. Axe, C.A. Crichlow, L.D. Foland, D.R. Scheuing, R.J. Wiersema, A.G. Zielske, Langmuir 7 (1991) 854.
[21] J. Yang, Curr. Opin. Colloid Interface Sci. 7 (2002) 276.
[22] G. Bournival, S. Ata, E.J. Wanless, Adv. Colloid Interface Sci. 225 (2015) 114.
[23] B.P. Binks, T.S. Horozov, Angew. Chem. 44 (2005) 3722.
[24] B.P. Binks, M. Kirkland, J.A. Rodrigues, Soft Matter 4 (2008) 2373.
[25] Q. Sun, Z. Li, J. Wang, S. Li, L. Jiang, C. Zhang, RSC Adv. 5 (2015) 67676.
[26] F. Nettesheim, M.W. Liberatore, T.K. Hodgdon, N.J. Wagner, E.W. Kaler, M. Vethamuthu, Langmuir 24 (2008) 7718.
[27] R. Bandyopadhyay, A.K. Sood, J. Colloid Interface Sci. 283 (2005) 585.
[28] G.A. Gaynanova, A.R. Valiakhmetova, D.A. Kuryashov, N.Y. Bashkirtseva, L.Y. Zakharova, J Surfactants Deterg. 18 (2015) 965.
[29] F. Carn, A. Colin, O. Pitois, M. Vignes-Adler, R. Backov, Langmuir 25 (2009) 7847.
[30] A. Sharma, E. Ruckenstein, Langmuir 3 (1987) 760.
[31] T.S. Horozov, Curr. Opin. Colloid Interface Sci. 13 (2008) 134.
[32] T.G. Mezger, The Rheology Handbook: For Users of Rotational and Oscillatory Rheometers, (2006) , pp. 34 Vincentz Network.
[33] Z. Chu, C.A. Dreiss, Y. Feng, Chem. Soc. Rev. 42 (2013) 7174.
[34] R. Kumar, G.C. Kalur, L. Ziserman, D. Danino, S.R. Raghavan, Langmuir 23 (2007) 12849.
[35] M.J. Economides, K.G. Nolte, Reservoir Stimulation, (2000) .
[36] J.R. Fink, Hydraulic Fracturing Chemicals and Fluids Technology, Elsevier, Oxford, UK, 2013.
[37] M.E. Helgeson, T.K. Hodgdon, E.W. Kaler, N.J. Wagner, M. Vethamuthu, K.P. Ananthapadmanabhan, Langmuir 26 (2010) 8049.

Chapter 5: Foam stability and its effects on hydraulic fracture proppant placement and overall effectiveness

5.1 Introduction

This chapter discusses the inclusion of a foam stability factor into hydraulic fracture modelling based on an experimental study of foam stability, resulting in rheological properties that improve the hydraulic fracture performance. Previous experimental results provide a general guideline for sensitivity analysis of foam stability factor for fracture modelling. To minimise formation damage in foam fracturing designs, a 'living' polymer made of WLMs is used as the base fluid. Finally, a 3D hydraulic fracture modelling is used to evaluate the impact of foam stability on the resulting proppant distribution within the hydraulic fracture. This chapter is a modified and adjusted version of our paper submitted to Journal of Natural Gas and Engineering, 'Fei, Y., Pokalai, K., Johnson, R., Gonzalez, M., & Haghighi, M. (2017). Experimental and simulation study on foam stability and its effects on hydraulic fracture proppant placement'.

5.2 Methodology

This chapter has three sections: 1) foam stability experiments, 2) foam rheological characterisation, and 3) 3D hydraulic fracturing simulation. The details of the workflow are shown in **Figure 0.1**. First, based on the experimental results in Chapter 4, the foam rheological properties were calculated by using an existing rheological correlation from literature. The rheological properties of the micellar-based fluid system were obtained from a fracturing fluid database. For dynamic conditions, the liquid drainage rates were obtained from the experiment to consider that foam quality changes with time. Eventually, a rheology curve was created, which was matched with the observed input data points by adjusting the rheological parameters in the correlation. Next, a planar, fully 3D hydraulic fracturing simulation was developed to model the fracture propagation and proppant transport.

The details of the model development have been described in our published paper "3D Simulation of Hydraulic Fracturing by Foam Based Fluids Using a Fracture Propagation Model Coupled with Geomechanics in an Unconventional Reservoir in the Cooper Basin, South Australia"(Fei et al., 2016). In the simulation, the developed foam rheological model is integrated into the designed pumping schedule, which recalculates the rheological properties on a grid-by-grid basis and predicts proppant distribution and conductivity. As previously mentioned, there are four different cases: Case 1, constant foam quality (static condition), which assumes that the foam is entirely stable during the fracture progress with no gas fractional changes; Case 2, variable foam quality (dynamic condition), where foam quality is based on experimental drainage rate observations and gas fractional changes with time; and Cases 3 and 4 as less stable foams based on the duration of the critical time to analyse the influence of a stability factor on the treatment outcome.

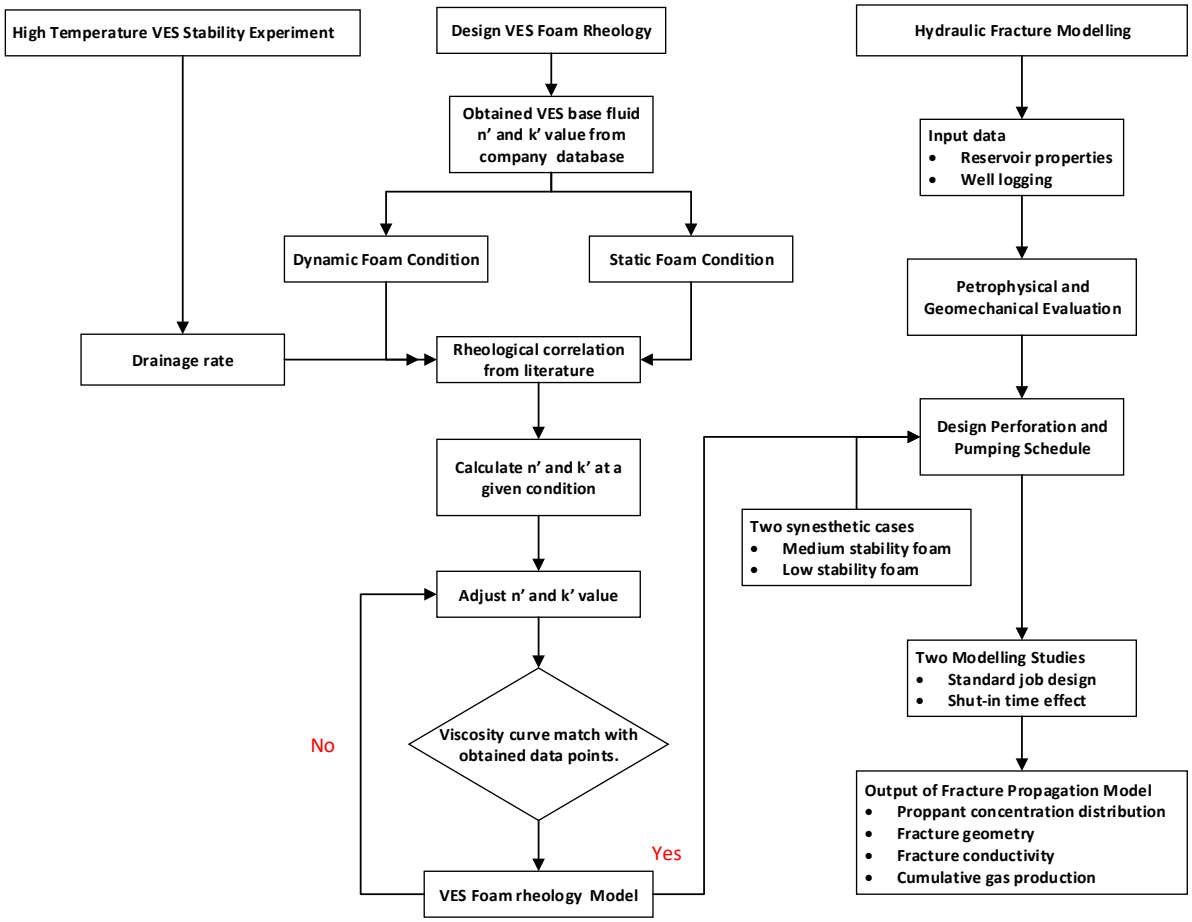

Figure 0.1. Workflow of experiment and model development

5.3 Experimental results

As analysed in Chapter 4, the initial foam volume is inversely proportional to the erucyl amidopropyl betaine (EAPB) concentration as presented in **Figure 0.2a**. The effect of EAPB on foam generation is significant—in one case reducing the foam volume from 525 ml to 170 ml (i.e. foam quality of 37.5%). As the viscosity of a foaming solution increases with the addition of EAPB, it is more difficult to diffuse gas into the solution at the same mixing rate (e.g. rotational speed of Warning blender), thereby reducing the foam volume. This observation also explains the difficulty of generating high foam qualities when high concentration of viscosifiers is employed to achieve better proppant transportation in hydraulic fracturing. For foam drainage and rupture test, 3% EAPB was used as the experimental case study to balance between foam quality and stability. Field practitioners have used delayed crosslinking of natural gums to achieve more stability in foamed fracturing fluids in order to transport higher concentrations of sand and limit the detrimental effects of crosslinking on foam generation (Freeman et al., 1986; Johnson, 1995).

After the foam formation, several processes occur, each of them leading to foam destruction. For further stability analysis, the trend of drainage profile for 3% EAPB samples is studied. **Figure 0.2b** displays the normalised drained liquid volume ($V_{(t)}$ / $V_{(l0)}$) versus time. $V_{(t)}$ is the foam volume that has been drained out of the foam, and $V_{(l0)}$ is the total volume of liquid in the foam at t = 0. As observed, the drainage half-time (τ) of 3% EAPB foam is 65 min;

however, this study has found that drainage half-life is not a key parameter to foam stability, particularly as it pertains to hydraulic fracture treatment simulation. Instead, the foam critical time (80 min), which is the intersection of drainage trend (from 30 min to 80 min) and disproportional trend (90 min to 140 min), is the key parameter defining foam stability.

In addition, **Figure 0.2c** shows the ratio of the remaining foam volume to the total volume, illustrating that the foam volume decreases gradually during the first 90 min, then sharply declines until no foam remains at 140 min. This is consistent with the drainage profile behaviour; thus, before the critical time, the samples are still in the drainage-dominated regime (still contain sufficient film thickness) and bubble diffusion remains at a minimum. After the critical time, the foam ruptures quickly as the capillary suction pressure is more dominant than the disjoining pressure. **Figure 0.2d** presents the volume change of the 3 wt% EAPB sample under 90 ℃. At 90 min, it can be observed that most of the liquid drains to the bottom and correspondingly the bubble size to grow significantly. The coupling effect of drainage and disproportionation eventually causes the foam rupture. The experiment presents the entire lifetime of the foam, from drainage to disproportionation and eventually to coalescence.

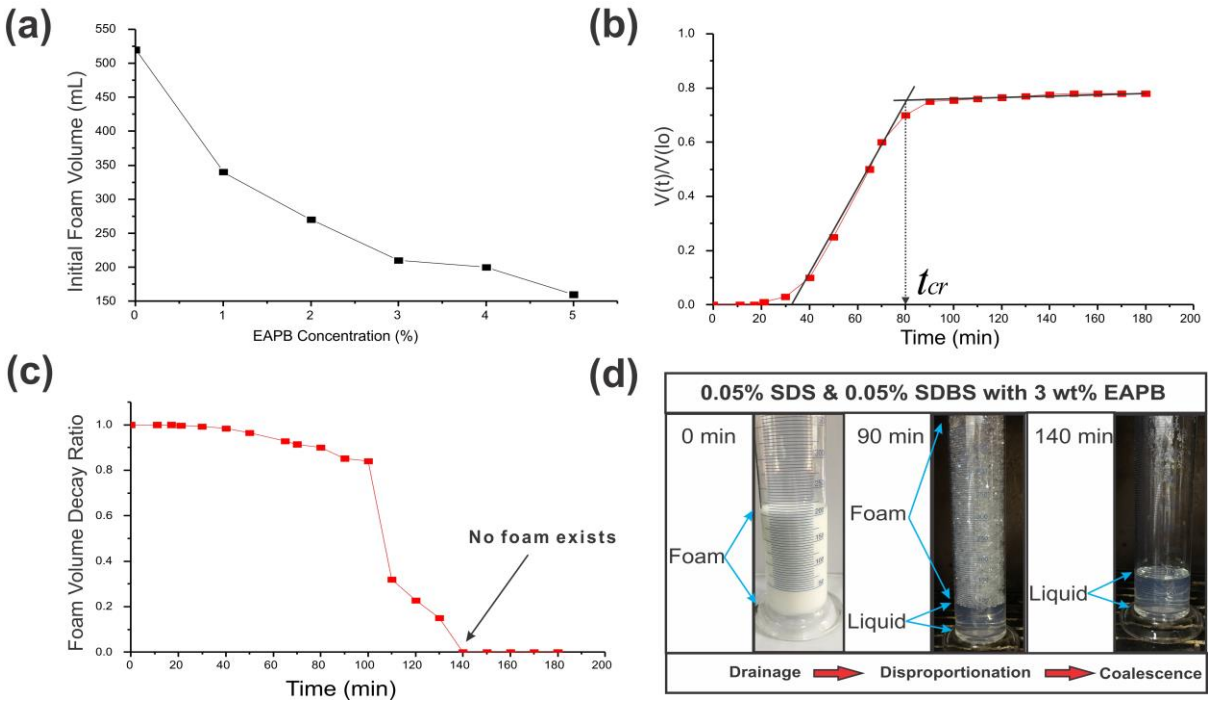

Figure 0.2. Foam stability varies with EAPB concentration under **90** ℃ based on (a) foamability, (b) foam drainage, (c) foam rupture, and (d) foam lifetime visualisation

5.4 Foam characterisation based on Carreau rheological model

Modelling of stability coupled with rheology of foam during a hydraulic fracturing treatment is a complex issue in this work. The time dependence of a non-Newtonian foam is modelled by predicting the variance of two primary base fluid (power law) parameters, n_{Liquid} and k_{Liquid}, and then coupling with the gas concentration to approximate the parameters for the foamed system, n_{Foam} and k_{Foam}. Published experimental correlations (Khade and Shah,

2004) have analogously predicted the consistency and flow behaviour index of foam fluids as a function of foam quality (Q_g):

$$\frac{n_{Foam}}{n_{Liquid}} = 1 - 0.6633Q_g^{5.168} \quad (9)$$

$$\frac{k_{Foam}}{k_{Liquid}} = e^{(0.4891Q_g + 5.6203Q_g^2)} \quad (10)$$

In this study, a planar, fully 3D hydraulic fracturing model known as GOHFER (Barree, 1983) was built. This model uses a Carreau rheological model to describe the time-dependent fluid properties as a function of position in the hydraulic fracture, shear rate, temperature, and sand concentration. The Carreau model relies much on the same data as the power law model, based on a foam power law exponent (n_{Foam}) and fluid consistency index (k_{Foam}). In addition, values of zero-shear viscosity (μ_o) (Asadi et al., 2002), high-shear viscosity (μ_∞), and slurry rheology exponent (a) are required to determine the apparent viscosity (μ_{app}) as follows:

$$\mu_{app} = \mu_\infty + \frac{S_f\mu_o - \mu_\infty}{(1 + (\frac{S_f\gamma}{\gamma_l})^2)^{\frac{1-n_{foam}}{2}}} \quad (11)$$

$$\gamma_l = (\frac{U_o k_{foam}}{47879})^{\frac{1}{n_{foam}-1}} \quad (12)$$

$$s_f = (1 - \frac{C_v}{C_{v_{max}}})^{-a} \quad (13)$$

Where γ_l is the curve-fit low shear transition, γ is the shear rate, C_v is the volume fraction of solids, and S_f is the sand factor. Each parameter is time dependent and changes with temperature and breaker reactivity affecting μ_o and μ_∞.

The foam quality in static conditions is always constant during the treatment, and the apparent viscosity could only be controlled by the time dependency of n_{Foam} and k_{Foam}. In the experiment, the model was run with a dynamic foam quality based on drainage observation. Thus, the apparent viscosity of the dynamic foam is controlled by an additional time-dependent foam quality variable Q_g^t. The calculated results are summarised in **Table 0.1**. From $t = 0$ min to $t = 30$ min, there is almost no liquid drainage in the experiment; the viscosity of the dynamic and static foam is the same. From $t = 30$ min to $t_{cr} = 80$ min, the viscosity of the dynamic foam increases owing to the effect of drainage. From $t_{cr} = 80$ min to $t_{rup} = 140$ min, the viscosity of the dynamic foam decreases by disproportionation, then after $t_{rup} = 140$ min, the foam totally collapses and no single structure remains. Following disassociation, the fluid is characterised by the base fluid rheology, which is assumed to be completely degraded by breakers added to the foam and eventually reverts to the viscosity of water (1 cP).

Using the above results, the apparent viscosity versus time can be plotted (see **Figure 0.3(a)**) as increasing from an initial base fluid viscosity to a threefold static foam viscosity (based on $Q_g = 52\%$) as a result of the foam structure. The static and dynamic foam do not differ in the first 30 min, a period where the foam is completely stable. After 30 min, the foam drainage starts to increase, then the viscosity of the dynamic foam increases until it reaches a critical time; after that period the foam viscosity decreases as the foam structure collapses. The

behaviours from the static and dynamic foam studies were matched to the Carreau rheological model as shown in **Figure 0.3(b)** and **Figure 0.3(c).**

In addition to the above models, two synthetic cases were created to illustrate the effect of foam stability on hydraulic fracturing outcome. These cases were created by horizontally shifting the apparent viscosity of the dynamic curve ($t_{cr} = 80$ min) to the critical time $t_{cr} = 20$ min (medium stability) and to the critical time $t_{cr} = 3$ min (low stability), as illustrated in **Figure 0.4**. Then, the same process of curve matching was performed with respect to the Carreau rheological model.

Table 0.1. Rheological properties of static foam and dynamic foam

	Constant foam quality (Static)		**Variable foam quality (Dynamic)**		
Time	Foam Quality	Apparent Viscosity	Foam Drainage Ratio	Foam Quality	Apparent Viscosity
(min)	(%)	(cP)		(%)	(cP)
1	52.381	234.778	0	52.381	234.778
10	52.381	234.778	0	52.381	234.778
20	52.381	234.778	0.01	52.632	237.737
30	52.381	230.214	0.03	53.140	239.152
40	52.381	199.670	0.1	55.000	228.091
50	52.381	166.624	0.25	59.459	241.290
60	52.381	124.648	0.425	65.672	256.768
70	52.381	96.162	0.6	73.333	311.331
80	52.381	75.496	0.7	78.571	331.151
90	52.381	59.524	0.75	81.481	307.620
100	52.381	44.280	0.755	81.784	230.997
140	52.381	1.000	0.78	83.333	1.000

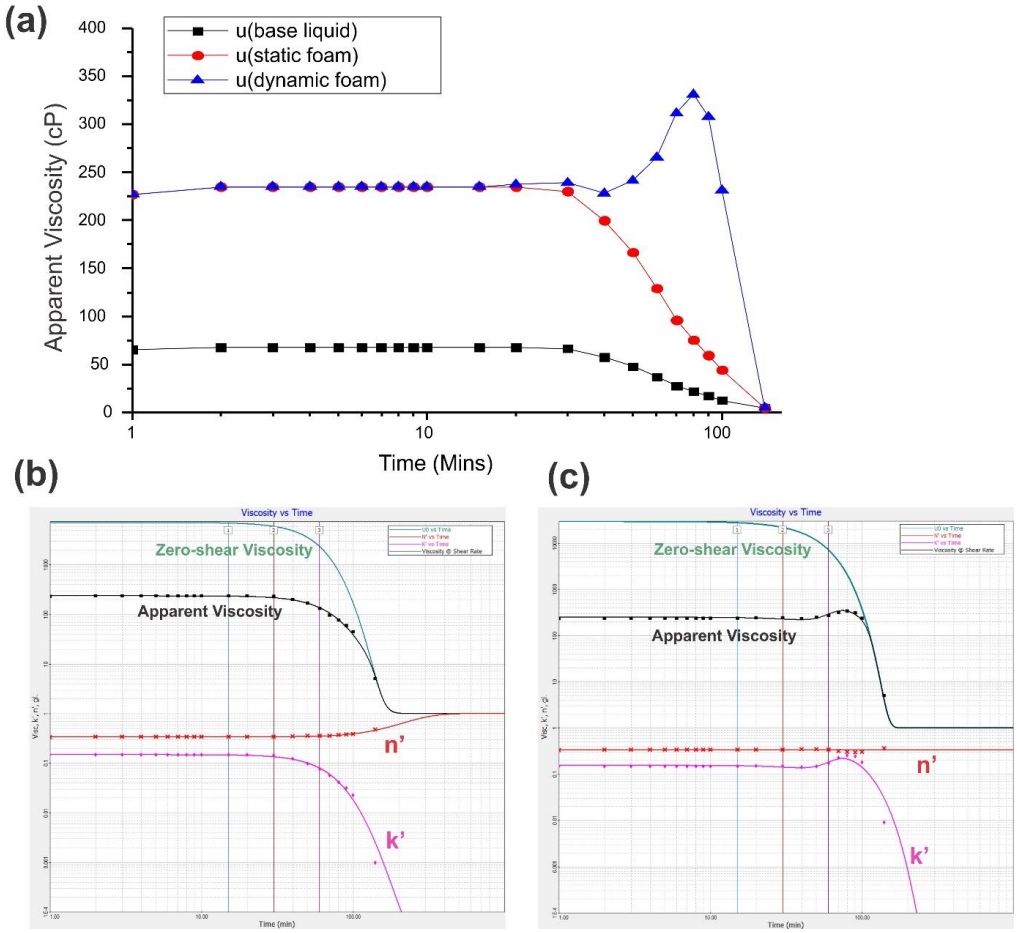

Figure 0.3. (a) Rheological properties of base fluid, static foam, and dynamic foam; (b) Carreau rheological model matching with obtained data points of static foam quality and (c) dynamic foam quality

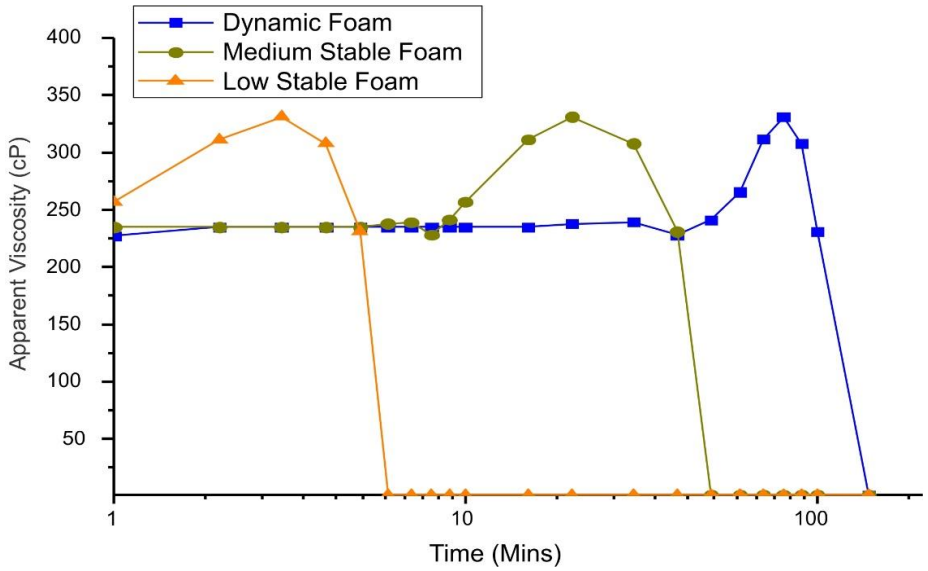

Figure 0.4. Development of synesthetic (medium and low stability) rheology curves from the reference curve (dynamic)

5.5 Hydraulic fracturing modelling

A 3D hydraulic fracturing simulation was developed using GOHFER (Barree, 1983). After running four different stability scenarios, the relationship between foam stability and fracture properties was obtained. The reservoir properties and the treatment parameters are assumed based on a typical tight sand reservoir in the simulation and they are listed in **Table 0.2**.

Table 0.2. Input data for standard treatment condition

Well Parameters	***Value***
Measured depth, ft	7325
Thickness, ft	77
Reservoir pressure, psi	1857
Permeability, md	0.17
Porosity, %	10
Water saturation, %	50
Gas saturation, %	50
Fracturing Treatment Parameters	
Type of Fracturing Fluid	*Foam*
Clean volume, gal	46,000
Proppant type, mesh	*Ceramic 20/40*
Proppant amount, lb	*135000*
Initial foam quality, %	52
Total pumping time, min	60
Shut-in time, min	30
Pumping rate, bpm	20

As discussed previously, we first modelled the created fracture geometry and resulting proppant distribution within the hydraulic fracture as per a standard job design in the industry (**Table 0.2**) and based on the degree of foam stability (**Figure 0.4**).

Second, a sensitivity study of the shut-in time is performed. Longer or shorter shut-in periods affect the foam stability, which subsequently influence the proppant distribution, conductivity, and post-treatment production. Foam rheology at any point of the treatment depends on foam stability as shown in **Figure 0.5.** The rheology profile can be split into two main parts: a stable region during pumping, where the experimental data matches the static data, and an unstable

region outside the stable envelope, where foam drainage and disproportionation affect the rheological properties. The shut-in period, varying from 0 to 1000 min, is investigated in this study, with fixed pumping time of 60 min.

The following models show (1) the relationship between foam stability and fracture properties under standard treatment conditions, and (2) the relationship between shut-in time and production performance. These include fracture geometry and proppant distribution impacted by the shut-in time, when considering significantly shorter or longer foam life. Consequently, the overall well production is affected by the foam behaviour during both pumping and shut-in periods.

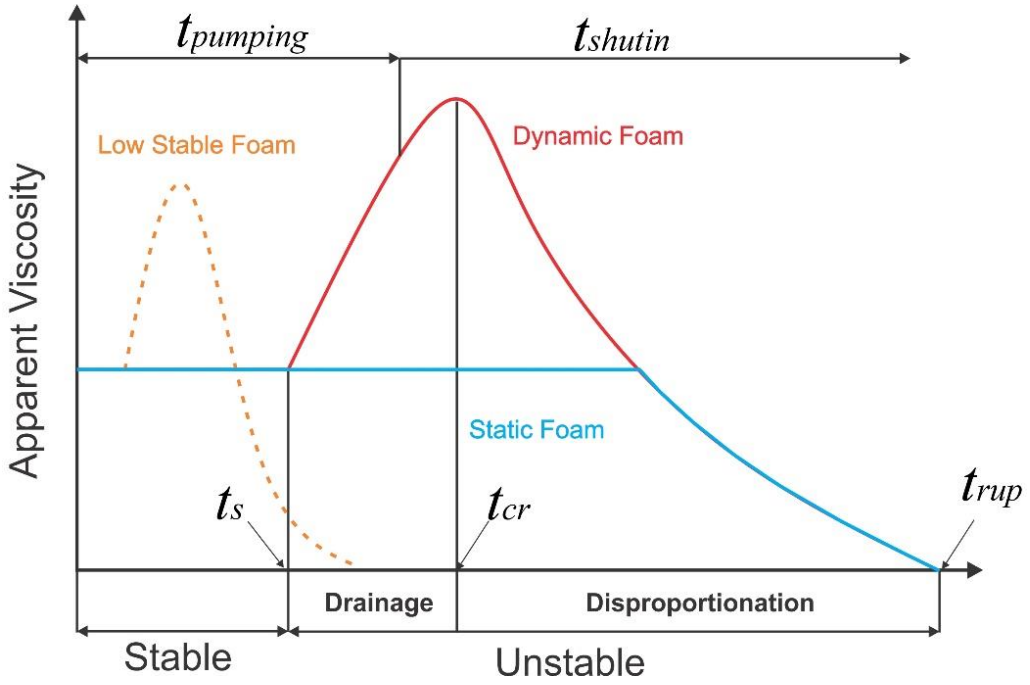

Figure 0.5. Generic foam rheology vs. foam stability under fracture treatment time

5.6 Results and discussion

5.6.1 Foam stability study

In the standard treatment condition, it can be observed that larger propped areas are created and proppant is placed homogeneously in the static and dynamic cases **(Figure 0.6)**. This is because the job time (60 min pumping and 30 min shut-in) is not significantly longer than the critical time for the dynamic foam (80 min). This indicates good foam stability results and good proppant transportation capabilities. In the medium stability case, the proppant carrying capacity decreases with foam stability, which causes more discontinuity in post-fracture production. In the low stability case, the low viscosity fluid and net pressure lead to a narrow aperture and hence, a long penetration distance according to the total mass balance. This behaviour is due to an early rupture of the foam film during the treatment, which causes the apparent viscosity to drop significantly and to promote proppant settling, leading to poor proppant placement. Therefore, for the unstable foam, there was a tendency to develop

excessive and undesirable fracture length as it could not transport the proppant to a further distance into the fracture.

Besides the fracture geometry, the fracture conductivity is another important treatment output that has a direct impact on the fracture productivity. **Table 0.3** shows the summary of fracture geometries, average proppant concentration, and conductivity for different foam stability. Generally, relatively stable foam provides a better proppant transportation, higher propped area, and higher conductivity. However, the average fracture conductivity of the low stability case is the highest. This is because the proppant accumulates in the nearby wellbore area owing to poor transportation.

Table 0.3. Results of hydraulic fracturing for different foam stability

Properties	**Static**	**Dynamic**	**Med Stability**	**Low Stability**
Fracture height, ft	110	115	100	60
Average fracture width, in	0.28	0.28	0.21	0.16
Propped half-length, ft	285	270	210	285
Propped area, ft^3	1463	1449	735	456
Average proppant concentration, lb/ft^2	0.86	0.87	0.20	0.16
Average fracture conductivity, $md \cdot ft$	369	370	312	872

Figure 0.7 shows the first year cumulative gas productions created by the four cases. The static and dynamic foam cases exhibit the best productivity; their curves are almost the same (overlapping). While the low stability foam provides a higher production during the initial 120 days compared with the medium foam case owing to higher fracture conductivity, it yields the worst cumulative production owing to the limitation of propped area. This phenomenon can be much more significant in ultra-low permeability reservoirs.

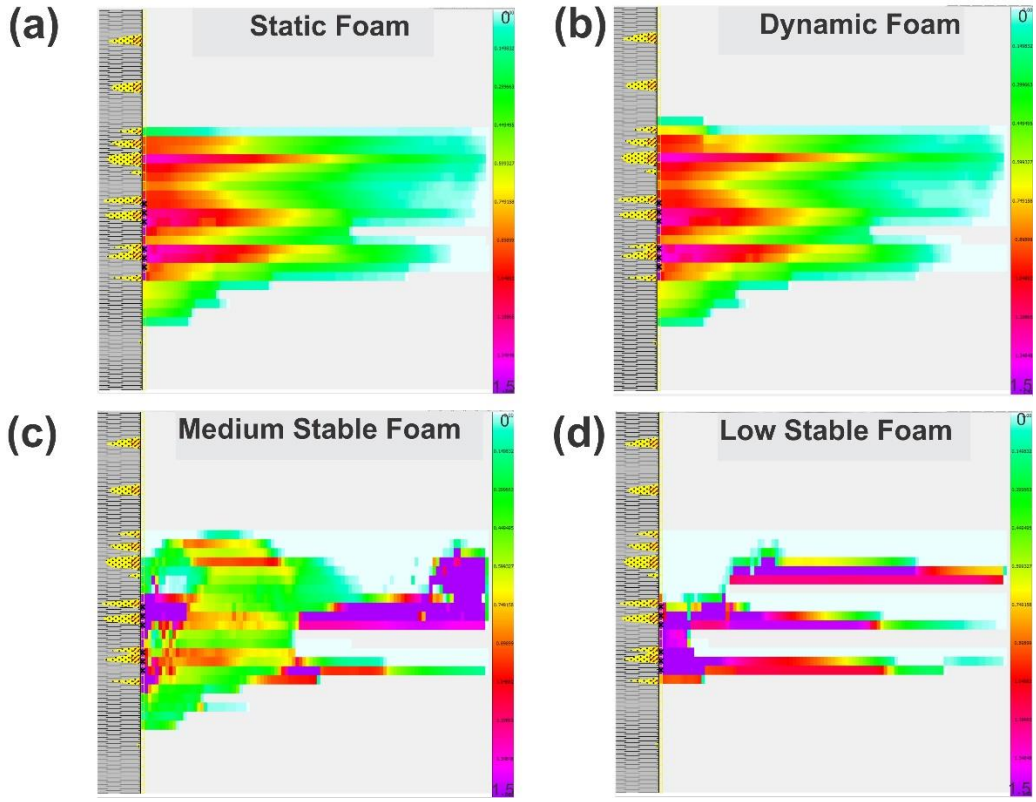

Figure 0.6. Proppant concentration distribution for four different scenarios. Proppant concentration is scaled from 0 $\mathbf{lb/ft^2}$ (light green) to 1.5 $\mathbf{lb/ft^2}$ (purple)

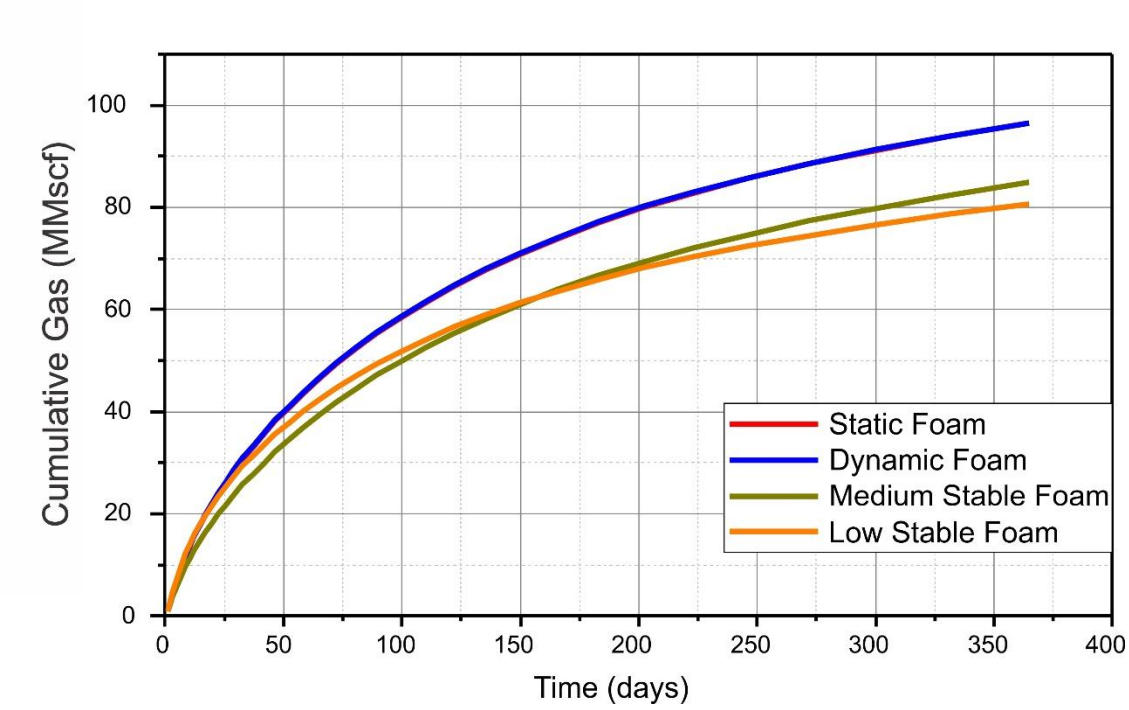

Figure 0.7. Cumulative gas production for four different cases

5.6.2 Shut-in conditions study

After reviewing the above results, it is concluded that foam stability is one of the essential parameters to be considered in designing a foam fracturing treatment.

From the results shown in **Figure 0.8**, it can be observed that the static and dynamic foam exhibit almost the same fracture productivity during the first 80 min shut-in. The initial 140 min (60 min from pumping and 80 min from shut-in) is consistent with the foam rupture time ($t_{rup} = 140$ min) from the experiment stability result. When the foam structure is completely ruptured, only the base fluid remains, resulting in leak-off increase; moreover, the proppant tends to drop at the bottom of the fracture, and the total propped area decreases. Thus, the production significantly decreases. Interestingly, the dynamic foam shows 5 MMscf of cumulative production, which is higher than the static case after 80 min shut-in. We believe that this is because the designed pumping time ($t_{pumping}$) ranges between the stable time (t_s) and critical time (t_{cr}). The proppant transportation in the fracture is improved by the drainage effect. For the low stability case, the foam critical time is much less than the pumping time, and the loss of apparent viscosity during proppant placement leads to less propped area and productivity. From these observations, it is shown that foam drainage, to some extent, improves the fracturing productivity, depending on the location of pumping time between foam stable time and foam critical time (see pumping time example on dynamic foam in **Figure 0.5**). The issue of long shut-in time leads to complete coalescence of foam, and the remaining low viscosity liquid can be detrimental to the final propped area and conductivity while the formation is still in the period of closure. Hence, it is recommended that the design pumping time is just less than the foam critical time and shut-in before the foam would be ruptured.

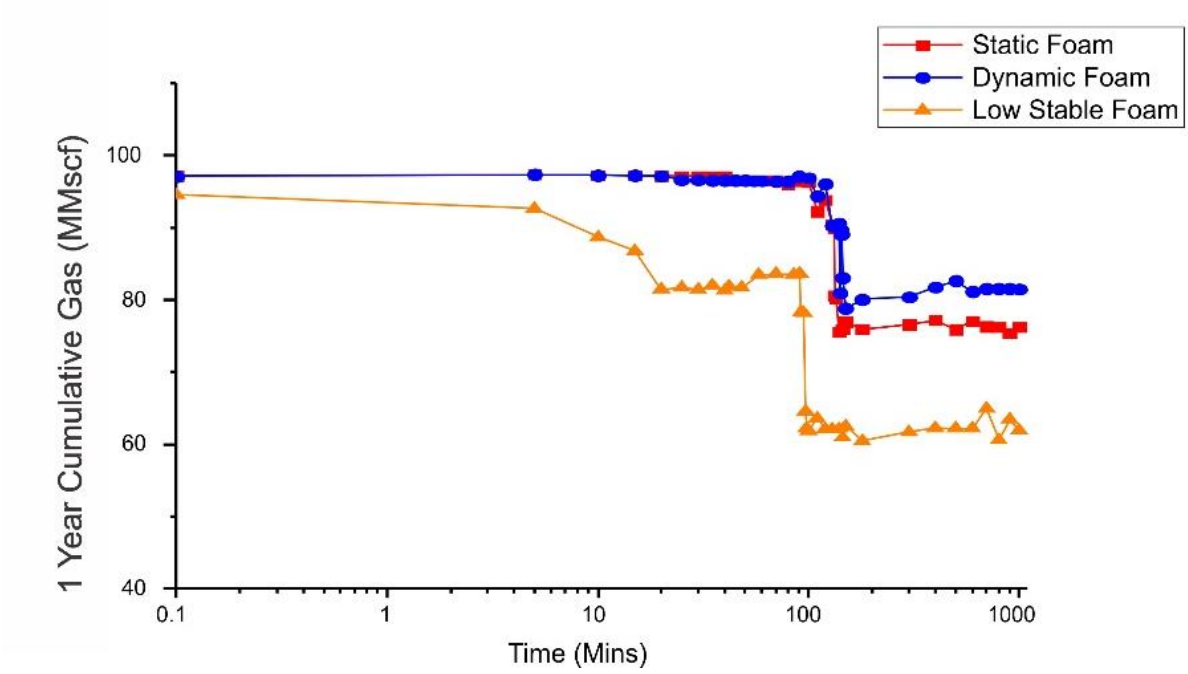

Figure 0.8. Cumulative gas production vs. shut-in time

5.7 Model challenge

In the simulation model, the proppant settling (Harris et al., 2009) is mainly based on the classical Stokes' law, ignoring the effect of microstructure of the liquid foam. In a microscopic study, we can explain the settling mechanism by the amount of net force on a proppant during drainage and gas diffusion process. Generally, as illustrated in Chapter 3 (**Figure 0.8**), there are three different forces of gravity (g), pressure force (F_p), and pulling network force (F_n) that act on each proppant. The network force and the pressure force are the two main force components against proppant settling. This can be analysed by the quasi-static 'surface evolver' method (Brakke, 1992; Davies and Cox, 2009; Jing et al., 2016). Raufaste et al. (2007) proposed that the contribution of the resultant uplift force (network force and pressure force) exerted on a round particle could be expressed by

$$F_{ny} = \frac{0.516}{(1-Q_g)^{0.25}} \frac{\gamma d_o}{\sqrt{A_b}} \tag{10}$$

Where γ is surface tension, d_o is the particle diameter, and A_b is the bubble area. This formula is consistent with **Figure 0.8**, which implies that a high foam quality improves the apparent viscosity owing to an increase in the resultant uplift force by drainage. However, after the critical foam quality has been reached, the uplift force exhibits a sharp decline because the bubble diffusion significantly increases the bubble area (A_b). Therefore, the focus of future work should be on a dynamic analysis of foam structure changes (bubble size distribution) to predict a more realistic proppant transport from rheological data.

5.8 Summary

In this chapter, the experimental and simulated study discovered the relationship between foam stability and fracturing efficiency. Foam stability has been found directly proportional to fracture productivity, as it influence foam rheology which coupled fracture geometry and proppant transportation. Long closure time leads to proppant settling and accumulation at the bottom of the formation, which causes reduction of proppant area and fracture productivity. In addition, foam stability is mainly controlled by foam drainage and disproportionation. The crossover point of those two mechanisms is called foam critical time; and it is an essential parameter for fracturing design. This topic will be further discussed in the following section.

Chapter 6: Hydraulic fracturing by nano-assisted foam-based fluid using a fracture propagation model

6.1 Introduction

This study follows the previous experimental work that used a viscoelastic surfactant with addition of silica nanoparticles. This chapter is a modified and adjusted version of the manuscript, 'Fei, Y., Johnson, R., Gonzalez, M., Haghighi, M., & Pokalai, K. (2017). Experimental and numerical investigation into nano-stabilised foam on hydraulic fracturing application (submitted manuscript)'.

6.2 Experimental results

Figure 0.1a–b show the foam drainage rate of EAPB foam and EAPB-SiO_2 foam, based on a normalized drained liquid ($V_{(t)}$ / $V_{(l0)}$) versus time. $V_{(t)}$ is the liquid volume that has been drained out of the foam, and $V_{(l0)}$ is the total liquid volume in the foam at t = 0. Based on this comparison, silica nanoparticles appear to reduce the gravitational drainage time. In addition, **Figure 0.1c** illustrates that the EAPB foam volume decreases gradually during the first 80 min, then sharply declines until no foam remains at 140 min. However, for EAPB-SiO_2 foam (**Figure 0.1d**), there is still 40% foam volume remaining after 180 min. The foam morphologies (**Figure 0.1e–f**) based on SEM images of the gas-water interface of EAPB foam and EAPB-SiO_2 foams also confirm the nanoparticle-adsorption phenomena that result in nanoparticle foam stabilisation.

The purpose of the particle adsorption at the gas-water interface is to maintain the film thickness, which counters bubble diffusion. When two bubble surfaces become sufficiently close, attractive forces (i.e. van der Waals forces) become significant. As the amplitude of the disturbance increases, the likelihood of film rupture becomes more prevalent. Therefore, having a large number of particles in the adsorbed layers results in a large film thickness, leading to a lower probability of film rupture. A schematic representation of the geometrical configurations for particles at the bubble interface associated with DLVO force is shown in **Figure 0.2**. In summary, foam stabilisation occurs by nanoparticle attachment in the film, thickening it, and preventing film rupture.

Finally, foam stability times or lifetimes are defined and compared in **Table 0.1**. The stable time indicates the period prior to the start of liquid drainage; the critical time indicates the period when the foam shifts from a drainage-dominated regime to a disproportionation-dominated regime; and the rupture time indicates the point at which the foam structure completely collapses. The inclusion of 0.8 wt% silica nanoparticles increases the foam lifetime (stable, critical, and rupture time) between 43% and 100%, enhancing the overall foam stability.

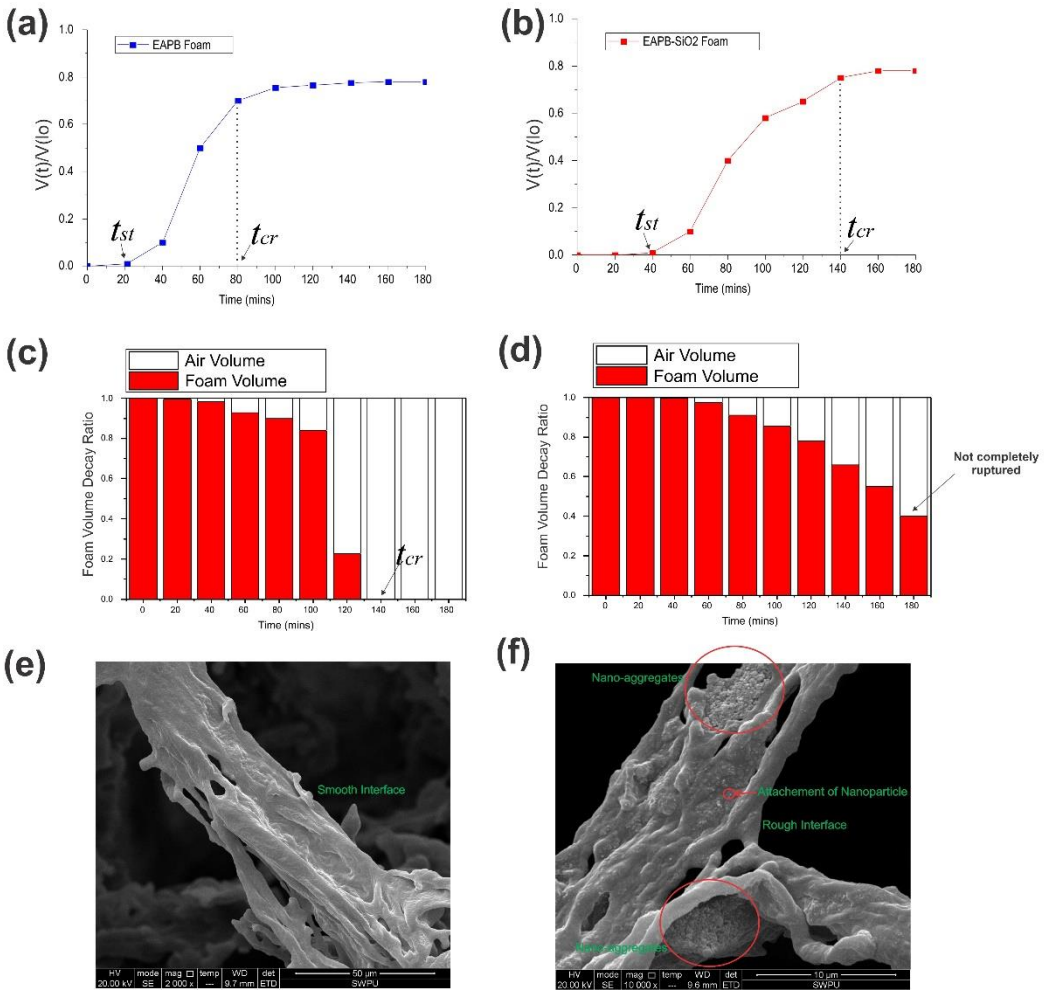

Figure 0.1. Results of foam stability experiments with 3% EAPB and EAPB-SiO_2 foam at 90 ℃: (a)–(b) foam drainage rate of EAPB foam and EAPB-SiO_2 foam; (c)–(d) decay rates of EAPB and EAPB-SiO_2-stabilised foams; (e)–(f) SEM images of EAPB foam and EAPB-SiO_2 foam gas-water interfaces

Table 0.1. Experimental results of foam stability time enhanced by silica nanoparticle

Name	**Value (min)**		**Incremental Ratio**
	Without SiO_2	With SiO_2	
Stable Time	20	40	+ 100%
Critical Time	80	140	+ 75%
Rupture Time	140	200	+ 43%

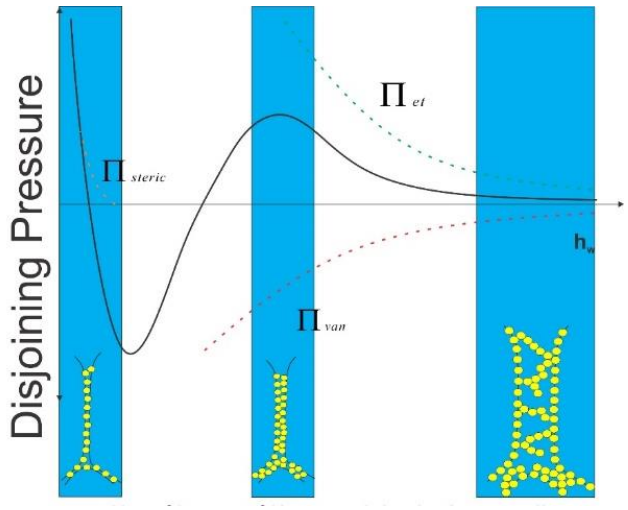

Figure 0.2. An example of disjoining pressure vs. film thickness. Increased layers of nanoparticles in the lamella decrease film thinning. The scale of the nanoparticle layer is for illustration purposes only

6.3 Hydraulic fracturing model

To evaluate the foam stability effect on hydraulic fracturing performance, several foam simulations were performed in a planar-3D hydraulic fracturing model, GOHFER (Barree, 1983). Three different fluid scenarios were evaluated in the simulator: an EAPB foam, an EAPB-SiO_2-stabilised foam, and a low viscosity or slickwater, non-foamed fluid. The reservoir properties and treatment parameters were based on a typical tight sand reservoir and are listed in **To investigate** the relationship between foam stability and post-fracture conductivity, the main outputs of proppant concentration were evaluated at the end of the injection period (i.e. initial shut-in time), and then during various shut-in periods. Finally, the resulting proppant conductivity for each treatment was evaluated at each treatment point of fracture closure. Fracture proppant concentration is a proxy for tracking potential fracture conductivity prior to fracture closure, as it is based on the final proppant concentration and closure stress on the proppant.

Table 0.2. To investigate the relationship between foam stability and post-fracture conductivity, the main outputs of proppant concentration were evaluated at the end of the injection period (i.e. initial shut-in time), and then during various shut-in periods. Finally, the resulting proppant conductivity for each treatment was evaluated at each treatment point of fracture closure. Fracture proppant concentration is a proxy for tracking potential fracture conductivity prior to fracture closure, as it is based on the final proppant concentration and closure stress on the proppant.

Table 0.2. Input data for hydraulic fracturing simulation condition

Well Parameters	Value
Reservoir thickness, ft	200

Reservoir pressure, psi	1857
Permeability, md	0.1
Porosity, %	10
Water saturation, %	50
Gas saturation, %	50
Fracturing Treatment Parameters	Value
Type of fracturing fluid	*EAPB foam, EAPB-SiO_2 foam, and slickwater*
Clean volume, gal	*57,000*
Proppant type, mesh	*Ceramic 20/40*
Proppant amount, lb	*175,500*
Initial foam quality, %	*52, 60, and 70*
Shut-in time, min	*0, 30, 60, 120, and 180*
Pumping rate, bpm	*10, 20, 30, 40, and 50*

6.4 Mathematical formulation

The fully 3D hydraulic fracturing simulator incorporates a series of sequential finite-difference solutions based on a fixed spatial grid (Barree, 1983). First, fracture-fluid pressures (P_f) are calculated based on Poiseuille's law for flow between parallel plates from the Navier–Stokes equations. The distribution of net pressure (P_{net}) resulting from fluid pressures is used to calculate the fracture width distribution (Barree and Conway, 1994):

$$\mathrm{w} = \int \frac{(1-\nu^2)}{\pi E r} P_{net} ds \tag{14}$$

Where ν is the Poisson's ratio and E is the Young's modulus. The fracture width (w) is obtained by integrating the displacement for a single point load over the surface of the fracture. In addition, the vertical and horizontal components of fluid velocity are provided by the implicit solution of the system of equations generated by the finite-difference fluid flow formulation. These velocity components are used to compute the proppant movement with the fracture. The vertical slurry velocity (ft/s) can be estimated (Barree and Conway, 1995) by

$$v_s = \frac{w^2}{12\mu_a} \frac{\partial(\Delta\rho_s g h + 144 P_f g_c)}{\partial z} \tag{15}$$

Where μ_a is apparent slurry viscosity and ρ_s is slurry bulk density. The slurry viscosity (μ_a) is dependent on the proppant volume fraction and liquid viscosity. During the proppant transport and placement in the fracture by the foam fracturing fluid, the liquid viscosity or foam viscosity was analyzed by considering the rheology of non-Newtonian fluids. The foam rheological characterization by EAPB with and without silica nanoparticles will be described in the next section.

In addition, the slurry bulk density (ρ_s) can be estimated by the combination of proppant density (ρ_p) and foam density (ρ_f) (Barree and Conway, 1995):

$$\rho_s = C_v\rho_p + (1 - C_v)\rho_f \tag{16}$$

Where C_v is the volume fraction of particles. The foam density, which relates to foam quality (Q_g), liquid phase density (ρ_l), and gas phase density (ρ_g) can be estimated by

$$\rho_f = Q_g\rho_g + (1 - Q_g)\rho_l \tag{17}$$

The gas phase density (ρ_g) can be either the CO_2 or N_2 density, which is a function of pressure (P) and temperature (T_F) (Barree et al., 2009):

$$\rho_{CO_2} = [0.6242e^{-0.0079T_F}] \times \frac{P^{(0.0007T_F+0.074)}}{(1 + (P/(800T_F/70))^{-2.8})^{0.357}} \tag{18}$$

$$\rho_{N_2} = \frac{(0.98 - 0.00045T_F)}{(1 + (P/(8800 + 13T_F))^{-1.1})^{0.95}} \tag{19}$$

Then, the calculated fluid velocity distribution from **Eq. 15** is used to estimate the concentration distributions of proppant at each point in the fracture, which results from the solution of the diffusivity equation in two dimensions (Barree and Conway, 1995):

$$-v = \frac{\delta C_v}{\delta x} = \frac{\delta C_v}{\delta t} \tag{20}$$

Finally, the proppant concentration associated with closure stress can determine the packed width (w_s), which is used to calculate the baseline conductivity distribution (C_f) (Barree et al., 2016):

$$C_f = k_f w_f = K_s * 1000 * \frac{w_s}{12} \tag{21}$$

Where K_s is the packed permeability at a given stress. The details of the mathematical formulation workflow are summarized in **Figure 0.3**.

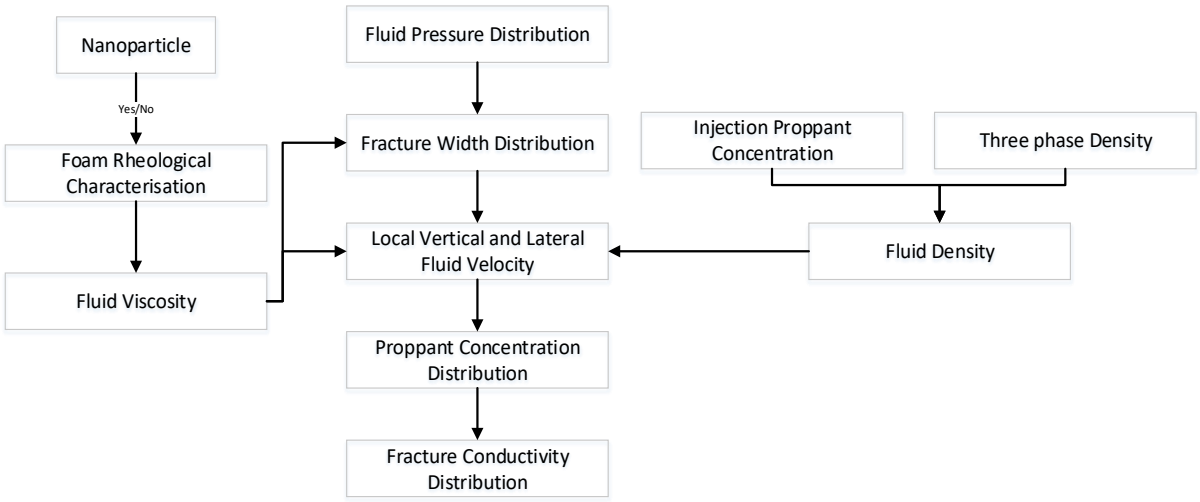

Figure 0.3. Workflow of the mathematical formulation for fracturing model

6.5 Foam rheological characterisation

In each case, an initial foam quality is assumed, and then varied upwardly (i.e. 52%, 60%, and 70% as most commonly used in actual treatment) with two types of foams: EAPB- and EAPB-SiO_2-stabilised. The drainage rate (v_d) from the experimental results (**Figure 0.1a–b**) are inputted into **Eq. 1** to calculate the time-dependent foam quality. The time dependence of a complex foam is modelled by predicting the variance of two primary base fluid (power law) parameters, n_{Liquid} and k_{Liquid}, and then by coupling with the foam quality (Q_g^t) to approximate the parameters, n_{Foam} and k_{Foam}, for the foamed system. Published experimental correlations (Khade and Shah, 2004) have analogously predicted the consistency and flow behaviour index of foam fluids using **Eq. 9** and **Eq. 10**. From the experimental results, the volume of EAPB-stabilised foam completely collapses at 140 min; however, the foam volume of EAPB-SiO_2-stabilised foam still remains at 40% foam volume after 180 min (**Figure 0.1c–d**). Following disassociation, the fluid is characterized by the base fluid rheology, which is assumed to be completely degraded by breakers; thus, the fluid eventually reverts to the viscosity of water (1 cP). Using the above results, then the apparent viscosity can be plotted as shown in **Figure 0.4**.

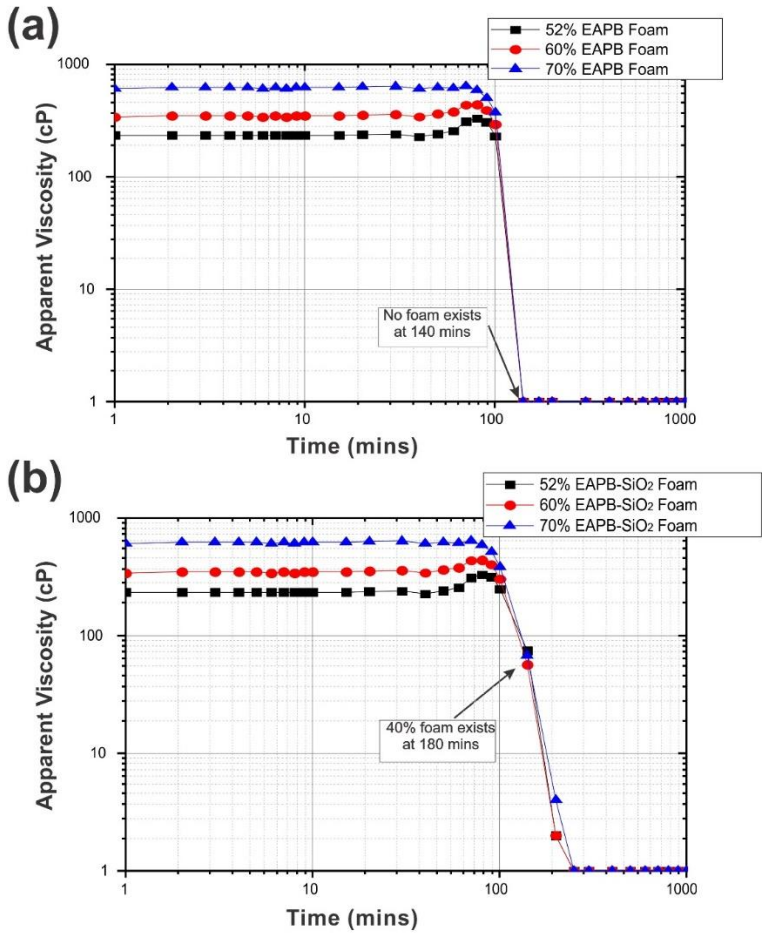

Figure 0.4. Characterisation of rheological properties of EAPB foam and EAPB-SiO_2 foam with three different foam qualities

6.6 Results and Discussions

Figure 0.5 shows the results of proppant concentration distribution predicted by the hydraulic fracture modelling using all three fluids: EAPB foams, EAPB-SiO_2 foams, and slickwater (100% water-based fluid) injected at a pumping rate of 30 bpm. It can be observed in the figure that the potential progression of proppant redistribution within the fracture develops within 0 min shut-in time (i.e. the end of injection) to 180 min shut-in before closure. For comparison purposes, the proppant concentration is observed at each of these times and is plotted from 0 (blue) to 1.5 (red) lb/ft^2. Certainly, the final dimensions at closure are the only dimensions. Apparently, the use of slickwater fracturing results in poorer proppant transport and less propped area compared with the two foam cases. The poor proppant transport is caused by the low viscosities and rapid leak-off rate of water, which results in rapid settling of the proppant particles. For both foam cases, the initial propped geometries (shut-in = 0 min) are almost the same. This indicates that both foams are stable and maintain a constant apparent viscosity during pumping, which provides a better proppant transport capability than slickwater treatment. However, the final fracture geometries are relatively different (at shut-in = 180 min). For EAPB foam, the propped area becomes more non-uniform, leaving more upper area unpropped within the propped length. For EAPB-SiO_2 foam, the propped area remains almost the same, and the minor proppant redistribution indicates a stabilised foam structure that

reduces the proppant settling rate. Alternatively, the results also suggest that in very low permeability formations, proppant settling becomes a major problem for proppant placement because it tends to gravitationally settle before fracture closure occurs.

Next, the modelling can illustrate the effect of pumping rate on the propped area as shown in **Figure 0.6.** For comparison purposes, the fracture conductivity is plotted from 0 (blue) to 50 (red) md ft. At shut-in time of 0 min, the total proppant laden area of slickwater is less than that created by the EAPB foam and EAPB-SiO_2 foam. This is because the proppant transport is affected by the low viscosity of slickwater. After shut-in time of 180 min, sand accumulates at the bottom of the fracture in the EAPB foam treatment. In general, the EAPB foam forms a thinner high-conductivity sand bed with a large amount of sand settling and convecting from the upper regions of the fracture regardless of the pumping rate. The propped area of EAPB-SiO_2 foam is higher than either that of the slickwater or EAPB treatments largely as a result of negligible foam decline (**Figure 0.6)**. However, if foam breakage occurs before fracture closure, the foams lose viscosity rapidly and proppant settling accelerates, significantly reducing the propped dimensions.

A parametric study of foam quality impact on the propped area is also shown in **Figure 0.7**, where the size of the propped area is directly proportional to the foam quality. It is observed that high foam qualities provide high viscosities. The high viscosity in this low permeability reservoir case increases the net pressure and results in fracture height growth and improved proppant transport. However, when fracturing a thin reservoir where there are negative consequences to height growth, using less stable, low quality foam may be desirable in order to minimize the net pressures and out-of-zone height growth.

As expected, less stable, low quality foam does not create longer propped fracture lengths than higher quality foams largely as a result of less effective proppant transport qualities. Similar to previous observations, using an EAPB foam causes proppant settling and high accumulation at the bottom of the fracture after 180 min shut-in. Similar to prior modelling studies (Johnson, 1995), proppant laden fluids convect downwardly towards the bottom of the fracture and more settling and poor proppant placement occur in the fracture. This is largely a result of the foam becoming more unstable during the shut-in period prior to fracture closure.

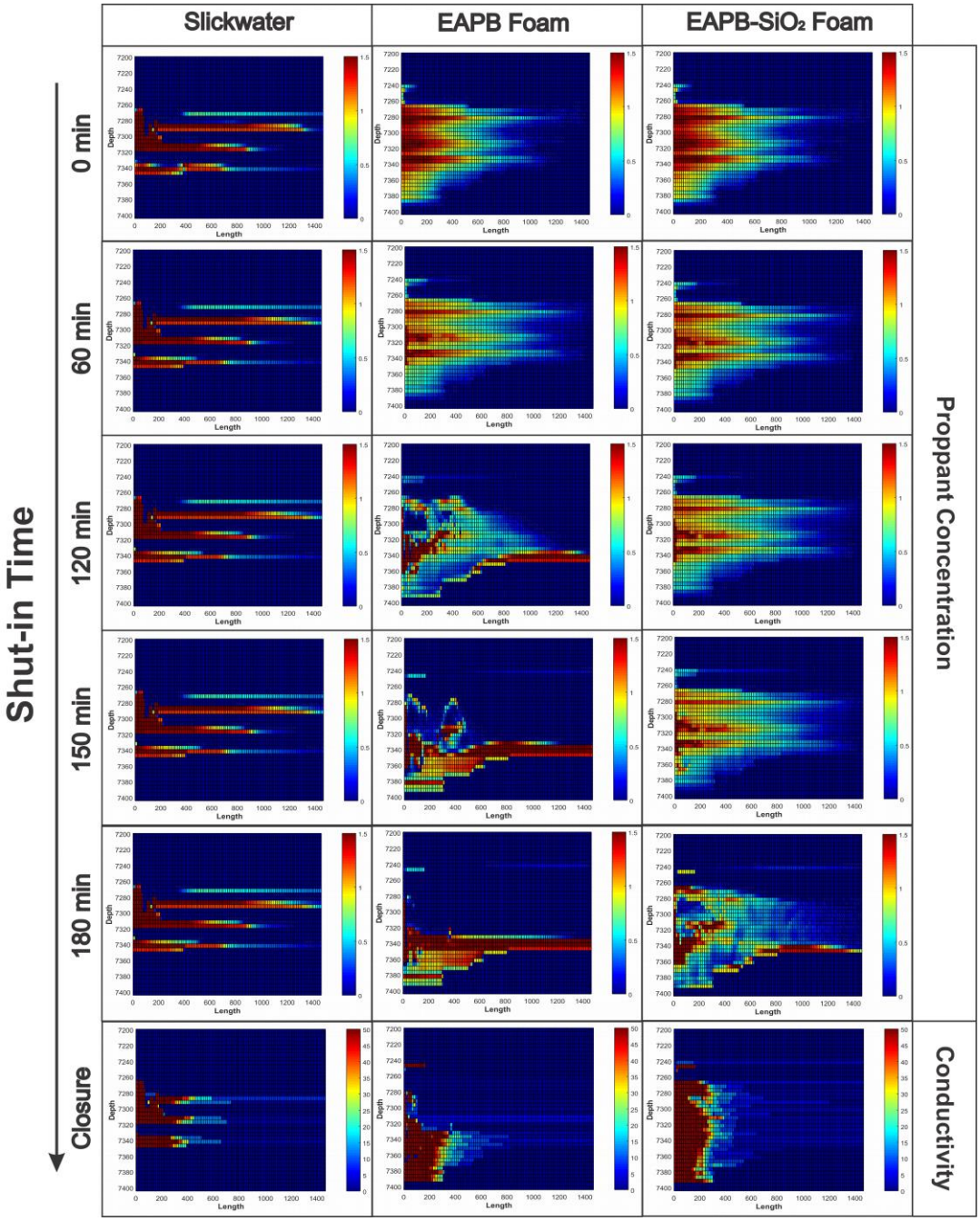

Figure 0.5. Proppant concentration distribution (lb/ft^2) vs. shut-in time for slickwater, EAPB foam, and EAPB-SiO_2 foam with 60% foam quality at 30 bpm of pumping rate

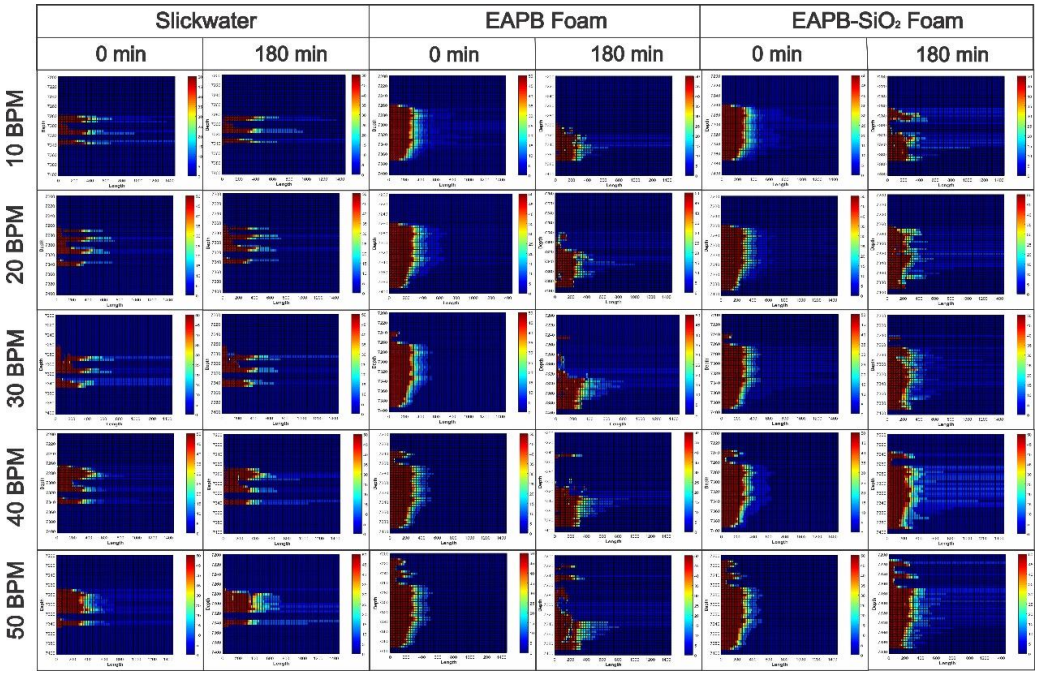

Figure 0.6. Fracture conductivity (propped area) vs. pumping rate for slickwater, EAPB foam, and EAPB-SiO_2 foam with 60% foam quality

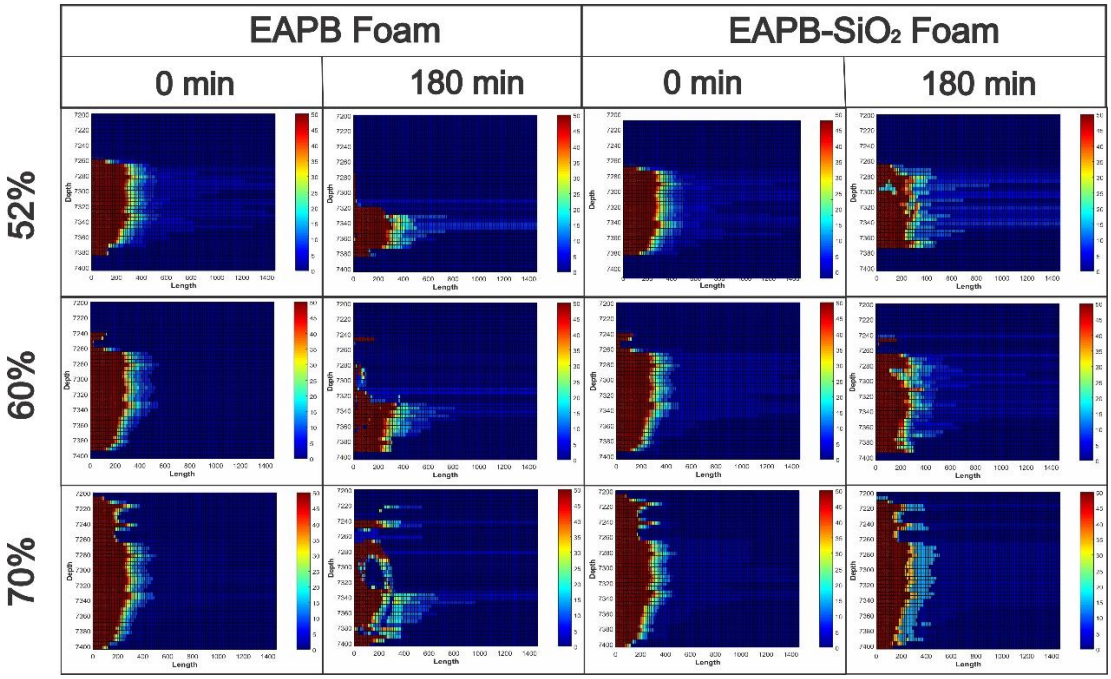

Figure 0.7. Fracture conductivity vs. foam quality for the two foam cases from 0 to 180 min shut-in time.

Simulations of one year cumulative production based on treatments using EAPB foam, EAPB-SiO_2 foam, and slickwater are shown in **Figure 0.8** based on varying injection rates. As expected, in a low permeability, tight gas case, the highest cumulative gas production is achieved by treatments using the highest injection rate, creating the longest propped lengths. When comparing between foam and slickwater treatments, the predicted productivity of

slickwater treatments are less sensitive to the pumping rate except in the cases of low injection rates, where proppant settling velocity is high. At the end of treatment (shut-in time = 0 min), the productivity of both foam cases is higher than that of slickwater. However, the productivity of EAPB foam decreases significantly after 60 min shut-in, particularly at low pumping rates of 10 bpm and 20 bpm. The longest shut-in actually yields the lowest cumulative production for EAPB foam as no foam exists to suspend the proppant, which leads to proppant accumulation at the bottom to form a smaller propped area. This observation is also consistent with previous proppant concentration studies. By contrast, for the EAPB-SiO_2 foam, the fracture geometry is uniformly propped and there is negligible proppant settling; the productivity therefore is maintained during long shut-in times. This comparison highlights the critical role of foam stability and the final position of the proppants, which contributes to the effectiveness of the post-fracture productivity.

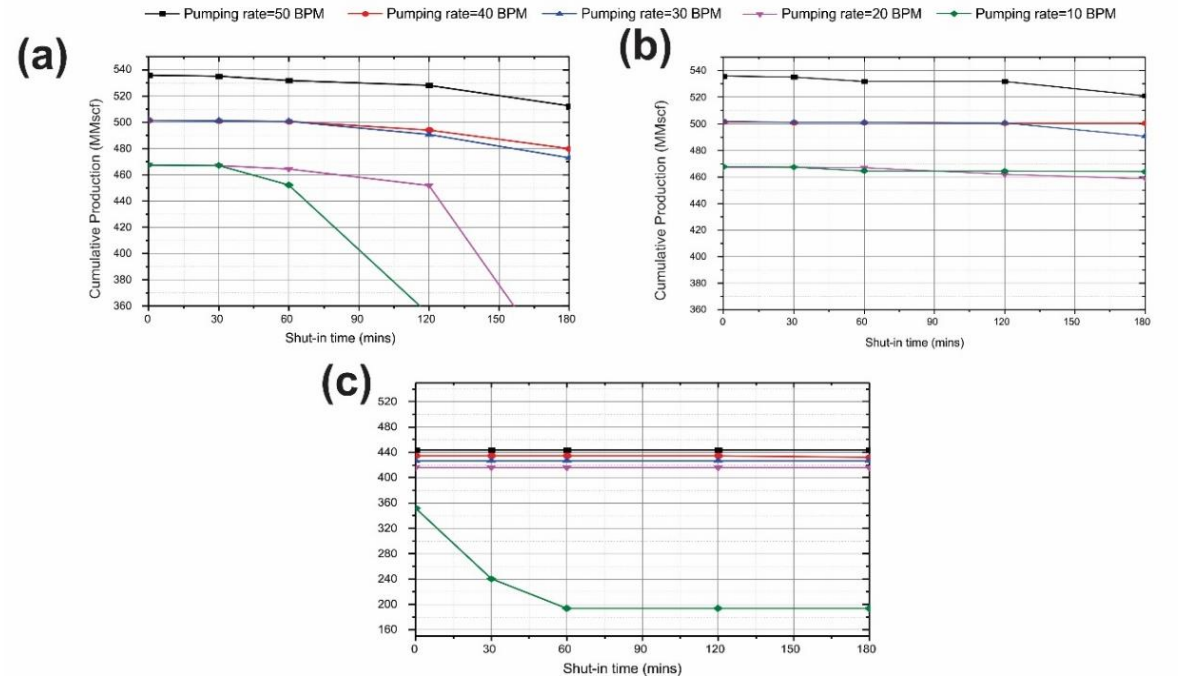

Figure 0.8. Fracture productivity generated by different pumping rates: (a) 60% EAPB foam, (b) 60% EAPB-SiO_2 foam, and (c) slickwater

6.7 General guideline for foam treatment design

In order to develop guidelines for foam fracturing design, understanding the foam rheology associated with foam stability behaviour is essential. **Figure 0.9** illustrates two different foam rheology profiles representing standard foam (black curve) and nano-stabilised foam (red curve), where the evolution process can be found from 1 to 4 and 5 to 8 respectively. For standard foam, the rheology experiences a stable period (1 to 2) and unstable period (2 to 4). In the stable period, the foam quality remains unchanged and maintains a constant foam viscosity. In the unstable period, the foam viscosity initially increases owing to foam drainage; then it decreases sharply by disproportionation (gas diffusion). The stable time (t_{st}), critical time (t_{cr}), and rupture time (t_{rup}) can be experimentally recorded to determine the change of foam behaviour (**see example in Table 0.1**). For the nano-stabilised foam, a longer stable

period and unstable period can be achieved, mainly because of the adsorption of nanoparticles that prevent bubble coalescence caused by thinning and rupture of the film between bubbles. The foam rheology associated with foam stability behaviour can therefore provide useful information for foam fracturing treatment, which is summarized in **Table 0.3**.

It is recommended that the pumping time should be less than or equal to the foam stable time. This is because the foam viscosity is constant during this period, which maintains a stable proppant carrying capacity. In addition, better accuracy is achieved for a hydraulic fracturing model that simulates proppant transport using foam with constant apparent viscosity. For a nano-stabilised foam, a long stable time can be attained, which allows more slurry volume to be pumped with constant apparent viscosity, resulting in higher productivity. In addition, it is not beneficial to use ultra-stable foams in highly permeable reservoirs because proppant settling can be prevented by rapid fracture closure before foam breakage occurs. However, for low permeability formations like unconventional reservoirs, a long closure time is observed, which leads to decrease in the propped area by migration of large amount of proppant to the bottom fracture layer. Therefore, the advantage of using ultra-stable foams is to prevent proppant settling, which will maintain the propped area and thus improve productivity. Those ultra-stable foams can be achieved by introducing nanoparticles.

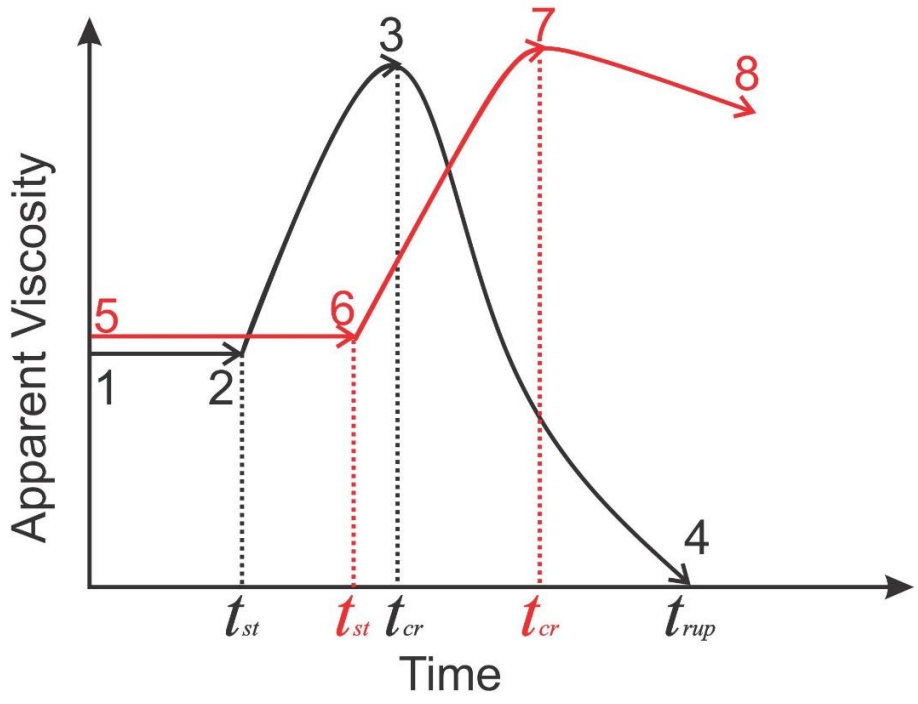

Figure 0.9. Generic of foam rheology profile coupled with foam stability factor. The black curve represents standard foam, while the red curve represents nano-stabilised foam. Time scale is for illustration purposes only

Table 0.3. Summary of foam fracturing treatment with different foam stability behaviour

Type	Process	Foam Behaviour	Fracturing Treatment
Without Nanoparticle	1→2	Stable Periods 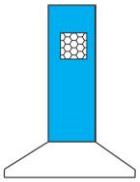	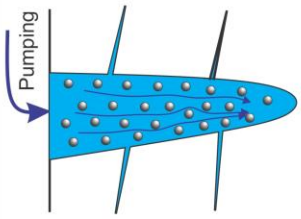
	2→3	Drainage Dominated 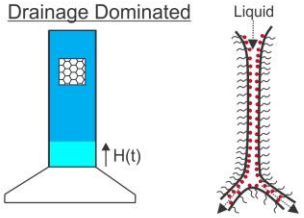	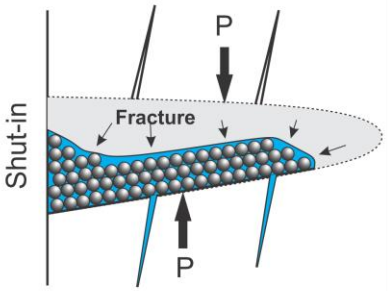
	3→4	Disproportionation Dominated 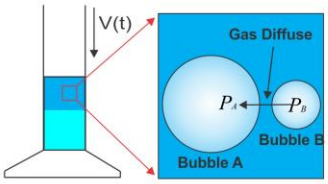	
With Nanoparticle	5→6	Stable Periods 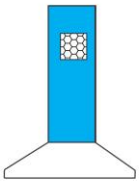	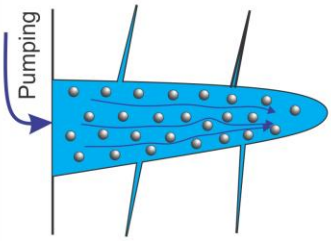
	6→7	Drainage Dominated 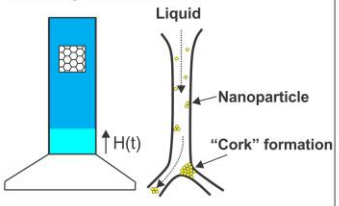	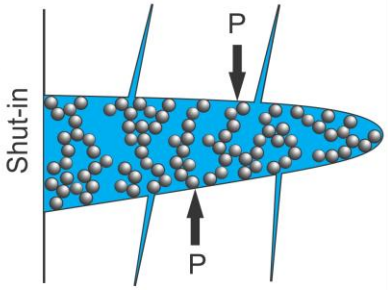
	7→8	Disproportionation Dominated 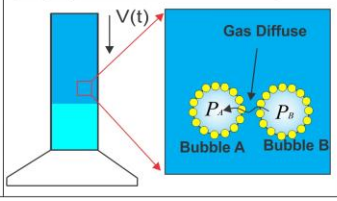	

6.8 Summary

The purpose of this chapter is to characterize foam stability and the effects of nanoparticle inclusion on proppant settling during fracture closure. Experimental observations indicate foam stability increases 2-3 fold in presence of 0.8wt% silica nanoparticles. The enhancement of foam life-time by nanoparticles can improve fracturing conductivity by preventing proppant settling during closure, thus minimize productivity loss.

Chapter 7: Simulation of hydraulic fracturing with liquefied petroleum gas.

Fei, Y., Gonzalez, M., Nguyen, V. Q., Lei, Z. Y., Pokalai, K., Sarkar, S., & Haghighi, M. (2016). Simulation of hydraulic fracturing with propane-based fluid using a fracture propagation model coupled with multiphase flow simulation in the Cooper Basin, South Australia. APPEA Journal, 56, 415-426.

Simulation of hydraulic fracturing with propane-based fluid using a fracture propagation model coupled with multiphase flow simulation in the Cooper Basin, South Australia

Lead author
Yang Fei

Y. Fei, M.E. Gonzalez Perdomo, V.Q. Nguyen, Z.Y. Lei, K. Pokalai, S. Sarkar and M. Haghighi
Australian School of Petroleum
The University of Adelaide
Adelaide, SA 5005
yang.fei@adelaide.edu.au

ABSTRACT

In many unconventional reservoirs, gas wells do not perform to their potential when water-based fracturing fluids are used for treatments. The sub-optimal fracture productivity can be attributed to many factors such as effective fracture length loss, low load fluid recovery, flowback time, and water availability. The development of unconventional reservoirs has, therefore, prompted the industry to reconsider waterless fracturing treatments as viable alternatives to water-based fracturing fluids.

In this paper, a simulation approach was used by coupling a fracture propagation model with a multiphase flow model. The Toolachee Formation is a tight sand in the Cooper Basin, around 7,200 ft in depth, and has been targeted for gas production. In this study, a 3D hydraulic fracture propagation model was first developed to provide fracture dimensions and conductivity. Then, from an offset well injection fall off test, the model was tuned by using different calibration parameters such as fracture gradient and closure pressure to validate the model. Finally, fracture propagation model outputs were used as the inputs for multiphase flow reservoir simulation.

A large number of cases were simulated based on different fraccing fluids and the concept of permeability jail to represent several water-induced damage effects. It was found that LPG was a successful treatment, especially in a reservoir where the authors suspected the presence of permeability jails. The authors also observed that total flowback recovery approached 76% within 60 days in the case of using gelled LPG. Modelling predictions also support the need for high-quality foam, and LPG can be expected to bring long-term productivity gains in normal tight gas relative permeability behaviour.

KEYWORDS

Tight gas, Cooper Basin, LPG fracturing fluid.

INTRODUCTION

Unconventional hydrocarbon reservoirs such as tight gas, shale gas and coalbed methane are becoming important resources for existing and future oil and gas supply; however, because of the low-permeable nature of unconventional reservoirs, they need hydraulic fracturing treatment. In this operation, a large volume of fracturing fluid is injected at high rates into the wellbore to overcome the rock and to induce fractures around the wellbore in the targeted formation. During a hydraulic fracture operation some of the fracturing fluid will leak-off from the fracture and invade the reservoir. In tight sand reservoirs the invaded water-based fracturing fluid may cause damage (water blockage) to reservoir permeability and fracture conductivity. Consequently, the use of water-based fracturing fluids in tight gas reservoirs may limit the potential of well productivity and result in longer flow-back times (Lestz et al, 2007).

Typically, water-based fluids are the simplest and most cost-effective solution to induce a fracture in a rock formation; however, alternatives to water-based fluids have significantly outperformed water treatments in many reservoirs. For instance, in 1970 foams were extensively used in various depleted reservoirs in which water fractures were not effective (Economides and Martin, 2007). More recently, the development of many unconventional reservoirs has prompted the industry to reconsider waterless fracturing treatments as viable alternatives to water-based fracturing fluids. In these reservoirs, the interactions between the rock formation and the fracturing fluids may be detrimental to hydrocarbon production (Ribeiro and Sharma, 2013).

The LPG fraccing technique has been commercially applied in unconventional reservoirs in North America. Gandossi (2013) reported that between 2008 and 2013, more than 2,000 LPG fracturing operations were carried out by a Canadian service company in North America. The LPG fluid's properties such as density, viscosity and surface tension with complete solubility in formation hydrocarbons are very beneficial (Gupta, 2009). In a field application, LPG is gelled before fracturing to allow transport of the proppant into the fracture (Leblanc et al, 2011).

In this paper, a diagnostics fracturing injection test (DFIT) was studied to validate instantaneous shut in pressure (ISIP), closure pressure, type of leak-off, and reservoir permeability. Then, based on mechanical rock properties from log data, minimum horizontal stress was estimated and a 3D hydraulic fracturing propagation model was developed (Pokalai et al, 2015). Eventually the results of the fracture dimension and conductivity were provided in a multiphase flow model to simulate the flowback and gas production of the fractured wells.

Since a hydraulic fracturing operation has already been carried out in well Merrimelia-62, the authors used nitrogen foam as a base case. After matching and validation with actual field flowback and history production, the new concept of permeability jail was investigated by a sensitivity analysis for three different fluid formulations: slickwater, N_2 foam, and LPG.

Conventional fracturing fluids include water-based and polymer-containing fluids. Unconventional fracturing fluids include non-polymer-containing fluids such as viscoelastic surfactant fluids, methanol-containing fluids, liquid CO_2-based fluids, and LPG-based fluids.

The ideal fracturing fluid should have:

1. compatibility with the formation to minimise formation damage;
2. sufficient viscosity to create a fracture and transport the proppant; and,
3. rapid viscosity breakdown after the proppant is placed to maximise fracture conductivity (Economides and Martin, 2007).

Figure 1 describes the significance of the fracturing fluid properties in hydraulic fracturing treatment (Economides and Martin, 2007; Economides and Nolte, 2000; Fink, 2013; Gidley et al, 1989; Valko and Economides, 1996).

The following are a few issues that need to be considered when using water-based fracturing fluids:

1. effective fracture length loss (Taylor et al, 2010);
2. low load fluid recovery (Economides and Martin, 2007);
3. flowback time (Al-Kanaan et al, 2013); and,
4. water availability.

Taylor et al (2010) suggested that the reason for phase trapping (fluid retention) is due to the high capillary threshold pressure. Values of the threshold pressure can be estimated using the Laplace-Young equation (Chalbaud et al, 2006) (Eq. 1).

$$P_C^{th} = P_{non\text{-}wetting} - P_{wetting} = \frac{2\gamma\cos\theta}{r} \quad (1)$$

In Equation 1, P_C^{th} is capillary threshold pressure (psi), γ is surface tension (dyn/cm), θ is the contact angle (degree), and r is pore radius (microns).

When pressure dropdown between reservoir pressure and flowing buttonhole pressure are not large enough to overcome the capillary threshold pressure, the fluids remain in the formation (Holditch, 1979). Taylor et al (2010) reported that capillary pressures of 1,450–2,900 psig, or much higher, can be present in low-permeability formations at low-water saturation levels. In addition, Economides and Martin (2007) presented that injecting water-based fracturing fluids into high-capillarity reservoirs results in creation of high water saturation in the near-wellbore. The relative permeability of gas will be dramatically reduced by the increasing water saturation (see Fig. 2).

Furthermore, the rock formation reacts both chemically and mechanically with the injected fluid. Clays may swell when placed in contact with water, but clays do not interact significantly with CO_2, N_2 and LPG. Many unconventional rock formations lose some of their mechanical integrity when placed in contact with water. As the rock becomes softer, the rock further closes on the proppant, thereby promoting proppant embedment (Ribeiro and Sharma, 2013).

LPG AS A FRACTURING FLUID

Hurst (1972) introduced a new stimulation technique using liquid gas. It is a fracturing treatment using an absolutely water-free fluid system. LPG gases are a mixture of petroleum natural gases (e.g. propane and butane) existing in a liquid state at ambient temperatures and moderate pressure (less than 200 psi). It behaves as other liquids do as long as they are under adequate pressure and below their critical temperature.

In field conditions, cold LPG at moderate pressure is frequently blended with proppant, gellant and breaker before being pumped into the formation for fracture. After pumping, the LPG changes phase behaviour as it converts to a gas phase due to reservoir conditions (increased pressure and temperature) and mixing with the reservoir gas (Lestz et al, 2007). Figure 3 demonstrates that with increasing the methane and propane mixture ratio, the saturation curve tends towards to the left. If the formation temperature is 160°F, with an initial 100% propane as fracturing fluid being pumped into the formation, the 100% liquid phase propane converts to a gas phase when the methane mixture ratio reaches 40%.

Leblanc et al (2011) presented a successful case for the application of a LPG-based fracturing fluid in the McCully gas field, in Canada. The results of using LPG, in comparison with a water-based fracturing fluid, show significant improvement in the McCully field, including:

1. the removal of water handling issues;
2. 100% of the propane was recovered within two weeks of the fracture treatment; and,
3. propane yielded an effective average fracture half-length that was double to that achieved by a water fracture.

In addition, laboratory tests have been conducted in the Montney Gas Reservoir in Canada, the results of which show that LPG is one of the best fracturing fluids and provides superior performance of regained methane permeability in comparison to all other conventional fluids (Taylor et al, 2010).

Gandossi (2013) demonstrated a comprehensive overview of hydraulic fracturing for shale gas production and presented a summary of the potential advantages and disadvantages of the LPG fracturing technique (see Table 1). One major disadvantage of LPG is that it is flammable and explosive; hence, it requires being carefully handled and pumped. Furthermore, nitrogen is usually mixed in either the pumping system or the fracturing fluid itself to prevent an explosion (Soni, 2014).

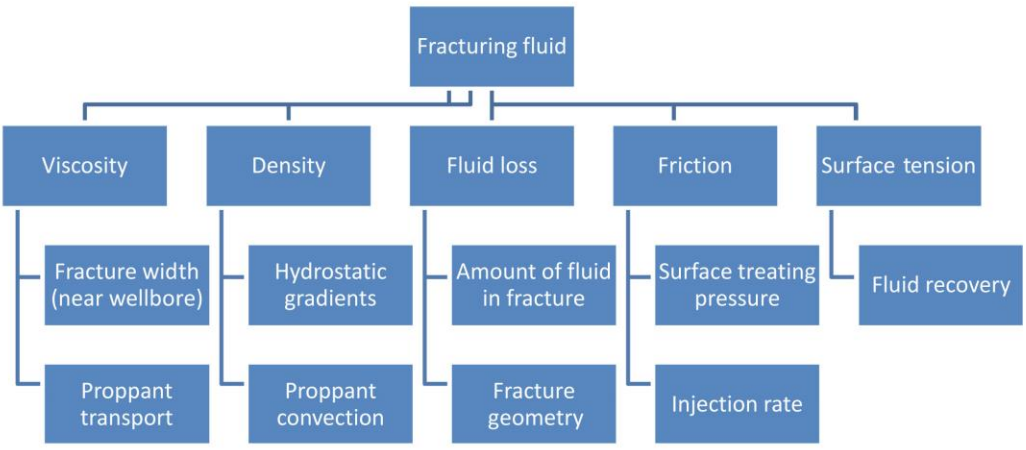

Figure 1. Physical and chemical properties of hydraulic fracturing fluid.

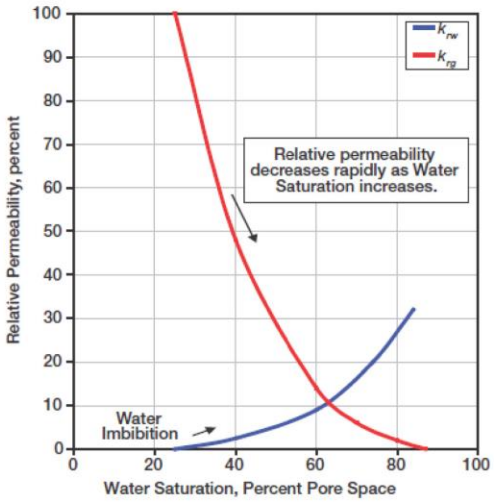

Figure 2. Effect of water imbibition on relative permeability change (Economides and Martin, 2007).

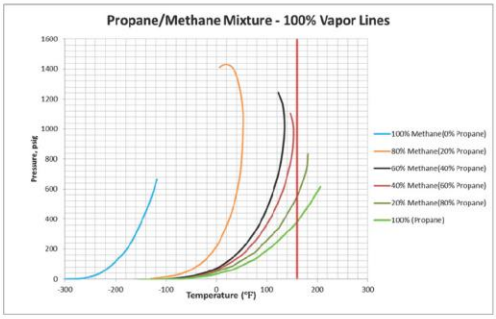

Figure 3. Propane-methane mixtures at formation conditions (Leblanc et al, 2011).

Table 1. Summary of potential advantages and disadvantages for LPG fracturing techniques (Gandossi, 2013).

Potential advantages	Potential disadvantages
• Water usage much reduced or completely eliminated. • Fewer or no chemical additives are required. • Flaring is reduced. • Truck traffic is reduced. • LPG is an abundant by-product of the natural gas industry. • Increases the productivity of the well. • Lower viscosity, density and surface tension of the fluid, which results in lower energy consumption during fracturing. • Full fluid compatibility with shale reservoirs (phase trapping virtually eliminated). • No fluid loss, recovery rates (up to 100%) possible. • Very rapid clean up.	• Involves the manipulation of large amounts of flammable propane, hence is potentially riskier than other fluids. • Higher investment costs. • Success relies on the formation's ability to return most of the propane back to surface to reduce the overall cost.

GEOLOGY AND HYDRAULIC FRACTURING IN THE COOPER BASIN

The Cooper Basin is a late Carboniferous to Middle Triassic, non-marine sedimentary basin in eastern–central Australia, spanning more than 130,000 km². The basin straddles the border of SA and Queensland, as illustrated in Figure 4. The Cooper Basin is the most significant onshore oil and gas province in Australia and is the primary onshore source for natural gas production (Gravestock and Jensen, 1998). Since the late 1960s significant volumes of oil, gas and LPG have been produced from more than 190 separate gas fields and 115 oil fields within the Cooper Basin (Santos, 2015). The primary fracture targets in the Cooper Basin tight gas are the Tirrawarra, Patchawarra and Toolachee formations. This paper's target formation is described in further detail below. The stratigraphic column of the Cooper Basin is shown in Figure 5.

The Toolachee Formation has large amounts of channels and crevasse splay deposits, with an average channel thickness of 15 ft and total gross thickness of 200–300 ft. The Toolachee Formation is widespread throughout the Cooper Basin and contains 25 of the basin's gas reserves (McGowen et al, 2007). There are two units within the Toolachee; the lower is carbonaceous shale with interbedded coal and sandstone, while the upper is sandstone with interbedded coals and shale. The reservoir permeability varies between 0.5 and 50 mD. Hydraulic fracturing in the Toolachee Formation accounts for 30% of all fracture treatments within the Cooper Basin.

Hydraulic fracturing has been used since 1968 to stimulate the Cooper Basin's oil and gas reservoirs. As of 2013, 700 wells in the Cooper Basin have been fracture stimulated and more than 1,500 individual fracture stimulation stages have been pumped (Braddeley, 2013). Figure 6 illustrates the increase in popularity of hydraulic fracturing in the Cooper Basin.

The main issues with hydraulic fracturing in the Cooper Basin have included high fracture gradients, high tortuosity and high pressure dependent leakoff (PDL) (Scott et al, 2013). Fracture gradients commonly range from 0.9–1.3 psi/ft because reservoir quality reduces or formation depth increases. High tortuosity is most likely caused by fracture tuning where the fracture remain principally vertical but is forced to counteract the maximum horizontal stress in the near wellbore region as it reorients after initiating from an unfavourable direction (Chipperfield and Britt, 2000). Lastly, McGowen et al (2007) reported that more than 65% of treatments in the Cooper Basin have observed high PDL. The typical fracturing fluids in the Cooper Basin that have been used are friction-reduced water (slickwater) and borate-crosslink gel. 100-mesh sand has been used throughout the basin to help reduce near wellbore pressure loss (NWBPL) and 20/40 to 40/70 mesh sands are the most commonly selected proppant (Pitkin et al, 2011). Special core analysis has, however, not been commonly conducted in this basin, so the relative permeability condition in most of the reservoirs remains unknown, which could potential cause low productivity and low flowback recovery by induced water-based fracturing fluid.

Merrimelia is a mature oil and gas producing field located approximately 45 km north of Moomba on the Gidgealpa-Merrimelia-Innamincka Ridge. This major positive structural feature runs the length of the SA sector of the Cooper/Eromanga Basin and separates the Patchawarra Trough from the Nappamerri Trough. Merrimelia–62 was drilled in mid-2011 as a gas development well in the Merrimelia field in SA (Fig. 7). The Toolachee was the primary target formation and the Callamurra Member was the secondary objective for Merrimelia–62. Hydrocarbon was indicated by the wireline logs. A total of 40 ft of net gas pay with a porosity of 11.6% was predicted for the Toolachee Formation. The Callamurra Member was prognosed to have 30 ft of net gas pay with a porosity of 11.9% (Santos, 2012).

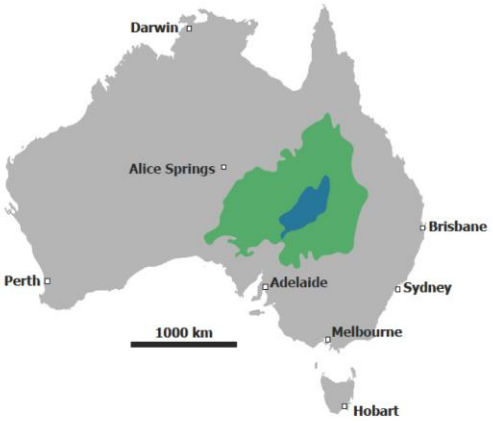

Figure 4. Cooper Basin location (blue) and overlying Eromanga Basin (green).

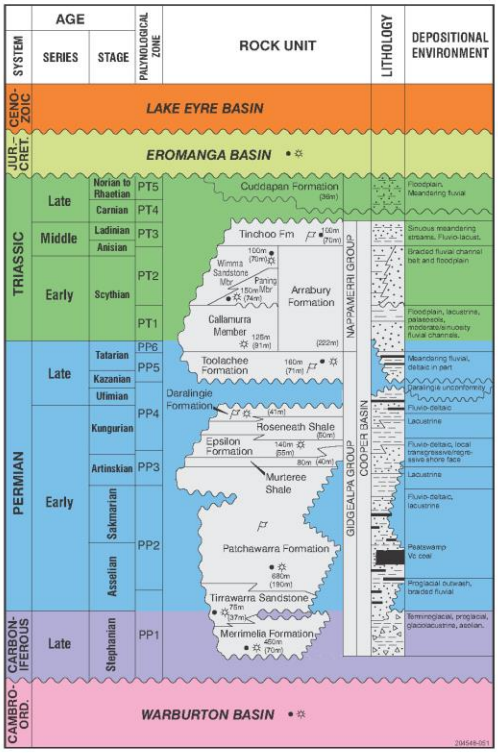

Figure 5. Stratigraphic summary of the Cooper Basin, SA (Alexander, 1998).

METHODOLOGY

In this paper, the authors used a fracture propagation model coupled with reservoir simulation. Figure 8 shows the details of the workflow.

First, the key reservoir properties—such as geomechanical stress and rock strength—that control the growth of hydraulic fracture needed to be determined from log data. IHS WellTest software was selected to simulate DFIT data due to its ability to model DIFT after-closure pressure without a full-scale fracture simulator. The

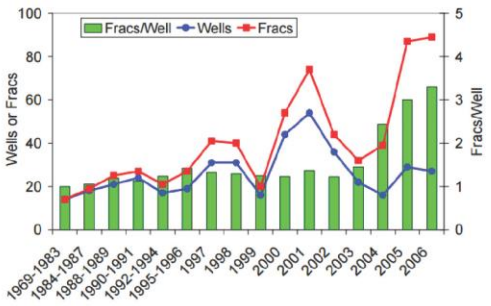

Figure 6. Fracture treatment in the Cooper Basin (McGowen et al, 2007).

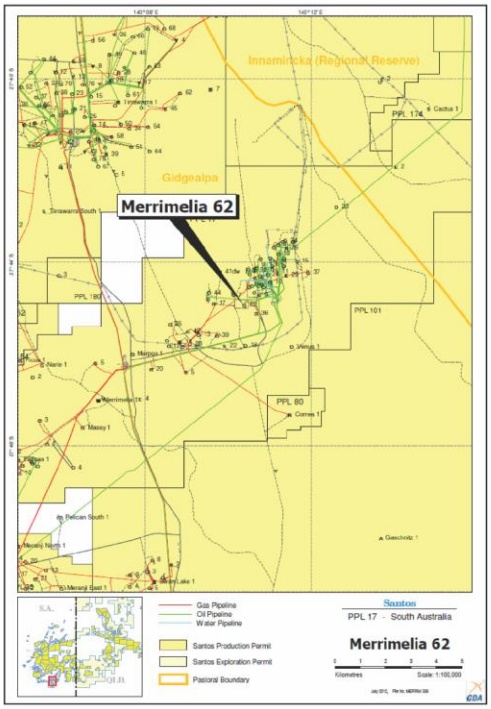

Figure 7. Location map of Merrimelia–62 (Santos, 2012).

result of pre-closure analysis are ISIP and closure pressure, which are the input parameters of the 1D mechanical earth model. Reservoir permeability and reservoir pressure are the after-closure analysis results, which are input into the fracture model. The pre-closure and after-closure results are summarised in Table 2.

Then, GOHFER (Grid-Orientated Hydraulic Fracture Extension Replicator) was used to model the fracture propagation to determine the fracture dimensions and conductivities. The actual pumping schedule for Merrimelia–62 is shown in Table 3. In this model, LPG fracturing fluid is generated from the viscosity versus time plot in the McCully field case study by Leblanc et al (2011). The temperature range is up to 150°F. As GOHFER can only generate the rheology curve based on a constant temperature, the viscosity data points on the graph are referring to this temperature. The viscosity is recorded to be 300 cP at a reference shear rate of 100 s^{-1} and a base fluid in the GOHFER database is selected with similar initial viscosity.

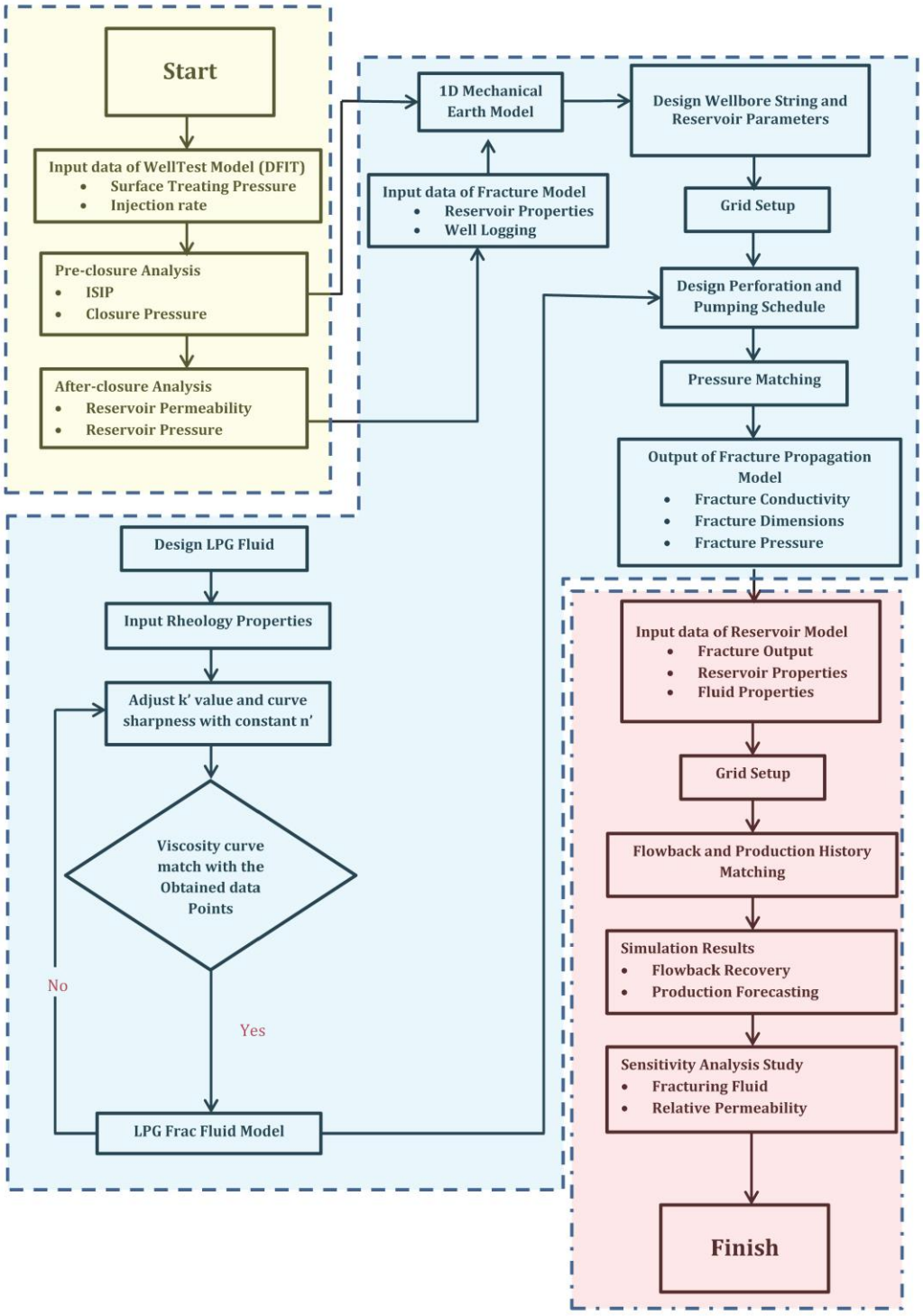

Figure 8. Workflow of the model development. Yellow indicates the IHS model process, blue indicates the GOHFER process, and red indicates the Eclipse process.

Table 2. Summary of Merrimelia–62 (stage 1) well injection fall off test results.

Pre-closure analysis	ISIP (psi)	4,871.87
	Closure pressure (psi)	4,091.79
	Closure gradient (psi/ft)	0.559
	Type of leak-off	Height recession
Nolte's after closure analysis	Permeability (mD)	0.1
	Flow capacity (mD.ft)	0.3079
	Fracture half-length (ft)	2.28
	Pore pressure (psi)	1,869

Table 3. Actual pumping schedule for Merrimelia–62 N_2 treatment.

Stage	1	2	3
Description	Pad	Slurry	Flush
Fluid type	HyborH_40	HyborH_40	Linear gel
Clean volume (gallons)	13,064	11,637	3,542
Breaker type	–	Vicon	Vicon
Start BH proppant concentration (ppg)	0	0.5–12	–
Proppant type	None	CarboProp 20/40	–
BH total rate (bpm)	26.7	26.7	26.7
N_2 foam quality (%)	50	50	50

Then the new rheology curve could be matched with the input data points by adjusting the n' and k' parameters. The simulator based on model inputs predicts the amount of proppant concentration, fracture half-length and fracture width. These key outputs (fracture conductivity, fracture dimensions and fracture pressure) are required for production modelling using Eclipse.

Finally, a reservoir simulator is used to model multiphase flow within the reservoir and the well production. In the actual field case, Merrimelia–62 has been fractured by 50% N_2 foam (base case). Eclipse was used to model the effect of fracture stimulation upon the productivity from Merrimelia–62. The reservoir properties of Merrimelia–62 are the main input parameters of Eclipse, as shown in Table 4. Pressure, volume, temperature (PVT) and relative permeability data was not available in the Merrimelia field so analogous data was required. Pressure, viscosity and formation volume factor data were sources from the Patchawarra Formation in the nearby Della field, while relative permeability (see Fig. 9a) and capillary pressure were provided from the Cowralli field. Flowback and history matching have been conducted to valid the model. The hydraulic fracturing results from GOHFER were used in Eclipse to model flowback recovery and production forecasting. Sensitivity analysis, which involves types of fracturing fluids and various relative permeability curves has also been studied in regards to gas productivity.

RESULTS AND DISCUSSION

From simulation of the fracture propagation model, the surface treating pressure has been matched with the post-job report (Fig. 10). The average pumping rate is 20 bpm, which has been injected into the Toolachee Formation at a depth of 7,000 ft. The breakdown pressure indicated 6,700 psi, and propagation pressure 5,700 psi. Then, the coupled simulation was run for the base case. Figure 11 shows good matching for the true production with the model results, and the history matching parameters and results are summarised in Table 5.

Table 4. Reservoir properties of the Merrimelia–62 well.

	Value	Unit
Measured depth	7,325	ft
Thickness	77	ft
Reservoir pressure	1,844.8	psi
Reservoir temperature	296	°F
Permeability	0.01	mD
Porosity	10.1–13.7	%
Water saturation	50	%
Gas saturation	50	%

Relative permeability curves are one of the major reservoir parameters controlling well productivity and, therefore, fracturing fluid selection. In some tight gas formations, water ceases to flow at a critical water saturation that is substantially greater than connate water saturation. Apart from phase trapping, the high effective stresses in the rock may impact the permeability to fluids so severely that classical theories for multiphase flow are no longer applicable (Shaoul et al, 2011). The relative permeabilities to both water and gas can be so low that neither phase has significant relative permeability across some range of saturations. This phenomenon is called permeability jail by Shanley et al (2004) . In addition, numerous authors (Cluff and Byrnes, 2010; Shanley et al, 2004; Shaoul et al, 2011) also discuss the existence of a permeability jail in tight gas reservoir rocks where the water is trapped by the high capillary pressure, thereby reducing the permeability to gas significantly. The sensitivity study will investigate this phenomenon as part of the post-fracture production analysis of tight gas reservoirs. The relative permeability curves presented in Figure 9 are in accordance with the theory described by Shanley et al (2004) and data from Cluff and Byrnes (2010). The relative gas permeability formula (Eq. 2) is (Shanley et al., 2004):

$$k_{rg} = (1 - S_w)^2 \left[1 - S_w^{\left(\frac{2+3\lambda}{\lambda}\right)}\right] \quad (2)$$

In Equation 2, k_{rg} is the relative permeability of gas (fraction), S_w is water saturation (percentage), and λ is the slope (dimensionless). Figure 9 shows four examples of relative permeability curves. The first scenario (a) is the base case. The second scenario (b) is named the weak permeability jail and is based on low but finite fluid mobility in the jail saturation range. The third and fourth scenarios (c and d) are named the median and strong permeability jails, where the relative permeability curves of the fluids do not intersect and where within a region with a width of 0–0.2 (in water saturation) no fluids are mobile at all. The sensitivity of the relative permeability jail concept is analysed based on these four scenarios. In each scenario, three different types of fraccing fluids were evaluated, as shown in Table 6.

Figure 12 shows the simulation results of flowback by different fraccing fluids with original reservoir conditions. In Figure 12a, it can be seen that water production rates for both cases of 50% N_2 foam and LPG are about two to three times higher than slickwater. This is mainly due to the water trap-

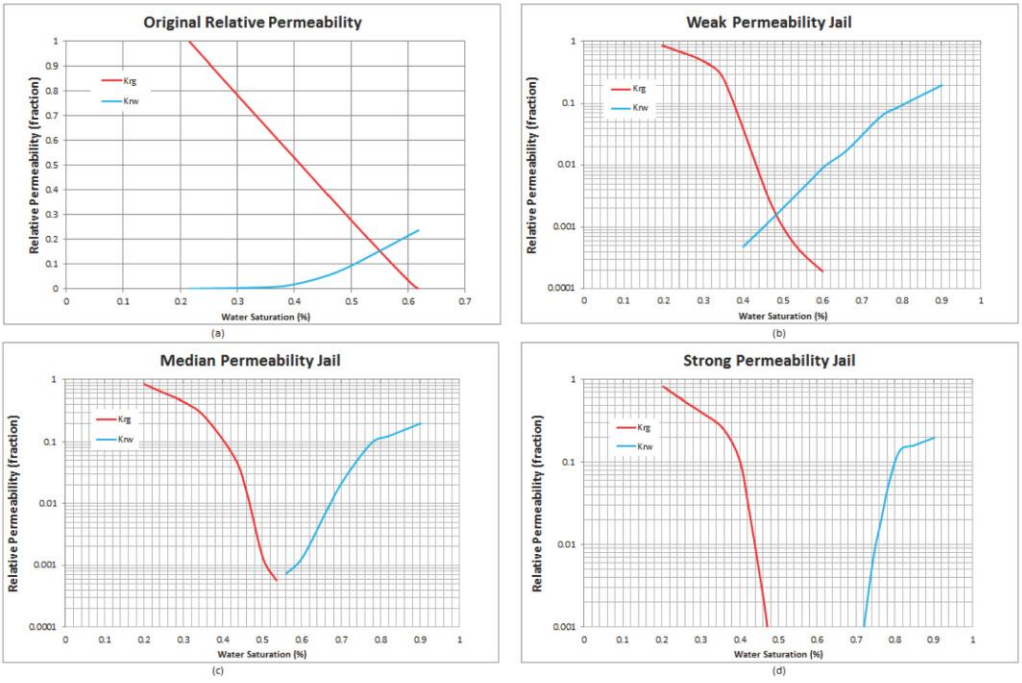

Figure 9. Sensitivity study of different relative permeability (rel-perm) curves. a) Original rel-perm curve for base case. b) Rel-perm curve for weak rel-perm jail. c) Rel-perm curve for median rel-perm jail. d) Rel-perm curve for strong rel-perm jail. (Shaoul et al, 2011.)

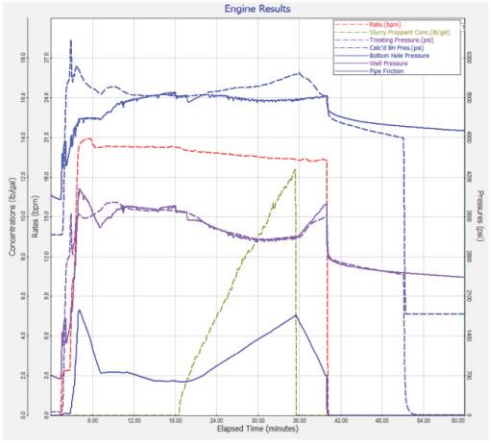

Figure 10. Surface treating pressure matching.

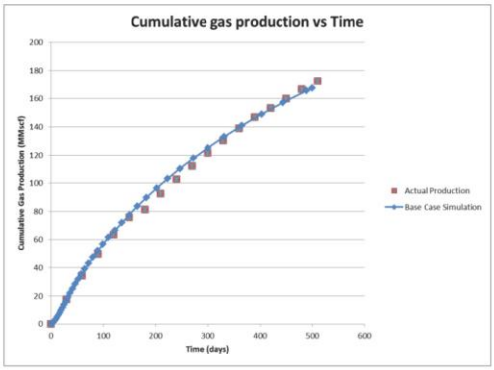

Figure 11. Production history matching of base case simulation.

ping phenomenon. The average conductivity of slickwater in the fraccing zone is 2,007 md-ft, whereas in the case of LPG the average conductivity is 2,598 md-ft. The lower conductivity contributed to higher capillary pressure, which would cause liquid retention at a low reservoir pressure environment. Furthermore, the stabilised fracturing pressure of LPG has 5,315 psi, whereas the fracturing pressure of the slickwater case only has 4,821 psi. This is because of the expansion mechanism from energised fluids that converts to gas in the formation, and the additional expansion energy at 500 psi would contribute to higher flowback. When comparing N_2 foam with LPG, LPG has a slightly better flowback rate in the initial stage (up to 50 days). This is because LPG is completely converted to the gas phase when it reaches the formation under reservoir conditions, and therefore less residual gel remains in the formation. Thus, the total flowback recovery was significantly enhanced to 76% within 60 days by using gelled LPG fracture stimulation. In addition, Figure 12b presents the cumulative water production with three fraccing fluids within 60 days. It can be seen that LPG has the highest total water production (509 STB), compared to 50% N_2 foam (433 STB) and slickwater (213 STB). The gas production rate as shown in Figure 13a shows that LPG reaches maximum gas production

Table 5. History matching results.

	Value	Unit
Permeability	1.9	mD
Porosity	0.08	Fraction
Drainage area	200	Acre
Clean-up time	50	Days
Skin	10	Dimensionless
Fluid efficiency	82.37	%
Retain permeability	68	%

Table 6. Sensitivity analysis of fluid type.

Rel-perm/ fluid type	50% N_2 foam	Slickwater	LPG
Original reservoir	Base case	Case 1	Case 2
Weak rel-perm	Case 3	Case 4	Case 5
Median rel-perm	Case 6	Case 7	Case 8
Strong rel-perm	Case 9	Case 10	Case 11

almost one day after the fraccing treatment, while N_2 foam and slickwater require 40–50 days , which also proves that LPG performs with a much faster flowback time. The total injection volume is 673 STB. The load of recoveries are 76% for LPG, 64% for 50% of N_2 foam, and 32% for slickwater.

Figure 13b shows cumulative gas production after a fracture treatment for three types of fraccing fluids, which are the same data as presented in Figure 13a. It can be seen that cumulative gas production will be higher if there is less water in the fraccing fluid. The cumulative gas production, however, does not differ much between N_2 foam and LPG. Also, if the fracture treatment uses slickwater, the cumulative gas production will decrease 50% in one year, which is about 0.8 Bscf for one well in a 200 acre spacing. Thus, proper selection of the fracturing fluid is critical to the success of the fracture treatment and long-term gas production.

The results of the sensitivity analysis are shown in Figures 14–16, and are summarised in Table 7. Figure 14 shows cumulative gas production for the weak relative permeability jail scenario. It can seen that cumulative gas production of LPG presents higher gas production (137 MMscf), followed by N_2 foam (110 MMscf) and slickwater (51 MMscf) at 230 days. In the median relative permeability jail scenario, Figure 15 shows the cumulative gas production of LPG (107 MMscf) remains the highest gas production, followed by N_2 foam (79 MMscf) and slickwater (51 MMscf). Similarly, with the weak and median cases, the strong case in Figure 16 also shows that LPG performs better than other fraccing fluids.

Figure 17 shows the results of reservoir simulation of cumulative gas production with different fraccing fluids at various reservoir scenarios. Case 2 (LPG, original rel-perm) pro-

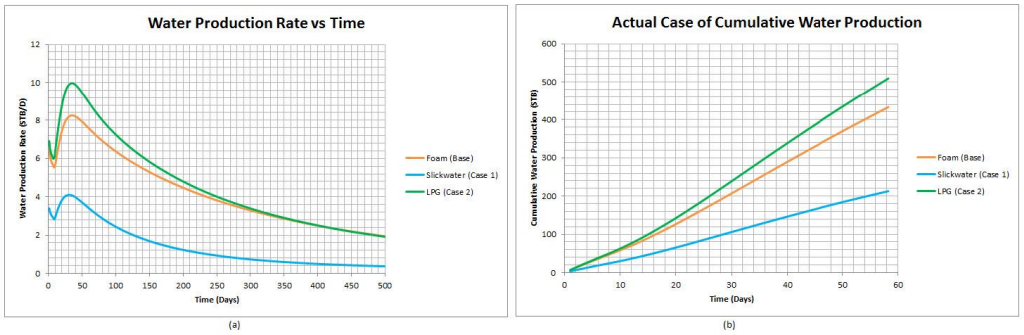

Figure 12. Effect of different fluid types on original reservoir condition. a) Water production rate versus time. b) Cumulative water production versus time.

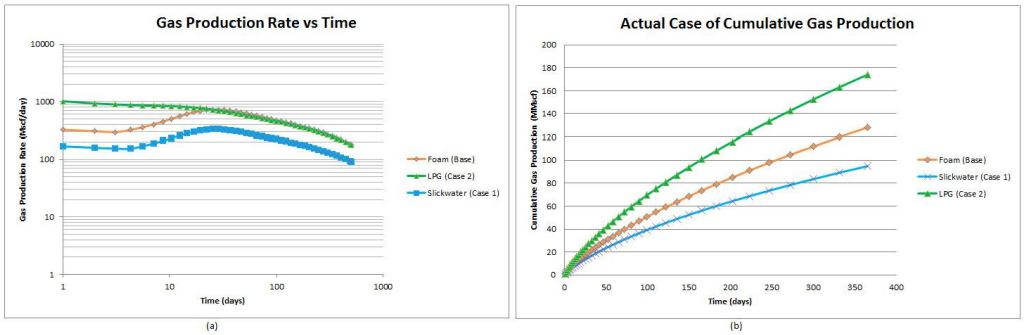

Figure 13. Effect of different fluid types on original reservoir condition. a) Gas production rate versus time. b) Cumulative gas production versus time.

vides the highest gas production of 170.9 MMscf compared to the base case (50% of N_2 foam, original rel-perm) and case 1 (slickwater, original rel-perm). The authors found that with more severe liquid sensitive formations (from original to strong rel-perm), the cumulative gas production of all the fraccing fluid would decrease to 47%. Comparing between case 2 and case 1, if no water trapping was assumed in LPG (case 2), slickwater (case 1) could cause 53% of water blocking in the original rel-perm formation. This is also true at other reservoir scenarios when comparing with slickwater, which consequently induce 53% effective fracture half-length loss. The authors also found that when comparing with 50% N_2 foam, the results of LPG show that in the case of normal relative permeability behaviour, there is no significant benefit on the post-fraccing production. In the case of the weak relative permeability jail, however, there is a benefit to be gained in the early-time production during the clean-up period that lasts several months.

CONCLUSIONS

LPG fracturing has the potential to eliminate all issues associated with water use and disposal, which is a key challenge in conventional hydraulic fracturing. Also, there are many advantages in using liquefied petroleum gases for hydraulic fracturing if it can be done safely. This paper introduced a fracture propagation model coupled with a multiphase flow model for an unconventional reservoir in the Cooper Basin by using actual field data. The simulation demonstrated the effectiveness of liquid retention and gas productivity enhancement under a low-pressure, high-temperature environment. The permeability jail has a negative impact on gas production. In a highly liquid sensitive formation (from original to strong rel-perm), the cumulative gas production of all the fraccing fluids would decrease to 47%.

In the model, the resulting water production rates of foam and LPG are about two to three times higher than slickwater due to additional fracturing pressure. When comparing N_2 foam to LPG, LPG has slightly better flowback rates in the initial stage (up to 50 days). Thus, the total flowback recovery was significantly enhanced to 76% within 60 days by using gelled LPG fracture stimulation. In a normal tight relative permeability case, the results show that there is a potential of getting up to 53% of effective fracture half-length loss by slickwater. When looking at the possibility of removing the water phase completely (gelled LPG fraccing), there is a potential of obtaining up to 53% of incremental gain comparing with slickwater in all the cases. In the case of 50% N_2 foam, however, the results show that there is no significant benefit on the post-fraccing production under this permeability behaviour. Thus, higher quality foam is recommended in a low pressure water sensitivity formation. The permeability jail concept needs to be explored further with core testing in the Cooper Basin. Laboratory experiments are necessary to verify the presence of a permeability jail in low permeability sandstones. Moreover, to further validate the fracturing model, rheology experimental laboratory tests are recommended.

NOMENCLATURE

k	Formation permeability (mD)
k_{rg}	Relative permeability of gas (dimensionless)
μ	Viscosity (cP)
P_C^{th}	Capillary threshold pressure (psi)
r	Pore radius (microns)
θ	Contact angle (degree)
S_w	Water saturation (percentage)

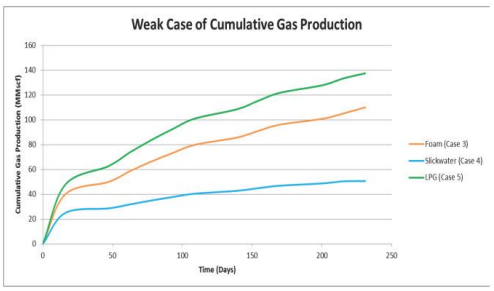

Figure 14. Effect of different fluid types on gas production (weak case).

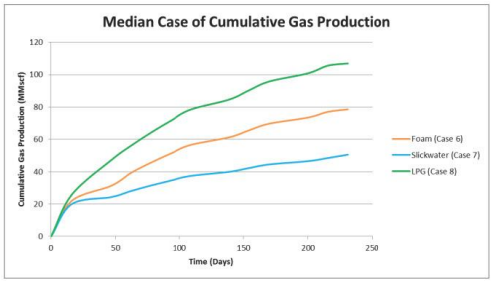

Figure 15. Effect of different fluid types on gas production (median case).

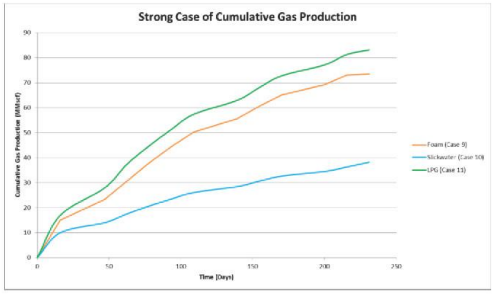

Figure 16. Effect of different fluid types on gas production (strong case).

Table 7. Results of sensitivity analysis.

Properties	Fraccing fluid type	Rel-perm type	Gas cumulative at 230 days (MMscf)
Base case	N_2 foam	Original reservoir	167.5
Case 1	Slickwater	Original reservoir	80.7
Case 2	LPG	Original reservoir	170.9
Case 3	N_2 foam	Weak perm jail	110.2
Case 4	Slickwater	Weak perm jail	50.7
Case 5	LPG	Weak perm jail	137.7
Case 6	N_2 foam	Median perm jail	78.5
Case 7	Slickwater	Median perm jail	50.6
Case 8	LPG	Median perm jail	106.9
Case 9	N_2 foam	Strong perm jail	73.5
Case 10	Slickwater	Strong perm jail	38.2
Case 11	LPG	Strong perm jail	83.2

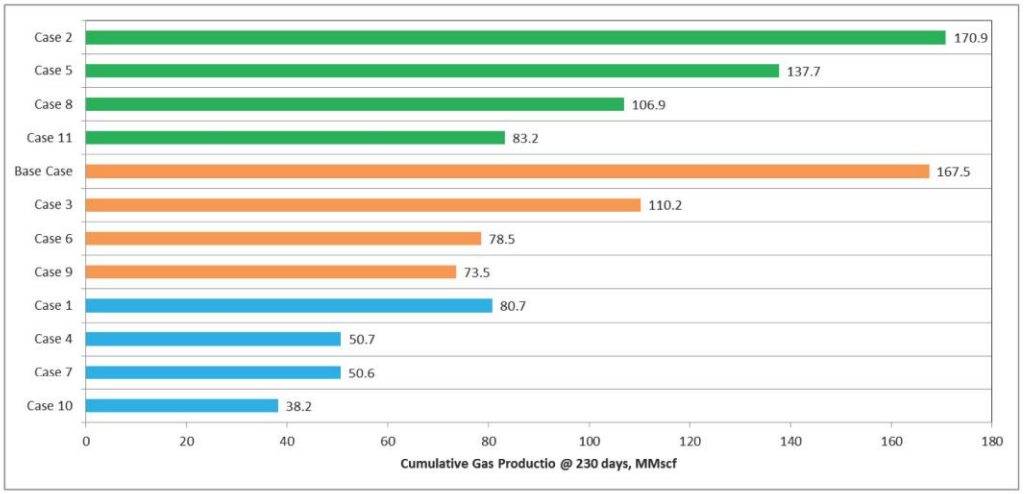

Figure 17. Cumulative production for reservoir simulation with various scenarios. The green colour represents LPG fluid, orange represents 50% N_2 foam, and blue represents slickwater.

REFERENCES

ALEXANDER, E.M., 1998—Lithostratigraphy and environments of deposition. In: Gravestock, D.I. and Jensen, S.B. (eds) The Petroleum Geology of South Australia, volume 4. Adelaide: Primary Industries and Resources South Australia.

AL-KANAAN, A., RAHIM, Z. AND AL-ANAZI, H., 2013—Selecting Optimal Fracture Fluids, Breaker System, and Proppant Type for Successful Hydraulic Fracturing and Enhanced Gas Production - Case Studies. SPE Unconventional Gas Conference and Exhibition, Muskat, Oman, 28–30 January, SPE-163976.

BADDELEY, T., 2013—Parliamentary inquiry into the implications for Western Australia of hydraulic fracturing for unconventional gas. Letter from Santos, 4 October 2013. Perth: Santos.

CHALBAUD, C.A., ROBIN, M. AND EGERMANN, P., 2006—Interfacial Tension Data and Correlations of Brine-CO_2 Systems under Reservoir Conditions. SPE Annual Technical Conference and Exhibition, San Antonio, Texas, 24–27 September, SPE-102918.

CHIPPERFIELD, S.T. AND BRITT, L.K., 2000—Application of after-closure analysis for improved fracture treatment optimisation: a Cooper Basin case study. SPE Rocky Mountain Regional/Low-Permeability Reservoirs Symposium and Exhibition, Denver, Colorado, 12–15 March, SPE-60316.

CLUFF, R.M. AND BYRNES, A.P., 2010—Relative Permeability In Tight Gas Sandstone Reservoirs - The "Permeability Jail" Model. SPWLA 51st Annual Logging Symposium, Perth, Western Australia, 19–23 June, SPWLA-2010-58470.

ECONOMIDES, M.J. AND MARTIN, T., 2007—Modern fracturing: enhancing natural gas production. Houston: Energy Tribune Publishing Inc.

ECONOMIDES, M.J. AND NOLTE, K.G., 2000—Reservoir stimulation. Chichester, West Sussex: John Wiley & Sons.

FINK, J.R., 2013—Hydraulic fracturing chemicals and fluids technology. Oxford: Elsevier.

GANDOSSI, L., 2013—An overview of hydraulic fracturing and other formation stimulation technologies for shale gas production. Joint Research Centre of the European Commission report. Report EUR: 26347. Luxembourg: Publications Office of the European Commission.

GIDLEY, J.L., HOLDITCH, S.A., NIERODE, D.E. AND VEATCHJR, R.W., 1989—Recent advances in hydraulic fracturing. Richardson, Texas: Society of Petroleum Engineers.

GRAVESTOCK, D.I. AND JENSEN, S.B., 1998—The petroleum geology of South Australia, volume 4. Adelaide: Primary Industries and Resources South Australia.

GUPTA, D.V.S., 2009—Unconventional Fracturing Fluids for Tight Gas Reservoirs. SPE Hydraulic Fracturing Technology Conference, Woodlands, Texas, 19–21 January, SPE-119424.

HOLDITCH, S.A., 1979—Factors affecting water blocking and gas flow from hydraulically fractured gas wells. Journal of Petroleum Technology, 31 (12), 1,515–24

HURST, R.E., 1972—Gas Frac - A New Stimulation Technique Using Liquid Gases. SPE Rocky Mountain Regional Meeting, Denver, Colorado, 10–12 April, SPE-3837.

LEBLANC, D.P., MARTEL, T., GRAVES, D.G., Tudor, E. AND Lestz, R., 2011—Application of Propane (LPG) Based Hydraulic Fracturing in the McCully Gas Field, New Brunswick, Canada. North American Unconventional Gas Conference, Woodlands, Texas, 14–16 June, SPE-144093.

LESTZ, R.S., WILSON, L., TAYLOR, R.S., FUNKHOUSER, G.P., WATKINS, H. AND ATTAWAY, D., 2007—Liquid petroleum gas fracturing fluids for unconventional gas reservoirs. Journal of Canadian Petroleum Technology, 46 (12), 68–72.

MCGOWEN, J.M., GILBERT, J.V. AND SAMARI, E., 2007—Hydraulic Fracturing Down Under. SPE Hydraulic Fracturing Technology Conference, College Station, Texas, 29–31 January, SPE-106051.

POKALAI, K., FEI, Y., AHMAD, M., HAGHIGHI, M. AND GONZALEZ, M., 2015—Design and optimisation of multi-stage hydraulic fracturing in a horizontal well in a shale gas reservoir in the Cooper Basin, South Australia. The APPEA Journal, 55, 1–14.

RIBEIRO, L. AND SHARMA, M., 2013—Fluid Selection for Energized Fracture Treatments. SPE Hydraulic Fracturing Technology Conference, Woodlands, Texas, 4–6 February, SPE-163867.

SANTOS, 2012—Merrimelia 62 well completion report. Adelaide: Santos Ltd.

SANTOS, 2015—Cooper Basin (overview). Accessed December 2015. <https://www.santos.com/what-we-do/activities/south-australia/cooper-basin/>.

SCOTT, M.P., STEPHENS, T., DURANT, R., MCGOWEN, J., THOM, W. AND WOODROOF, R., 2013—Investigating hydraulic fracturing in tight gas sand and shale gas reservoirs in the Cooper Basin. SPE Unconventional Resources Conference and Exhibition–Asia Pacific, Brisbane, Queensland, 11–13 November, SPE-167073.

SHANLEY, K.W., CLUFF, R.M. AND ROBINSON, J.W., 2004—Factors controlling prolific gas production from low permeability sandstone reservoirs: implications for resource assessment, prospect development, and risk analysis. AAPG Bulletin, 88 (8), 1,083–121.

SHAOUL, J.R., VAN ZELM, L.F. AND DE PATER, C.J., 2011—Damage mechanisms in unconventional gas well stimulation--a new look at an old problem. SPE Production & Operations, 26 (04), 388–400.

SONI, T.M., 2014—LPG-Based Fracturing: An Alternate Fracturing Technique in Shale Reservoirs. IADC/SPE Asia Pacific Drilling Technology Conference, Bangkok, Thailand, 25–27 August, SPE-170542.

TAYLOR, R.S., FYTEN, G., ROMANSON, R., MCINTOSH, G., LITUN, R., MUNN, D., BENNION, B., PLWOWAR, M. AND HOCH, O., 2010—Montney fracturing-fluid considerations. Journal of Canadian Petroleum Technology, 49 (12), 28–36.

VALKÓ, P. AND ECONOMIDES, M.J., 1996—Hydraulic fracture mechanics. Chichester, West Sussex: John Wiley & Sons.

THE AUTHORS

Yang Fei is presently undertaking a PhD in petroleum engineering at the Australian School of Petroleum (ASP). Before starting his PhD, Yang received his BE (Hons) in petroleum engineering from the University of Adelaide. Previously, Yang worked as a technical assistant at Santos Ltd for four years.

Yang's area of expertise is in production engineering and optimisation, where he focuses on the development and maintenance of GAP/PROSPER/MBAL models of satellites from the Cooper Basin. In addition to that, he provided support in running various scenarios to identify potential projects to fully optimise satellite performance. Yang's PhD involves researching waterless and foam-based hydraulic fracturing alternatives for Australian unconventional reservoirs. Member: SPE, PESA and AAPG.

yang.fei@adelaide.edu.au

Mary Gonzalez Perdomo is a lecturer of petroleum engineering, and the Engineering Honours Academic Coordinator for the ASP. Her research and teaching focus is on reservoir and production engineering, particularly production enhancement and optimisation.

She joined the ASP in 2009 after several years of experience in the oil and gas industry, where she provided practical petroleum engineering, consultancy services and solutions in the areas of subsurface and production engineering.

Mary has collaborated on APPEA papers, and has BSc and a post-graduate degrees in petroleum engineering, and post-graduate studies in higher education. Member: SPE and PESA.

maria.gonzalezperdomo@adelaide.edu.au

Authors' biographies continued next page.

Authors' biographies continued from previous page.

THE AUTHORS

Viet Quoc Nguyen is undertaking a Bachelor of Petroleum Engineering degree at the ASP. Viet's area of interest is in reservoir stimulation by using hydraulic fracturing. He is focusing on the benefits of applying LPG as a fracturing fluid in the Cooper Basin as a project for his final-year thesis. In Viet's work, hydraulic fracturing and reservoir production models are developed and incorporated with each other using IHS Welltest, GOHFER and Eclipse. Member: SPE.

vietquoc.nguyen@student.adelaide.edu.au

Zhongyu Lei is a recent graduate in the Bachelor of Petroleum Engineering (Honours) degree at the ASP, and has completed a three-month internship with Petro-China, researching and commissioning hydraulic fracturing in 2014. The title of Zhongyu's thesis, completed for her honour project, was Enhanced gas recovery using LPG fracturing fluid in tight/shale gas reservoirs (Cooper Basin). She focuses on simulating and researching the viability of using LPG as a hydraulic fluid for tight gas reservoirs in the Cooper Basin. In addition to that, Zhongyu is presently assisting Yang Fei with his PhD project involving research about waterless and foam-based hydraulic fracturing alternatives for Australian unconventional reservoirs. Member: SPE.

a1613566@student.adelaide.edu.au

Kunakorn Pokalai is presently a PhD candidate of petroleum engineering at the University of Adelaide. He has a BE in petrochemical engineering from Silpakorn University (Thailand), and completed a Graduate Certificate in Management and Masters in petroleum engineering from the University of Adelaide.

Kunakorn's research interests are in the simulation of unconventional reservoirs and hydraulic fracturing. He mainly focuses on the issue of fracturing fluid flowback in the Cooper Basin. Kunakorn was the recipient of the prestigious AAPG Imperial Barrel Award in the Asia Pacific Region in 2014. Member: SPE and AAPG.

kunakorn.pokalai@adelaide.edu.au

Sume Sarkar is a PhD candidate at the ASP. She has experience in petroleum sector regulation in a south Asian context. She holds a MSc degree in petroleum engineering with specialisation in reservoir engineering from Norwegian University of Science and Technology, and a BSc degree in chemical engineering from Bangladesh University of Engineering and Technology. Sume is conducting research on two major areas for unconventional reservoirs in the Cooper Basin: fracturing fluid flowback modelling, and geomechanical modelling for multi-stage hydraulic fracture operations.

sume.sarkar@adelaide.edu.au

Manouchehr (Manny) Haghighi is an associate professor of petroleum engineering. His research and teaching focus is on unconventional reservoirs, reservoir simulation, well testing, and formation evaluation. He has supervised more than 40 MSc and 10 PhD students. Before joining the University of Adelaide in 2009, Manouchehr was associate professor of petroleum engineering at the University of Tehran (Iran). During 2000–07, he was the head of the petroleum engineering program at the University of Tehran. In 2000, Manouchehr established Simtech, a consulting company for integrated reservoir simulation in which he has been project director of several full-field simulation projects for oil and gas reservoirs.

From 1995 to 2000 Manouchehr worked with the National Iranian Oil Company (NIOC) and was the director of a program for the training of NIOC staff at several universities in the US, UK, Canada, France, Australia and Norway. Manouchehr was a visiting professor at the University of Calgary from 2007–08.

Manouchehr has published more than 80 articles in peer-reviewed journals or presented in international conferences. He has served as a reviewer for various journals including the Journal of Petroleum Science and Engineering. Member: SPE.

manouchehr.haghighi@adelaide.edu.au

Chapter 8: Conclusion and Future Work

8.1 Conclusive Remarks

The purpose of this thesis is to characterise foam stability as a fracturing fluid and to study the effects of nanoparticles on foam stability and proppant placement during hydraulic fracturing.

The experimental and simulation studies highlight the enhancement of foam stability and proppant settling by silica nanoparticles and the overall improvement in the efficiency of foam as a fracturing fluid at high temperature environment.

The experimental conclusions are as follows:

1. Foam drainage can help in suspending more proppant. However, the major question is how long can the proppant be kept in suspension, which is related to maintaining stability.

2. In the presence of high ionic strength, the foam structure can be damaged even more quickly and the particle suspension becomes worse. In addition, it is generally easy to suspend particles in highly viscous foam owing to the high total pulling force and long free drainage regime. Nanoparticle-stabilised foam has been found to create a transition regime that delays the foam coarsening and coalescence.

3. The experimental results showed that SiO_2 nanoparticles and EAPB had a synergistic effect, which significantly improves the foam stability. At a temperature of 90 ℃, it is observed that the decrease in foam volume of WLMs-nanoparticles mixture was two times greater than that of WLMs alone. Foam node blockage and plateau border adsorption by nanoparticles have been identified by cryo-scanning electron microscopy (cryo-SEM). This phenomenon leads to reduced liquid drainage and increase in the rigidity of the interface to prevent foam coarsening resulting to the increase of foam stability.

4. The rheological measurements show that the addition of 0.8% nanoparticles into EAPB foam leads to a dramatic increase in the foam viscosity at an initial time of 30 min, which appears to be due to the formation of micelle-particle junctions. The enhancement of viscosity in a high temperature environment could result in reducing the free drainage rate to improve foam stability.

The simulation conclusions are as follows:

1. Foam stability is mainly controlled by foam drainage and disproportionation. The crossover point of those two mechanisms called foam critical time which is indication of foam viscosity breakdown. Therefore, it is an essential parameter for pumping schedule design.

2. A long shut-in period leads to proppant settlement and accumulation at the bottom of the formation, which causes reduction of the propped area and fracture productivity.

The total pumping time and shut-in time need to be carefully designed with respect to the foam critical and rupture time.

3. The hydraulic fracture modelling suggests that the effective propped area or final proppant distribution can be controlled by varying the injection rate and foam quality during proppant injection towards higher foam stabilisation.

4. Low stability foam as a fracturing fluid can only achieve sufficient proppant coverage over a thick pay interval when closure time is relatively shorter than foam stability.

5. Foam stability is related to the treatment time; it influences proppant transportation during placement and redistribution of proppant during closure. Therefore, it also provides useful information for production history matching.

6. LPG fracturing has the potential to eliminate all the issues associated with water use/disposal and formation damage and has the potential to be an ideal fracturing fluid in many unconventional reservoirs if applied safely. Simulation results show that LPG has slightly better flowback rate and post-fracture production when compared to other water based fracturing fluids.

7. There are other variables such as surfactant types, concentrations, shear history, and system pressure, which are also important in foam rheology characterisation. The best approach is to develop an understanding of foam properties and performance and onsite quality control tests. This process requires good onsite quality control to avoid any unnecessary changes in the treatment condition that will result in a less stable foam.

8.2 Future Work

This study is focused on the impact of nanoparticles on foam stability to minimize proppant settling during hydraulic fracturing application. The research conducted involved the technical aspects of silica nanoparticle in a particular type of WLMs (Erucyl amidopropyl betaine) only at a temperature of 90℃ .

Future work on this topic should consider the following aspects:

1. Different types of nanoparticles and foaming agents are suggested to be studied. Foamability and foam stability are the main variables to be optimized in the parameter selection.
2. To study foam stability at a high pressure and higher temperature range (above 90 ℃) this could be achieved with a high temperature and high pressure visualization cell.
3. Systematic experimental study of nanoparticle-stabilised foam rheology. It is suggested to consider high pressure high temperature condition (i.e., up to 5000 psi & 200 ℃), gas type (i.e., liquid or supercritical CO_2), and nanoparticle type (i.e., partially hydrophobic silica nanoparticle or MgO/ZnO/FeO nanoparticle).
4. In the current fracture model, foams are assumed to be non-Newtonian fluids with a local apparent viscosity determined by shear rate, pressure, and foam quality when

predicting proppant settling in foams. For better modelling, a dynamic settling test should be designed for foams.

5. This study has limited field verification. Collaboration with field operators is necessary to confirm the fracturing performance of polymer-free nanoparticle-stabilised foams as observed in the simulations of this study.

References

Alargova, R.G., Warhadpande, D.S., Paunov, V.N. and Velev, O.D., 2004. Foam Superstabilization by Polymer Microrods. Langmuir, 20(24): 10371-10374.

Alotaibi, M.A. and Miskimins, J.L., 2015. Slickwater Proppant Transport in Complex Fractures: New Experimental Findings & Scalable Correlation, SPE Annual Technical Conference and Exhibition. Society of Petroleum Engineers, Texas, USA.

Angarska, J., Stubenrauch, C. and Manev, E., 2007. Drainage of foam films stabilized with mixtures of non-ionic surfactants. Colloids and Surfaces A: Physicochemical and Engineering Aspects, 309(1–3): 189-197.

Asadi, M., Conway, M.W. and Barree, R.D., 2002. Zero Shear Viscosity Determination of Fracturing Fluids: An Essential Parameter In Proppant Transport Characterizations, SPE International Symposium and Exhibition on Formation Damage Control. Society of Petroleum Engineers, Lafayette, Louisiana.

Barree, R.D., 1983. A Practical Numerical Simulator for Three-Dimensional Fracture Propagation in Heterogeneous Media, Reservoir Simulation Symposium. Society of Petroleum Engineers, San Francisco, CA.

Barree, R.D., Conway, M. and Gilbert, J.V., 2009. An Effective Model for Pipe Friction Estimation in Hydraulic Fracturing Treatments, SPE Rocky Mountain Petroleum Technology Conference. Society of Petroleum Engineers, Denver, Colorado, USA.

Barree, R.D. and Conway, M.W., 1994. Experimental and Numerical Modeling of Convective Proppant Transport, 69th SPE Annual Technical Conference. Society of Petroleum Engineers, New Orleans, LA, USA.

Barree, R.D. and Conway, M.W., 1995. Experimental and Numerical Modeling of Convective Proppant Transport. SPE Journal.

Barree, R.D., Miskimins, J.L., Conway, M.W. and Duenckel, R., 2016. Generic Correlations for Proppant Pack Conductivity, SPE Hydraulic Fracturing Technology. Society of Petroleum Engineers, The Woodlands, Texas, USA.

Beg, M.S., Kunak, A.O., Gong, M., Zhu, D. and Hill, A.D., 1998. A Systematic Experimental Study of Acid Fracture Conductivity. SPE Production & Facilities.

Bhakta, A. and Ruckenstein, E., 1995. Drainage of a Standing Foam. Langmuir, 11(5): 1486-1492.

Binks, B.P. and Horozov, T.S., 2005. Aqueous Foams Stabilized Solely by Silica Nanoparticles. Angewandte Chemie, 44: 3722-3725.

Binks, B.P., Kirkland, M. and Rodrigues, J.A., 2008a. Origin of stabilisation of aqueous foams in nanoparticle-surfactant mixtures. Soft Matter, 4(12): 2373-2382.

Binks, B.P., Kirkland, M. and Rodrigues, J.A., 2008b. Origin of stabilisation of aqueous foams in nanoparticle–surfactant mixtures. Soft Matter, 4: 2373-2382.

Blauer, R.E. and Kohlhaas, C.A., 1974. Formation Fracturing with Foam, 49th Annual Fall Meeting of the Society of Petroleum Engineers of AIME. Society of Petroleum Engineers, Houston, Texas.

Bournival, G., Ata, S. and Wanless, E.J., 2015. The roles of particles in multiphase processes: Particles on bubble surfaces. Advances in Colloid and Interface Science, 225: 114-133.

Brakke, K.A., 1992. The surface evolver. 141-165.

Burke, L.H., Nevison, G.W. and Peters, W.E., 2011. Improved Unconventional Gas Recovery With Energized Fracturing Fluids: Montney Example. Society of Petroleum Engineers.

Carl, A., Bannuscher, A. and von Klitzing, R., 2015. Particle Stabilized Aqueous Foams at Different Length Scales: Synergy between Silica Particles and Alkylamines. Langmuir, 31(5): 1615-1622.

Carn, F., Colin, A., Pitois, O., Vignes-Adler, M. and Backov, R., 2009. Foam Drainage in the Presence of Nanoparticle−Surfactant Mixtures. Langmuir, 25(14): 7847-7856.

Chang, O., Dilmore, R. and Wang, J.Y., 2017. Model development of proppant transport through hydraulic fracture network and parametric study. Journal of Petroleum Science and Engineering, 150: 224-237.
Churaev, N.V., 2003. Derjaguin's disjoining pressure in the colloid science and surface phenomena. Advances in Colloid and Interface Science, 104(1–3): xv-xx.
Clark, P.E. and Guler, N., 1983. Prop Transport in Vertical Fractures: Settling Velocity Correlations, SPE Symposium on Low Permeability. Society of Petroleum Engineers, Denver, Colorado.
Cosima, S. and Regine von, K., 2003. Disjoining pressure in thin liquid foam and emulsion films—new concepts and perspectives. Journal of Physics: Condensed Matter, 15(27): R1197.
Cox, S.J., Dollet, B. and Graner, F., 2006. Foam flow around an obstacle: simulations of obstacle–wall interaction. Rheologica Acta, 45(4): 403-410.
Craft, J.R., Waddell, S.P. and McFatridge, D.G., 1992. CO2 -Foam Fracturing With Methanol Successfully Stimulates Canyon Gas Sand.
Davies, I.T. and Cox, S.J., 2009. Sedimenting discs in a two-dimensional foam. Colloids and Surfaces A: Physicochemical and Engineering Aspects, 344(1–3): 8-14.
Dickinson, E., Ettelaie, R., Kostakis, T. and Murray, B.S., 2004. Factors Controlling the Formation and Stability of Air Bubbles Stabilized by Partially Hydrophobic Silica Nanoparticles. Langmuir, 20(20): 8517-8525.
Economides, M.J. and Nolte, K.G., 2000. Reservoir Stimulation, 18. Wiley, New York.
Farajzadeh, R., Krastev, R. and Zitha, P.L.J., 2008. Foam film permeability: Theory and experiment. Advances in Colloid and Interface Science, 137(1): 27-44.
Fei, Y. et al., 2016. Simulation of hydraulic fracturing with propane-based fluid using a fracture propagation model coupled with multiphase flow simulation in the Cooper Basin, South Australia. APPEA Journal, 56: 415-426.
Fredd, C.N., McConnell, S.B., Boney, C.L. and England, K.W., 2001. Experimental Study of Fracture Conductivity for Water-Fracturing and Conventional Fracturing Applications. SPE Journal.
Freeman, E.R., Bilden, D.M. and Hossaini, M., 1986. Delayed Crosslinked Gels: Their Role in Aqueous Foam Fracturing, 56th California Regional Meeting. Society of Petroleum Engineers, Oakland, CA.
Fujii, S., Ryan, A.J. and Armes, S.P., 2006. Long-Range Structural Order, Moiré Patterns, and Iridescence in Latex-Stabilized Foams. Journal of the American Chemical Society, 128(24): 7882-7886.
Garbis, S.J. and Taylor, J.L., III, 1986. The Utility of CO2 as an Energizing Component for Fracturing Fluids.
Gaydos, J.S. and Harris, P.C., 1980. Foam Fracturing: Theories, Procedures And Results. Society of Petroleum Engineers.
Goelitz, R. and Evertz, G.E., 1982. Foam Fracturing In The Uinta Basin - A Field Study Of The Dakota And Wasatch Formations. Society of Petroleum Engineers.
Gu, M. and Mohanty, K.K., 2015. Rheology of polymer-free foam fracturing fluids. Journal of Petroleum Science and Engineering, 134: 87-96.
Harris, P.C., 1985. Dynamic Fluid Loss Characteristics of Foam Fracturing Fluids. SPE Journal.
Harris, P.C., 1992. Application of Foam Fluids To Minimize Damage During Fracturing, International Meeting on Petroleum Engineering. Society of Petroleum Engineers, Beijing, China.
Harris, P.C. and Health, S.J., 1996. Rheology of Crosslinked Foams. SPE Journal.
Harris, P.C. and Heath, S.J., 1996. High-Quality Foam Fracturing Fluids, Gas Technology

Symposium. Society of Petroleum Engineers, Calgary, Alberta, Canada.
Harris, P.C. and Reidenbach, V.G., 1987. High-Temperature Rheological Study of Foam Fracturing Fluids. SPE Journal.
Harris, P.C., Walters, H.G. and Bryant, J., 2009. Prediction of Proppant Transport From Rheological Data. SPE Journal.
Höhler, R. and Cohen-Addad, S., 2005. Rheology of liquid foam. Journal of Physics: Condensed Matter, 17(41): R1041.
Hunter, T.N., Pugh, R.J., Franks, G.V. and Jameson, G.J., 2008. The role of particles in stabilising foams and emulsions. Advances in Colloid and Interface Science, 137(2): 57-81.
Hutzler, S., Cox, S.J. and Wang, G., 2005. Foam drainage in two dimensions. Colloids and Surfaces A: Physicochemical and Engineering Aspects, 263(1–3): 178-183.
Jansen, T.A., Zhu, D. and Hill, A.D., 2015. The Effect of Rock Mechanical Properties on Fracture Conductivity for Shale Formations, SPE Hydraulic Fracturing Technology Conference. Society of Petroleum Engineers, Woodlands, Texas, USA.
Jing, Z., Wang, S. and Wang, Z., 2016. Detailed Structural and Mechanical Response of Wet Foam to the Settling Particle. Langmuir, 32(10): 2419-2427.
Johnson, R.L., Jr., 1995. Fracture Treatment Modifications And Bottomhole Treating Pressure Analysis In The Pictured Cliffs Formation, Rio Arriba County, New Mexico, Production Operations Symposium. Society of Petroleum Engineers, Oklahoma City, Oklahoma, USA.
Karakashev, S.I. and Manev, E.D., 2001. Frothing Behavior of Nonionic Surfactant Solutions in the Presence of Organic and Inorganic Electrolytes. Journal of Colloid and Interface Science, 235(1): 194-196.
Khade, S.D. and Shah, S.N., 2004. New Rheological Correlations for Guar Foam Fluids. SPE Journal.
Koehler, S.A., Hilgenfeldt, S. and Stone, H.A., 2000. A Generalized View of Foam Drainage: Experiment and Theory. Langmuir, 16(15): 6327-6341.
Koehler, S.A., Hilgenfeldt, S. and Stone, H.A., 2004. Foam drainage on the microscale: I. Modeling flow through single Plateau borders. Journal of Colloid and Interface Science, 276(2): 420-438.
Leonard, R.A. and Lemlich, R., 1965. A study of interstitial liquid flow in foam. Part I. Theoretical model and application to foam fractionation. AIChE Journal, 11(1): 18-25.
Li, N. et al., 2016. Laboratory Testing on Proppant Transport in Complex-Fracture Systems. SPE Journal.
Liu, Y., Leung, J.Y., Chalaturnyk, R. and Virues, C.J.J., 2017. Fracturing Fluid Distribution in Shale Gas Reservoirs Due to Fracture Closure, Proppant Distribution and Gravity Segregation, Unconventional Resources Conference. Society of Petroleum Engineers, Calgary, Alberta, Canada.
Lv, Q., Li, Z., Li, B., Li, S. and Sun, Q., 2015. Study of Nanoparticle–Surfactant-Stabilized Foam as a Fracturing Fluid. Industrial & Engineering Chemistry Research, 54(38): 9468-9477.
Lv, Q. et al., 2017. Silica nanoparticles as a high-performance filtrate reducer for foam fluid in porous media. Journal of Industrial and Engineering Chemistry, 45: 171-181.
Maestro, A., Rio, E., Drenckhan, W., Langevin, D. and Salonen, A., 2014a. Foams stabilised by mixtures of nanoparticles and oppositely charged surfactants: relationship between bubble shrinkage and foam coarsening. Soft Matter, 10(36): 6975-6983.
Maestro, A., Rio, E., Drenckhan, W., Langevin, D. and Salonen, A., 2014b. Foams stabilised by mixtures of nanoparticles and oppositely charged surfactants: relationship between bubble shrinkage and foam coarsening. Soft Matter, 10: 6975-6983.

Magrabi, S.A., Dlugogorski, B.Z. and Jameson, G.J., 2001. Free drainage in aqueous foams: Model and experimental study. AIChE Journal, 47(2): 314-327.
Neethling, S.J., Lee, H.T. and Cilliers, J.J., 2002. A foam drainage equation generalized for all liquid contents. Journal of Physics: Condensed Matter, 14(3): 331.
Pyrak-Nolte, L.J. and Morris, J.P., 2000. Single fractures under normal stress: The relation between fracture specific stiffness and fluid flow. International Journal of Rock Mechanics and Mining Sciences, 37(1–2): 245-262.
Raufaste, C., Dollet, B., Cox, S., Jiang, Y. and Graner, F., 2007. Yield drag in a two-dimensional foam flow around a circularobstacle: Effect of liquid fraction. The European Physical Journal E, 23(2): 217-228.
Safouane, M., Saint-Jalmes, A., Bergeron, V. and Langevin, D., 2006. Viscosity effects in foam drainage:Newtonian and non-newtonian foaming fluids. The European Physical Journal E, 19(2): 195-202.
Sani, A.M., Shah, S.N. and Baldwin, L., 2001. Experimental Investigation of Xanthan Foam Rheology, SPE Production and Operations Symposium. Society of Petroleum Engineers, Oklahoma City, Oklahoma.
Saye, R.I. and Sethian, J.A., 2013. Multiscale Modeling of Membrane Rearrangement, Drainage, and Rupture in Evolving Foams. Science, 340(6133): 720-724.
Shiozawa, S. and McClure, M., 2016. Simulation of proppant transport with gravitational settling and fracture closure in a three-dimensional hydraulic fracturing simulator. Journal of Petroleum Science and Engineering, 138: 298-314.
Stevenson, P., 2005. Remarks on the shear viscosity of surfaces stabilised with soluble surfactants. Journal of Colloid and Interface Science, 290(2): 603-606.
Stevenson, P., 2010. Inter-bubble gas diffusion in liquid foam. Current Opinion in Colloid & Interface Science, 15(5): 374-381.
Stocco, A., Garcia-Moreno, F., Manke, I., Banhart, J. and Langevin, D., 2011. Particle-stabilised foams: structure and aging. Soft Matter, 7(2): 631-637.
Stokes, G.G., 1851. On the effect of the internal friction of fluids on the motion of pendulums, 9. Pitt Press.
Sun, Q. et al., 2015a. Properties of multi-phase foam and its flow behavior in porous media. RSC Advances, 5(83): 67676-67689.
Sun, Q. et al., 2015b. Aqueous foam stabilized by partially hydrophobic nanoparticles in the presence of surfactant. Colloids and Surfaces A: Physicochemical and Engineering Aspects, 471: 54-64.
Sun, X., Liang, X., Wang, S. and Lu, Y., 2014. Experimental study on the rheology of CO2 viscoelastic surfactant foam fracturing fluid. Journal of Petroleum Science and Engineering, 119: 104-111.
Toney, F.L. and Mack, D.J., 1991. The Next Generation of Foam: A Field Study of Northwestern Oklahoma Foam Fracturing, Production Operations Symposium. Society of Petroleum Engineers, Oklahoma City, Oklahoma.
Urs T. Gonzenbach, André R. Studart Dr., Elena Tervoort Dr. and Dr., L.J.G.P., 2006. Ultrastable Particle-Stabilized Foams. Angew. Chem. Int. Ed.: 3526-3530.
Vance, B., 1999. Forces and structure in thin liquid soap films. Journal of Physics: Condensed Matter, 11(19): R215.
Wamock, W.E., Jr., Harris, P.C. and King, D.S., 1985. Successful Field Applications of CO2-Foam Fracturing Fluids in the Arkansas-Louisiana-Texas Region.
Wang, J., Nguyen, A.V. and Farrokhpay, S., 2016. A critical review of the growth, drainage and collapse of foams. Advances in Colloid and Interface Science, 228: 55-70.
Wanniarachchi, W.A.M. et al., 2015. Current opinions on foam-based hydro-fracturing in deep geological reservoirs. Geomechanics and Geophysics for Geo-Energy and Geo-

Resources, 1(3): 121-134.
Warpinski, N.R., 2010. Stress Amplification and Arch Dimensions in Proppant Beds Deposited by Waterfracs. SPE Production & Operations.
Watkins, E.K., Wendorff, C.L. and Ainley, B.R., 1983. A New Crosslinked Foamed Fracturing Fluid, 58th Annual Technical Conference and Exhibition. Society of Petroleum Engineers, San Francisco, CA.
Weaire, D., 2008. The rheology of foam. Current Opinion in Colloid & Interface Science, 13(3): 171-176.
Wu, W., Kakkar, P., Zhou, J., Russell, R. and Sharma, M.M., 2017. An Experimental Investigation of the Conductivity of Unpropped Fractures in Shales, Hydraulic Fracturing Technology Conference and Exhibition. Society of Petroleum Engineers, Woodlands, Texas, USA.
Wyn, A., Davies, I.T. and Cox, S.J., 2008. Simulations of two-dimensional foam rheology: Localization in linear Couette flow and the interaction of settling discs. The European Physical Journal E, 26(1): 81-89.
Yu, W., Zhang, T., Du, S. and Sepehrnoori, K., 2015. Numerical study of the effect of uneven proppant distribution between multiple fractures on shale gas well performance. Fuel, 142: 189-198.
Zargartalebi, M., Barati, N. and Kharrat, R., 2014. Influences of hydrophilic and hydrophobic silica nanoparticles on anionic surfactant properties: Interfacial and adsorption behaviors. Journal of Petroleum Science and Engineering, 119: 36-43.
Zhang, G., Li, M. and Gutierrez, M., 2016. Numerical simulation of proppant distribution in hydraulic fractures in horizontal wells. Journal of Natural Gas Science and Engineering.
Zhu, Y., Pei, X., Jiang, J., Cui, Z. and Binks, B.P., 2015. Responsive Aqueous Foams Stabilized by Silica Nanoparticles Hydrophobized in Situ with a Conventional Surfactant. Langmuir, 31(47): 12937-12943.

Appendix

A. Liquid Fraction Profile Calculation

The following four steps comprise the calculation procedure: 1) defining the flow drainage regime, 2) calculating the drainage velocity, 3) determining the theoretical drainage half-time, and 4) calibrating between the theoretical and experimental drainage half-time.

1. Assume that the DLVO forces of foam film are strong enough to stop the walls from breaking and there is no Ostwald ripening. This assumption will simplify the foam drainage so as not to couple with foam coarsening due to natural complexity of the drainage. Initial input parameters obtained from experimental measurements are initial foam height (H_i), solution viscosity (η_l), density (ρ_l) of the base fluid, initial liquid fraction (ε_o), and cross-sectional area of the cylinder (S). Assume an initial bubble diameter D, then calculate the length of Plateau border (L); the radius of length border (r_{PB}) is given by **Eq. 22** and **Eq. 23**:

$$L = {}^{D}/_{2.7} \tag{22}$$

$$r_{PB} = L \times \sqrt{\frac{\varepsilon_o}{0.17}} \tag{23}$$

2. Determine the drainage flow regime using the interfacial mobility (M) value from **Eq. 24**. $M \gg 1$ indicates that drainage is plug flow; the nodes play a significant role in flow resistance. Using a node-dominated drainage equation (**Eq. 25**), if $M \ll 1$, the drainage is Poiseuille flow, i.e. 'no slip' condition down the Plateau border. Using channel-dominated drainage equation (**Eq. 26**). In this study, we used the liquid viscosity (η_l) and initial liquid fraction (ε_o) obtained from an experiment (Stevenson, 2005)(Stevenson, 2005)(Stevenson, 2005)(Stevenson, 2005)(Stevenson, 2005)(Stevenson, 2005)(Stevenson, 2005). Furthermore, we used typical values of $\eta_s = 0.001$ g/s for all cases.

$$M = \frac{0.9\eta_l\sqrt{\varepsilon_o}}{\eta_s} \tag{24}$$

$$v_d^{channel} = \frac{0.007\rho_l g L^2 \varepsilon_o}{\eta_l} \tag{25}$$

$$v_d^{node} = \frac{0.002\rho_l g L^2 \sqrt{\varepsilon_o}}{\eta_l} \tag{26}$$

3. In addition to drainage velocity, calibrate the drainage half-time between theoretical (**Eq. 27)** and experimental results by adjusting the bubble diameter D.

$$\tau = {}^{H}/_{v_d} \tag{27}$$

4. After theoretical validation, rearrange **Eq. 25** and **Eq. 26** incorporated with **Eq. 27**. The liquid fraction is a function of foam height and time (**Eq. 28** and **Eq. 29**), where the foam height $H \subseteq [0, H_i]$ and the time $t \subseteq [0, \tau_1]$. Then, use Excel to calculate the liquid fraction value by varying the height and time.

$$\varepsilon^{channel} = \frac{\eta_l}{0.007\rho_l g L^2}\frac{H}{t} \tag{28}$$

$$\varepsilon^{node} = [\frac{\eta_l}{0.007\rho_l g L^2}\frac{H}{t}]^2 \tag{29}$$

5. Plot the liquid fraction (ε) with the foam height (H) and time (t). See example of foam B (0.8% SiO_2 nanoparticle, channel) and foam C (CMHPG, node) in Figures A1 and A2 respectively.

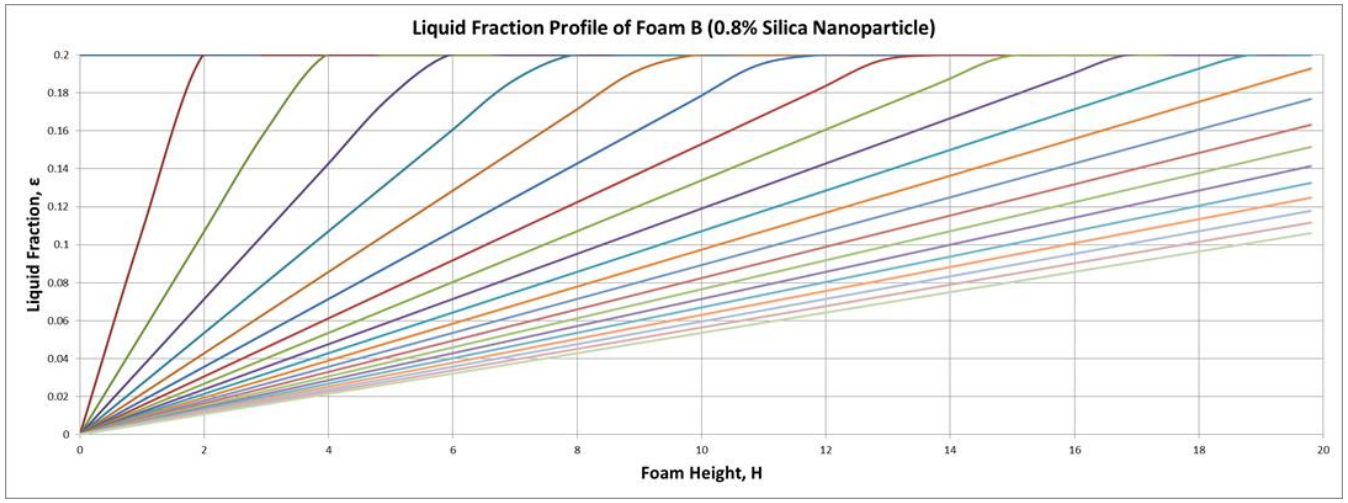

Figure A1. Liquid fraction profile of 0.8 wt% SiO_2 with 0.1 wt% regular anionic surfactant.

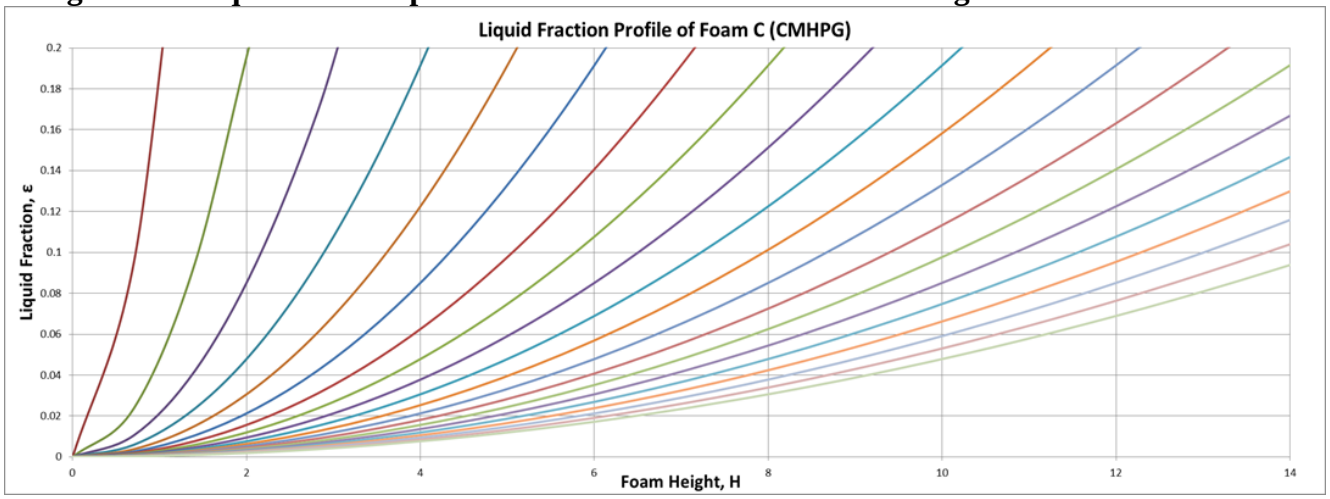

Figure A2. Liquid fraction profile of 0.36 wt% CMHPG with 0.1 wt% regular anionic surfactant.